AD A033101

(3)

STUDY OF THE FEASIBILITY OF CONDUCTING A WAKE-RIDING EXPERIMENT USING A T-2 AIRCRAFT BEHIND TWO P-3 AIRCRAFT

Aeronautical Research Associates of Princeton, Inc.
50 Washington Road, Princeton, New Jersey 08540

APPROVED FOR PUBLIC RELEASE;
DISTRIBUTION UNLIMITED

August 1976

Final Report for Period 19 April 1976 - 17 August 1976

Prepared for

NAVAL AIR DEVELOPMENT CENTER
Warminster, Pennsylvania 18974

UNCLASSIFIED
SECURITY CLASSIFICATION OF THIS PAGE (When Data Entered)

REPORT DOCUMENTATION PAGE		READ INSTRUCTIONS BEFORE COMPLETING FORM
1. REPORT NUMBER	2. GOVT ACCESSION NO.	3. RECIPIENT'S CATALOG NUMBER
4. TITLE (and Subtitle) (6) Study of the Feasibility of Conducting a Wake-Riding Experiment Using a T-2 Aircraft Behind Two P-3 Aircraft,		5. TYPE OF REPORT & PERIOD COVERED Final 4/19/76-8/17/76
		6. PERFORMING ORG. REPORT NUMBER A.R.A.P. Report No. 287
7. AUTHOR(s) (10) Coleman duP. Donaldson, Alan J. Bilanin, Guy G. Williamson, Richard Snedeker		8. CONTRACT OR GRANT NUMBER(s) (15) N62269-76-C-0305 new
9. PERFORMING ORGANIZATION NAME AND ADDRESS Aeronautical Research Associates of Princeton, Inc. 50 Washington Rd., Princeton, NJ 08540		10. PROGRAM ELEMENT, PROJECT, TASK AREA & WORK UNIT NUMBERS (14) ARAP-287
11. CONTROLLING OFFICE NAME AND ADDRESS Naval Air Development Center Warminster, PA 18974	(11)	12. REPORT DATE Aug [redacted] 76
		13. NUMBER OF PAGES
14. MONITORING AGENCY NAME & ADDRESS (if different from Controlling Office) (9) Final rept. 19 Apr-17 Aug 76,		15. SECURITY CLASS. (of this report) UNCLASSIFIED
		15a. DECLASSIFICATION/DOWNGRADING SCHEDULE

16. DISTRIBUTION STATEMENT (of this Report)

(12) 91 p.

17. DISTRIBUTION STATEMENT (of the abstract entered in Block 20, if different from Report)

APPROVED FOR PUBLIC RELEASE;
DISTRIBUTION UNLIMITED

18. SUPPLEMENTARY NOTES

19. KEY WORDS (Continue on reverse side if necessary and identify by block number)

Wake Riding
Aircraft Wakes
Vortex Wakes

20. ABSTRACT (Continue on reverse side if necessary and identify by block number)

A study has been made of a T-2 aircraft attempting to establish a wake-riding position behind two P-3 aircraft. The major objectives were to estimate structural loads in the wake rider and to evaluate wake entry and station keeping control techniques. The results of the study indicate that the root-bending load on the tail of the T-2 aircraft would be of the order of the design load if the aircraft were to inadvertently pass directly through the center of a trailing vortex from one of the P-3s. Thus the next

008 400

20. ABSTRACT (concluded)

flight tests, as originally envisaged, must be considered as high risk experiments unless the tail of the T-2 were to be strengthened. If wake riding experiments are carried out, approach to the wake-riding position should be made from above using a reduced-power, constant-airspeed approach. In calm air the piloting task appears reasonable if the trailing vortices are marked by smoke or condensation.

1. INTRODUCTION

As a result of the aircraft vortex hazard problem, there has been a revival of interest in the nature of aircraft wakes. While the interest is mostly directly towards avoiding or dissipating the vortices, one should also ask if the energy contained in the wake can be put to good use. Initial computations, done at A.R.A.P. (Ref. 1), indicate that the wakes generated by large aircraft contain enough energy in usable form to allow substantial reductions in power for a following or wake-riding aircraft. The Naval Air Development Center has expressed an interest in obtaining a proof of the concept of wake riding by flight testing a T-2 trainer in the wake of two P-3 patrol aircraft, as shown in Figure 1.

In order to assure that the flight test referred to above could be carried out safely, A.R.A.P. was asked by NADC to perform a pre-test study which had two principal objectives:

(1) Estimation of the structural loads that would be encountered by the T-2 were it to inadvertently pass directly through one of the trailing vortices left by the P-3s during the flight tests.

(2) Consider the nature of the piloting task that would be faced by the pilot of the T-2 and recommend piloting techniques and test procedures that might be helpful in assuring success of the flight tests under consideration.

The study that was undertaken by A.R.A.P. to accomplish these ends was divided into five tasks:

(1) The wake fluid velocity field was computed and entered into an existing simulation program.

(2) An existing A.R.A.P. simulation program was modified in order to calculate changes in the six force and moment coefficients due to the vortex velocity field. Also, a simple autopilot was incorporated into the program.

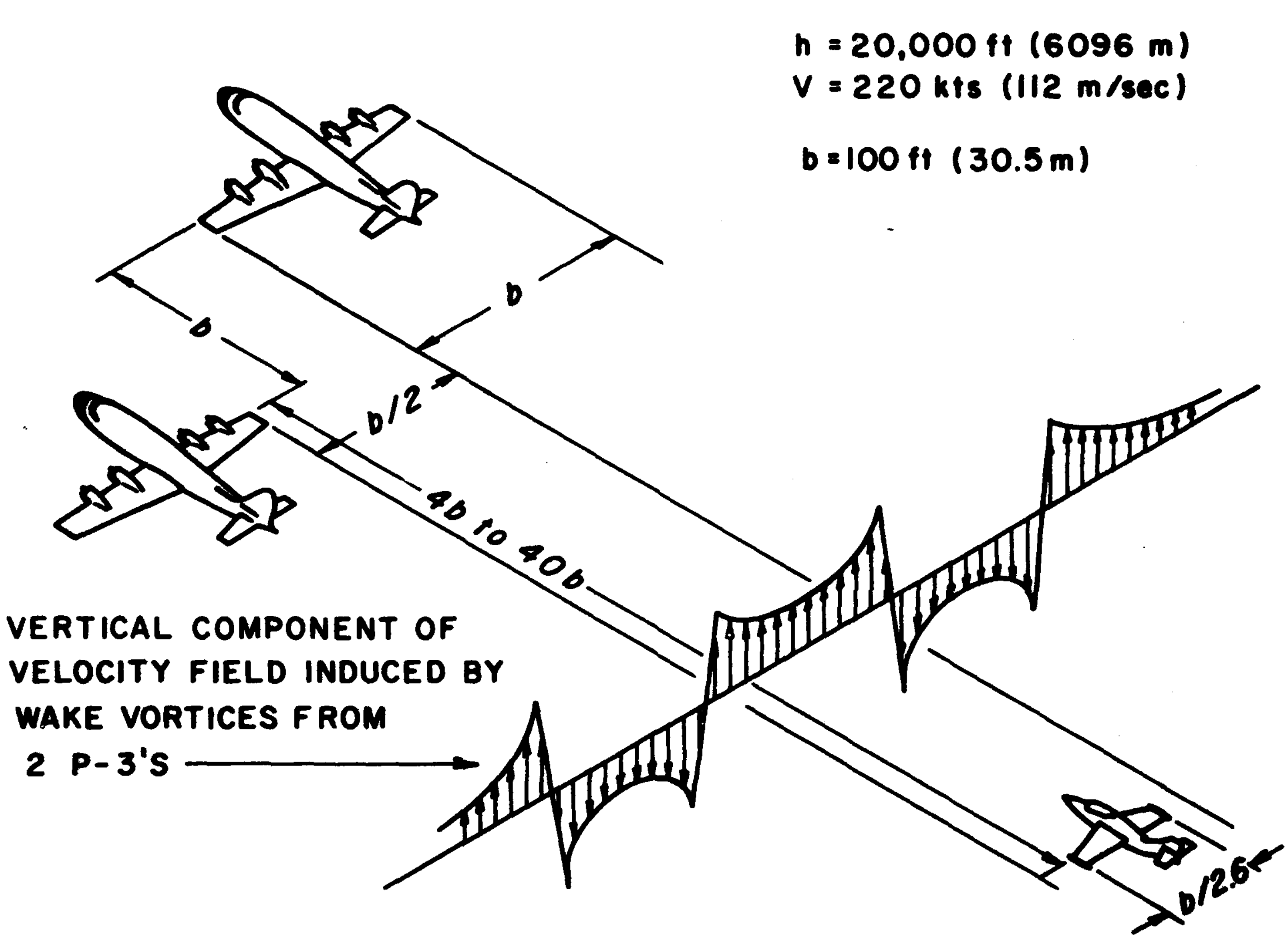

Fig. 1. Flight Configuration for Wake Rider Test

(3) Measurements of induced rolling moment on a model T-2 wing were made in a small-scale wind tunnel. These measurements were made to increase confidence in the analytic estimates of rolling moment coefficient computed by the digital simulation program.

(4) Using results from the above-noted three tasks, digital simulations of a T-2 aircraft entering, riding, and leaving the wakes of two P-3 aircraft were run. The series of simulations included worst case encounters where the aerodynamic loads are large. In addition, runs were made with simple autopilots to roughly evaluate the difficulty of the piloting task.

(5) Structural loads of the aircraft surfaces were estimated and compared with their maximum allowable values. These estimates were then considered in the light of NASA's flight test experience when probing the wake of a 747 with an instrumented T-37 aircraft.

In Section 2 of this report, the mathematical model used to describe the flow field left by the two P-3 aircraft is presented. Section 3 reports on a simple wind tunnel test that helps lend credence to the model presented in Section 2 and the calculation of forces and moments on the T-2 which are presented in Section 4. Section 5 deals with the dynamics of the T-2 as it enters the wake-riding region and the problem of maintaining this position. Section 6 discusses the structural loads that might be expected on the T-2 aircraft should vortex encounter occur. And, finally, Section 7 sets forth the conclusions and recommendations that resulted from this brief study.

2. THEORETICAL MODEL OF WAKE FLOW FIELD

The wake fluid velocity field was computed assuming an elliptic load distribution of the P-3 wing which ideally rolls up into two discrete vortices for each P-3 as shown in Figure 2. Each vortex is then ideally located at $\frac{\pi}{8}b$ from the centerline of the aircraft. The strength of each vortex is given in terms of the circulation Γ_o as

$$\Gamma_o = \frac{4L}{\pi \rho U b}$$

For the P-3 in steady level flight during testing at an altitude of 20,000 ft (6096 m) and at a flight speed of 220 knots (112 m/sec), this is characteristically

$$\Gamma_o = 2{,}700 \text{ ft}^2/\text{sec} \ (251 \text{ m}^2/\text{sec})$$

The flow field produced by each vortex can, for the purpose of this study, be characterized by the mean tangential velocity V_T. Based on the results of Ref. 2, the tangential velocity associated with each vortex is given by the following set of equations:

for $r < 3$ ft (.91 m)

$$V_T = \frac{\Gamma_o}{18\pi}\left[6\left(\frac{3}{b}\right) - 9\left(\frac{3}{b}\right)^2\right]^{1/2} r$$

for 3 ft (.91 m) $\leq r \leq$ 33 ft (10 m)

$$V_T = \frac{\Gamma_o}{2\pi r}\left[6\left(\frac{r}{b}\right) - 9\left(\frac{r}{b}\right)^2\right]^{1/2}$$

for $r > 33$ ft (10 m)

$$V_T = \frac{\Gamma_o}{2\pi r}$$

These relations should adequately define the flow field for the region downstream of the P-3s defined by

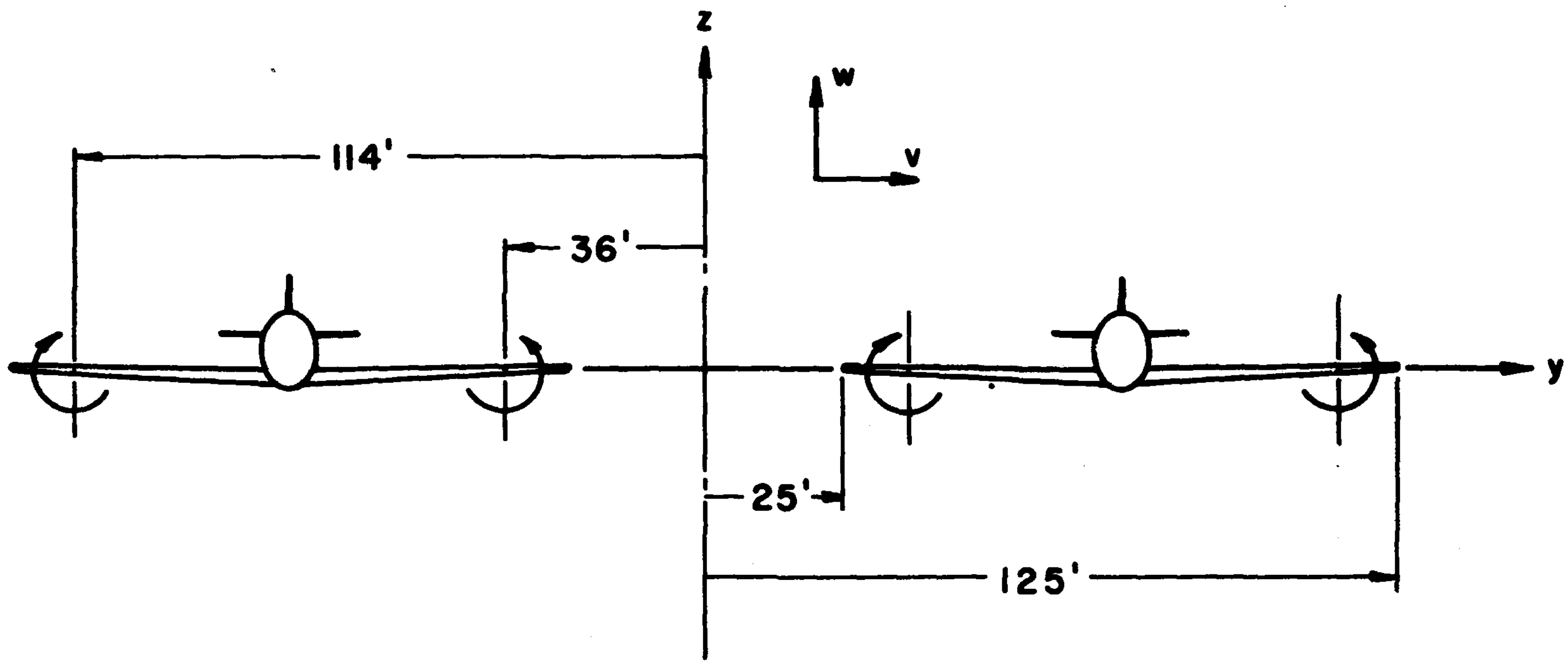

Figure 2. Lateral spacing of P-3 aircraft and their wake vortices.

$$400 \text{ ft } (122 \text{ m}) < x < 4000 \text{ ft } (1219 \text{ m})$$

The tangential velocity contributions from each of the four vortices are then summed in order to obtain the crossflow velocity at any particular lateral and vertical position.

This crossflow velocity information is then converted to geocentric velocity components v (horizontal) and w (vertical) and stored at 3-foot intervals in y and z over a square area 300 ft (91.4 m) on each side. A program then linearly interpolates among these values and converts to body axes in order to obtain the wake velocity normal to the wing at selected stations.

Figures 3 and 4 illustrate the vertical wake velocity w as a function of lateral position y at $z = 0$ and $z = 20$ ft (6.1 m) above the vortex centers. Two characteristics are worth noting. (1) w decreases as z departs from $z = 0$. This means that the aircraft will be stable with respect to altitude above the vortices and unstable below them. (2) For $|z| < 10$ ft (3.05 m), w increases for lateral positions away from the origin. This tends to stabilize the aircraft laterally by rolling the aircraft back towards the center.

Figure 5 illustrates the horizontal velocity v as a function of z at two selected values of y. Here it is worth noting that the horizontal velocity will tend to destabilize the aircraft with respect to lateral position for $z > 0$ and is stabilizing it for $z < 0$.

VERTICAL WAKE VELOCITY COMPONENT

$z = 0$

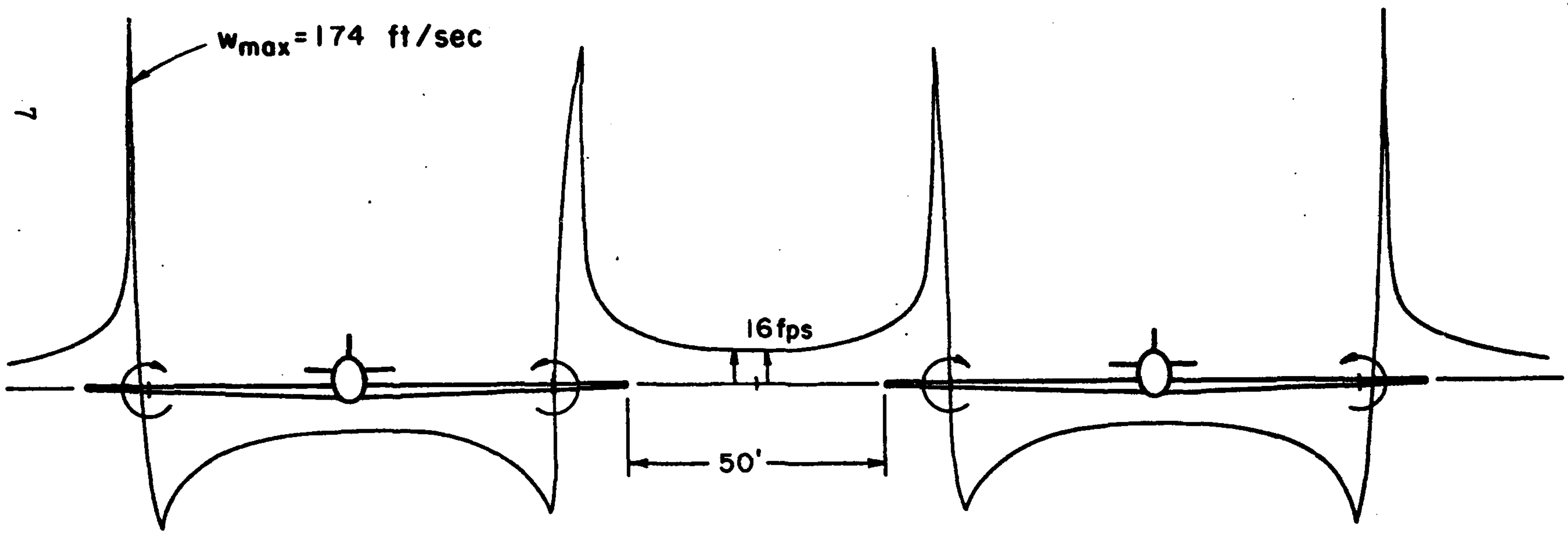

Figure 3.

VERTICAL WAKE VELOCITY COMPONENT

$z = 20$ feet

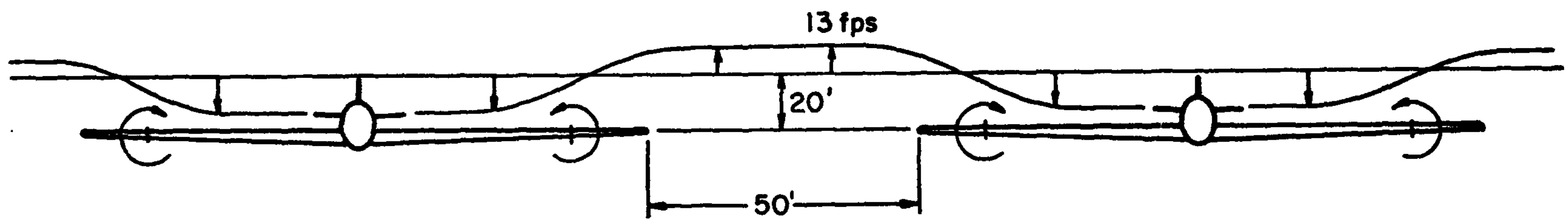

Figure 4.

HORIZONTAL WAKE VELOCITY COMPONENT

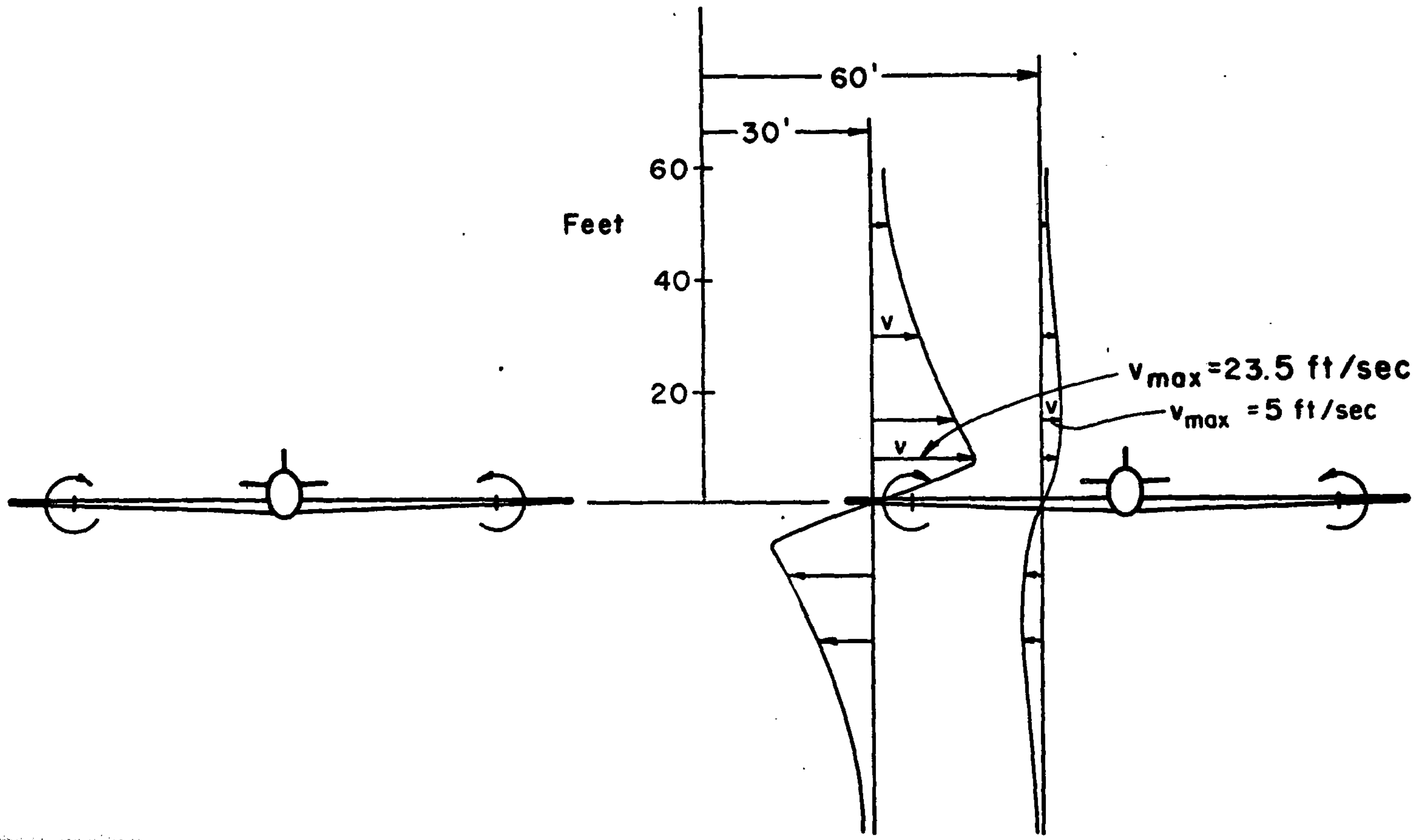

3. WIND TUNNEL TEST PROGRAM

In order to lend credence to the validity of the theoretical rolling moment values computed for the T-2 in the next section of this report, a wind tunnel test program was carried out in which rolling moment coefficients were measured on a scale T-2 wing immersed in a scale vortex wake. The apparatus and techniques used in this program and the results obtained are described in the following sections.

A. Apparatus and Instrumentation

The object of the tests was to measure the rolling moment coefficients on a wing model under conditions which simulated as closely as possible those of a full-scale encounter of a T-2 with the central portion of the wake produced by two P-3's flying side-by-side. The means of establishing the desired wake flow was already available in the A.R.A.P. subsonic wind tunnel. This tunnel has a 30.5 x 30.5 cm (12x12 in.) test section 2 m (6.5 ft) long. It is provided with vortex generator airfoils which can produce pairs of parallel vortices in various combinations of strength, sign and spacing. The tunnel test section and wake generating system are illustrated schematically in Figure 6, which also shows the flow visualization system available and some examples of vortex flow cross-sections photographed in the course of an earlier study of vortex merging. The tunnel is capable of speeds of up to 13.7 m/sec (45 ft/sec). The vortex generator airfoils are of NACA 0012 section and are hollow with holes at their tips to allow for the injection of smoke into the flow.

The choice of conditions for the tests was dictated by the desire to scale the T-2 wake encounter accurately while minimizing the effects of the tunnel walls. This choice, in turn, specified the size of the T-2 wing model to be used. The conditions chosen were based on a wake vortex spacing of 13.4 cm, or about 44% of the tunnel width. Since the nominal full-scale test configuration was to have the vortex spacing equal to twice the T-2 wingspan,

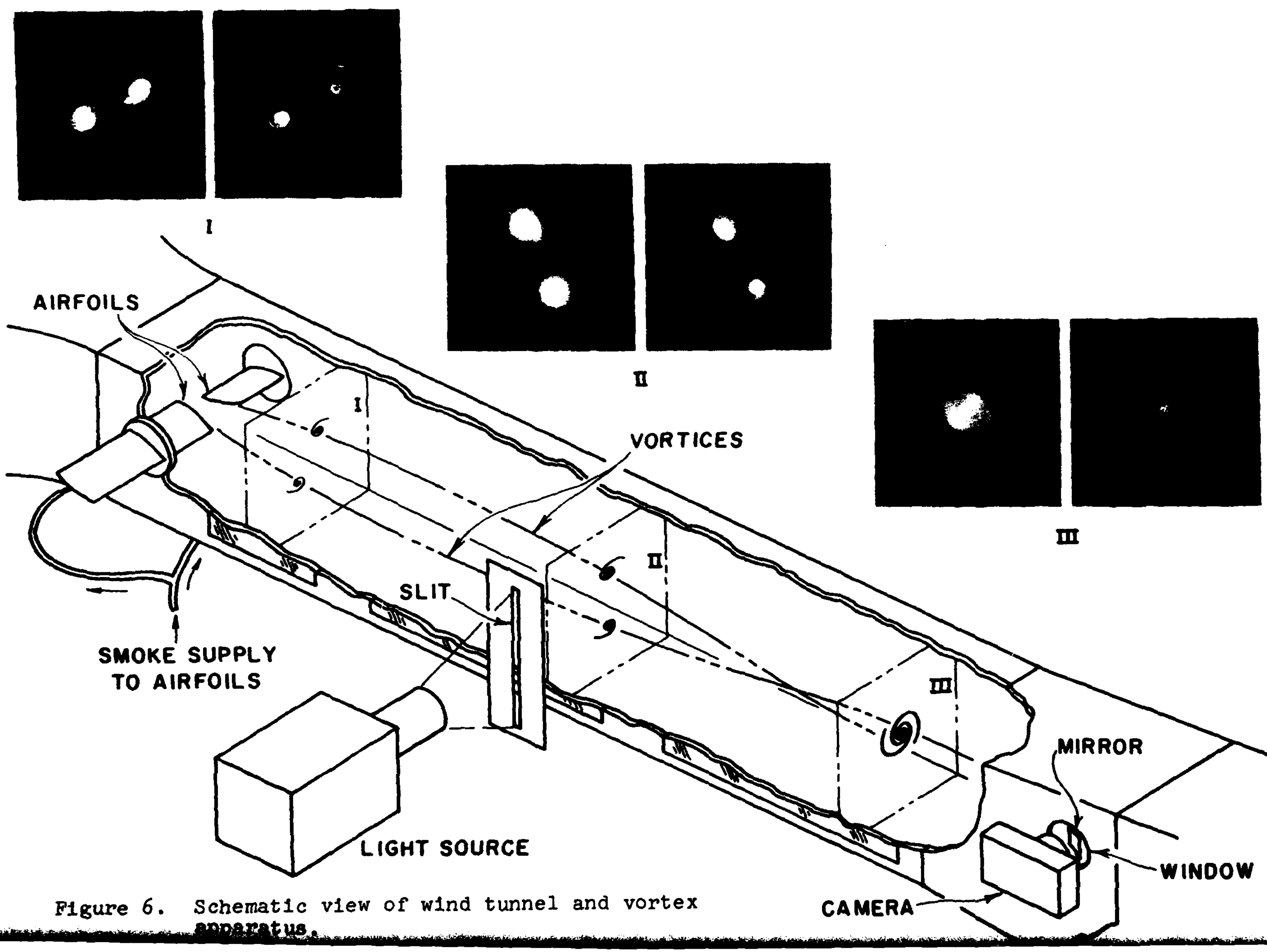

Figure 6. Schematic view of wind tunnel and vortex apparatus.

the T-2 wing model was made with a wingspan of 6.7 cm. These relative dimensions are shown in Figure 7.

The measurement of rolling moment on a wing model of this size presented several challenging problems. Not only would the instrument have to be highly sensitive to applied rolling moment, but it would also have to be insensitive to axial and normal forces and other applied moments. At the same time it would have to be small enough so as not to disturb the flow unduly, and simple enough to be constructed within the time available. An estimate of the moments to be encountered revealed that the maximum rolling moment would be of the order of 10 gm-cm. A number of possible instrumentation methods were explored, including strain-gauge torque tubes, reflected light beams, and servo-driven null systems. None met the combined requirements of high sensitivity, small size, and simplicity.

Finally, a torque meter design was arrived at which did prove satisfactory in all respects. The instrument incorporated a sensitive active element mounted coaxially in a fixed tubular case with the sensitive element suspended on springs of the flexural pivot type. A very slight angular rotation was allowed in response to the applied torque, and this rotation was sensed by a rotary variable differential transformer (RVDT). In a size that is rugged enough for the present application (.48 cm, 3/16-in. O.D.) the flexural pivots - manufactured by the Bendix Corporation - are available with torsional spring rates as low as .8 gm-cm/degree, which is more than adequate. Their response to torsion is virtually unaffected by radial and axial loads of the magnitudes anticipated. The RVDT used was manufactured by Pickering and Co., Inc., and had separate rotor and stator sections so that, when it was combined with the flexural pivots, the action of the instrument was frictionless. In principle, the resolution was only limited by the means used to detect the output of the RVDT. A cross-sectional view of the torque meter is shown in Figure 8. As can be seen, the frontal area of the instrument (3.81 cm diam) is mainly limited

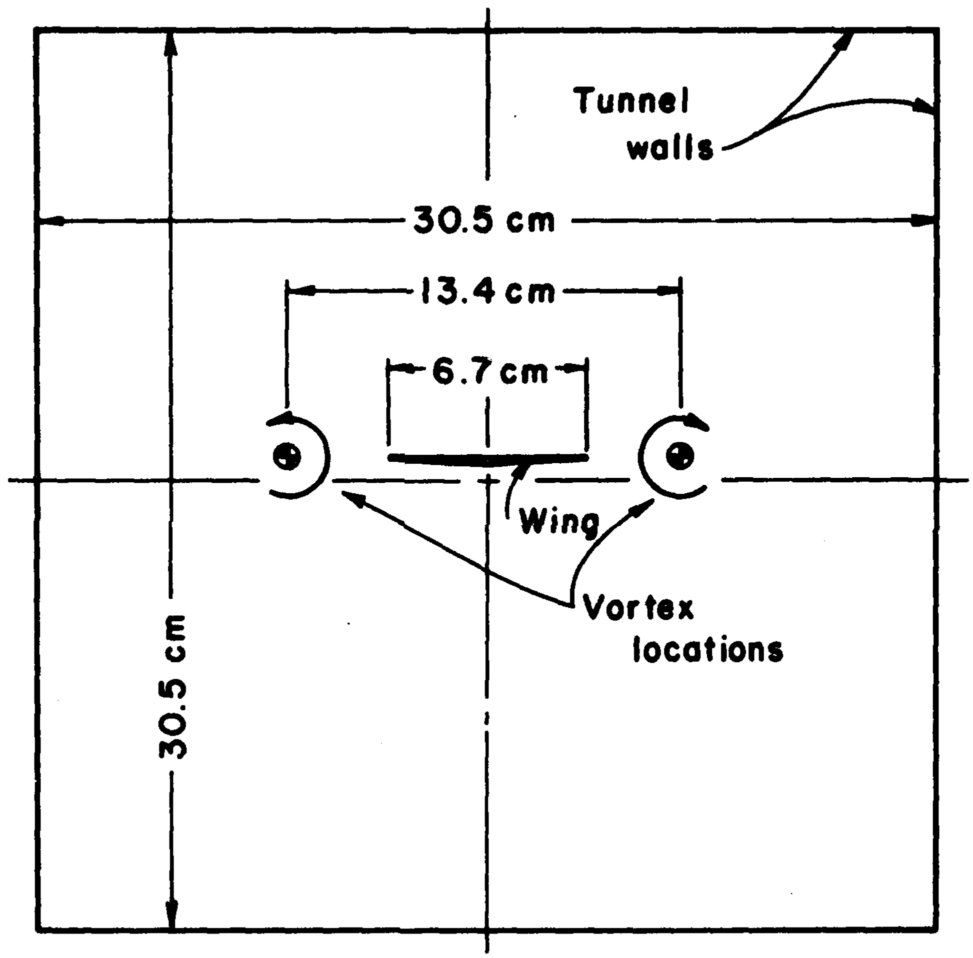

Figure 7. Relative dimensions of scale wind tunnel test of T-2 encounter with vortex wake.

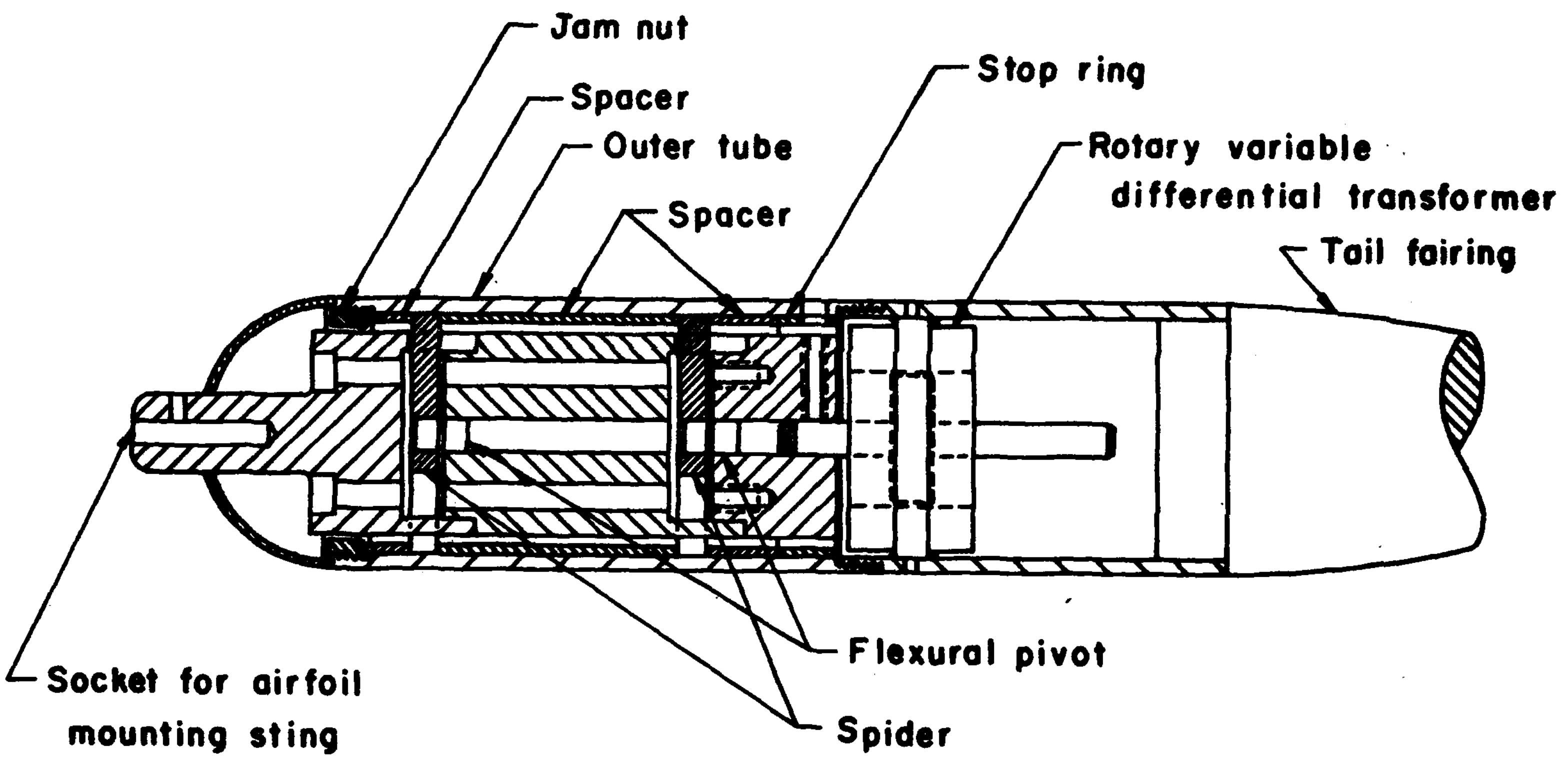

Figure 8. Cross-sectional view of torque meter.

by the size of the RVDT, which, in this case, was the smallest available of the desired type.

The RVDT was excited by a 10 kHz signal of 3-volt-rms amplitude. The output was demodulated and measured on a digital dc voltmeter on the ± 0.1 volt full-scale range. The resolution was .00001 volts dc and a potentiometer was used to adjust the zero setting.

With the spring suspension of the sensitive element, the only damping available for the torque meter was the aerodynamic damping due to the T-2 wing itself. During the tests it was found that the damping in roll of the wing was quite adequate to overcome any significant vibrationally induced oscillations of the torquemeter. In the design, the sensitive element was made as massive as possible to minimize its undamped natural frequency. It was found that this frequency was about 16 Hz. This low value effectively eliminated effects of vibration on the RVDT output.

The T-2 wing model was made of aluminum and was mounted at the end of a 15-cm long sting inserted in the forward end of the torque meter. The wing was to scale in planform, but somewhat thinner than scale in section.

The torque meter was mounted in a manually adjustable traversing mechanism which allowed the wing to be located at any point in the flow field up to within about 4 cm of the tunnel walls. In Figure 9, the torque meter and model T-2 wing are shown together with a view of the wind tunnel test section with the vortex generator airfoils and the torque meter installed.

The torque meter was calibrated by hanging weights at the tips of the model wing. The calibration was found to be linear throughout the full range of allowable angular rotation. Built-in stops limited this rotation to about $\pm 5°$. The two flexure pivots actually installed in the torque meter resulted in a combined spring rate of about 14 gm-cm/degree. Thus the maximum rolling moment to be expected (10 gm-cm) would produce a roll deflection of less than 1 degree, a negligible disturbance to the wing roll attitude. The torque meter calibration is shown in Figure 10.

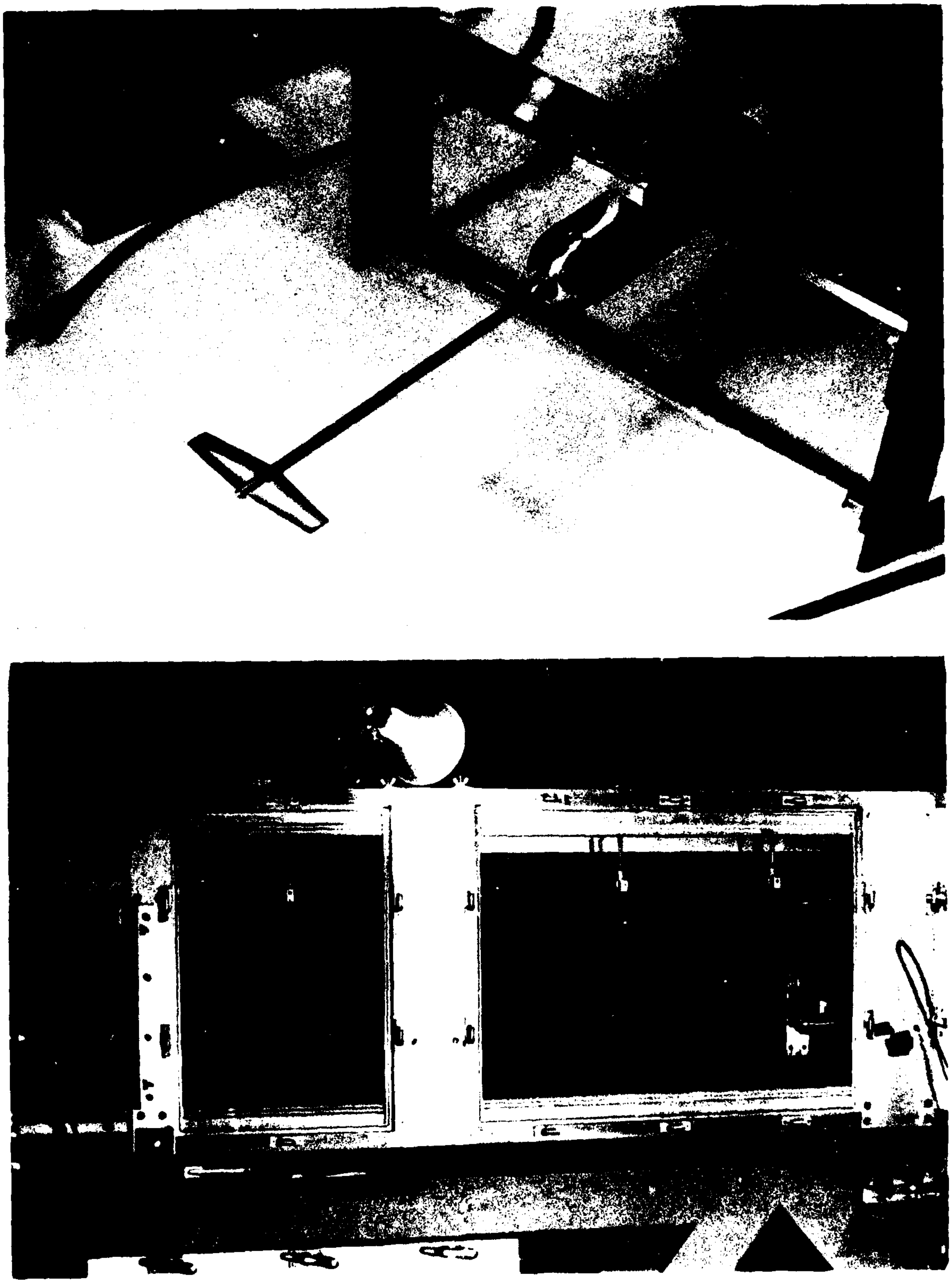

Figure 9. (Top) The T-2 wing model and torque meter mounted in the traversing mechanism. (Bottom) View of the wind tunnel showing the vortex generator airfoils at left and the torque meter in place at right.

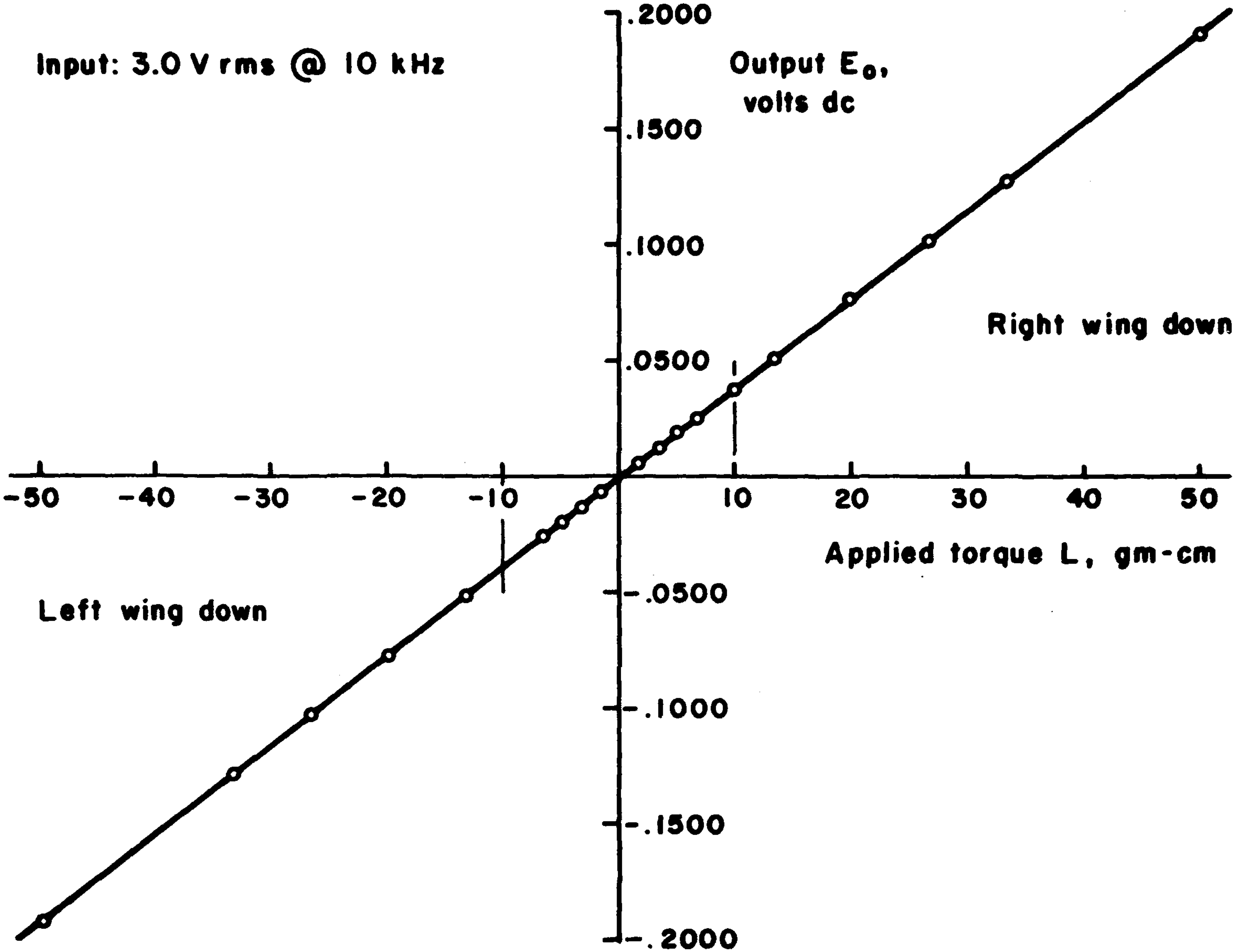

Figure 10. Torque meter calibration.

B. Procedure and Technique

To establish the proper wake flow field for these tests, it was first necessary to determine what vortex circulation strengh was needed and what conditions were required to produce it. For the full-scale flight test at 20,000-ft (6096-m) altitude and 220 kts (112 m/sec) the lift coefficient for a P-3 is $C_L = .88$ for a gross weight of 100,000 lbs (45,450 kg). The wind tunnel tests were scaled by adjusting the angle of attack of the vortex generator airfoils and the tunnel velocity to produce vortices equal in circulation strength Γ to those that would be produced by two hypothetical scale model P-3's. Assuming an elliptical loading for the P-3, the lift is

$$L = \frac{\pi}{4} \rho U \Gamma b$$

Substituting for L in the expression for lift coefficient

$$C_L = \frac{L}{\frac{1}{2} \rho U^2 S}$$

and rearranging, we have

$$\frac{\Gamma}{U} = \frac{2 C_L b}{\pi A}$$

where $A(=b^2/S)$ is the aspect ratio of the P-3 (A=7.5) and b is the wingspan of the hypothetical model P-3 scaled the same as the T-2 model. This latter value is $b = 19$ cm. For these conditions, then,

$$\frac{\Gamma}{U} = .0142 \text{ meter}$$

To find the proper settings of vortex generator angle of attack and tunnel speed to match this value, it was first necessary to calibrate the vortex generator system. This was accomplished by deducing the circulation strength Γ by measuring the mutual rotation induced on each other by a pair of like-sign and equal-strength vortices between two points downstream of the vortex generators. For one vortex of a parallel pair, the circulation Γ

can be shown to be

$$\Gamma = \frac{\pi^2 d^2 U}{x_{180}}$$

where d is the spacing of the pair, U is the stream velocity, and x_{180} is the distance downstream required to produce a rotation of 180 degrees. Using smoke for flow visualization, a series of photographs was taken showing cross-sections of like-sign vortex pairs at three distances downstream of the vortex generators. The initial spacing was the same as that to be used in the wake penetration tests. To minimize Reynolds number effects, the tunnel was run at its maximum speed of 13.7 m/sec. The angles of induced rotation and the spacing were then measured on the photographs and the values of Γ calculated. These values are plotted in Figure 11. The excellent agreement between the points based on the two axial intervals is taken to mean that the degree of vortex roll-up changed very little downstream of $x = .38$ m . It is thus assumed that roll-up was in fact complete at $x = 1.01$ m , the location of the T-2 wing model during the rolling moment measurements. From the Γ calibration, it is seen that the vortex generators should be set at an angle of attack of 3.2° to produce the desired scaling of Γ .

The remaining geometric specification needed for the tests was the vertical reference for location of the T-2 wing relative to the vortices. This was easily determined from smoke pictures at the proper axial location with the vortex generators set at the proper angle. The location was confirmed by again observing the smoke flow with the wing in position for a coaxial encounter. It is interesting to note that the latter observation showed the vortex flow to be quite steady around the wing model with no evidence of disturbance created by the model or its mounting sting.

Two additional factors which might be expected to affect the rolling moment measurements are the distribution of angular momentum in the vortex, as characterized by its tangential velocity profile, and the Reynolds number. Both of these factors were investigated in a limited way.

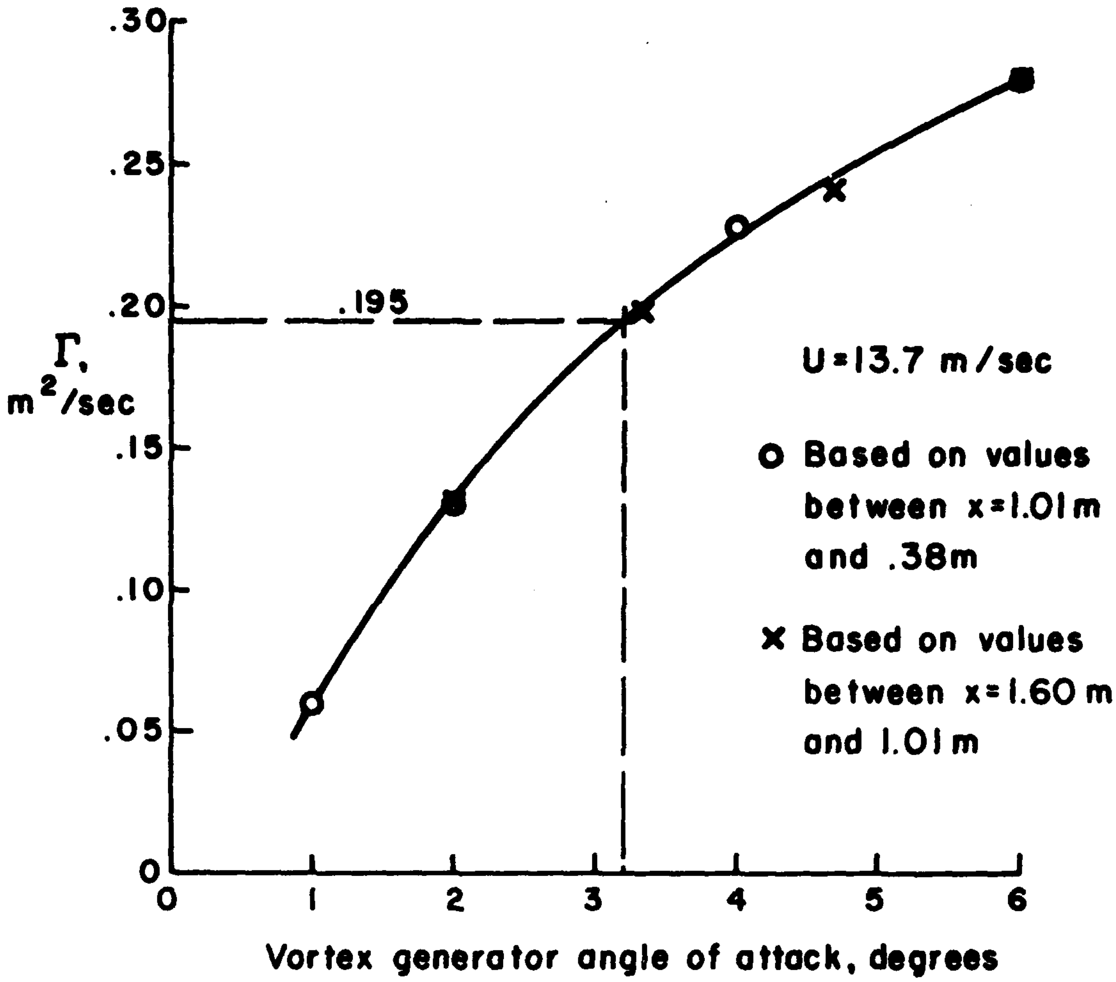

Figure 11. Calibration of vortex generator system.

Some idea of the tangential velocity profile was gained by holding a rake of sensitive tufts across the flow just upstream of the wing. The tufts were spaced at intervals of .48 cm (3/16 in.). It was observed that two adjacent tufts deflected in opposite directions indicating that the maximum tangential velocity occurred at a radius of no greater than .24 cm. The implied core diameter of no more than .48 cm (3/16 in.) is consistent with the observed smoke concentrations which imply a core diameter no larger than about .5 cm. It is estimated very roughly that the deflection angle of the adjacent tufts did not exceed about 8°. Thus the tangential velocity at that location probably did not exceed 13.7 tan 8° = 1.9 m/sec. For purposes of judging the relative scale of such a vortex, in Figure 12 is plotted a simple Betz-type profile based on the measured $\Gamma = .195\ m^2/sec$ and the elliptically loaded wing of the hypothetical scale model P-3 generator aircraft (b = .19m). Also shown are a potential vortex of the same strength, a point denoting the velocity estimate based on the tuft deflection, and the semispan of the T-2 wing drawn to the same scale. The conclusion that may be drawn from this plot is that the fluid velocity at one point is below that of the assumed vortex from the P-3. This point, however, is near the viscous core region of the vortex, and since no viscous effects are accounted for in the Betz model, the lower value would be expected.

To assess the possible effects of conducting these tests at low Reynolds numbers, the rolling moment coefficient C_ℓ was evaluated for a coaxial encounter for three tunnel speeds, 10.6, 12.2, and 13.7 m/sec. These speeds correspond to Reynolds numbers based on the T-2 model mean chord of 9,500, 10,900, and 12,300, respectively. Unfortunately, only this limited range was available with the existing vortex generators and wind tunnel. The greatest difference occurred when the value of C_ℓ at Re = 12,300 was found to be 7% below the value at Re = 9,500, a not too significant amount. This is within the range of expected experimental accuracy of these tests. Perhaps of more interest was an investigation of earlier airfoil testing at low Reynolds numbers which brought to light some useful data. Insofar

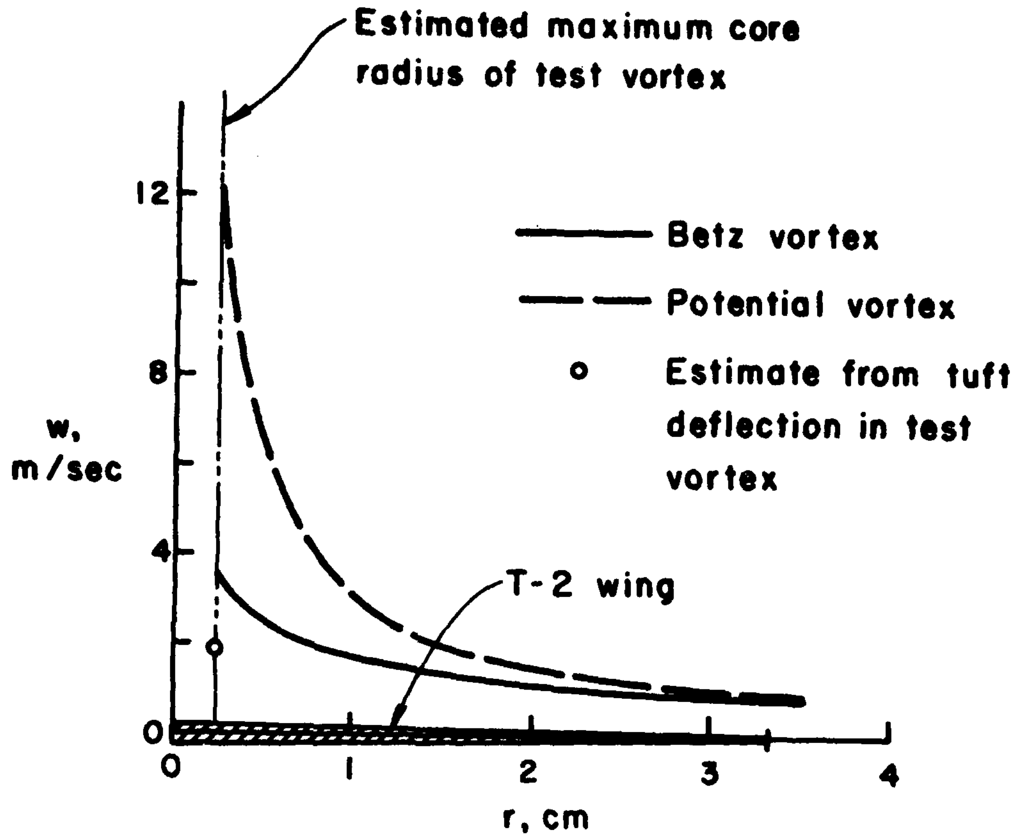

Figure 12. Comparison of illustrative vortex profiles and estimate from tuft deflection.

as rolling moment calculations are concerned, two parameters are of importance which are affected by Reynolds number. These are the section lift-curve slope and the value of $C_{L_{max}}$, the maximum lift coefficient. In Ref. 3 data for a number of thin airfoils are reported at Reynolds numbers as low as 42,000. The principal trend as Reynolds number is reduced is that $C_{L_{max}}$ is also reduced. For thin airfoils, the two-dimensional lift-curve slope changes very little down to $Re = 42{,}000$, remaining at approximately .1 per degree. At this value, the maximum angle of attack obtainable prior to stall is still above 10°. Additional data at still lower Reynolds numbers were found in a report (Ref. 4) on the testing of small paper gliders. In this case, the Reynolds number was 23,000 and the airfoils included a flat plate, several stepped wedges, an NACA 0012, and a circular arc. All had an aspect ratio of 3. The lift curve slopes were all similar, being approximately .05 per degree. This value is the result of the low aspect ratio and the reduced Reynolds number. The value of $C_{L_{max}}$ still occurred at angles of attack above 10°. The implication of these data seems to be that at least down to Reynolds numbers of about 20,000 the section characteristics contributing to rolling moment should remain valid as long as the local vortex-induced angle of attack does not exceed 10° and as long as the actual three-dimensional lift-curve slope can be approximated. Of course, even if the local angle of attack does exceed 10° for a portion of the encountered vortex profile, the over-all effect on rolling moment may not be large because of the small lateral extent of that portion.

To explore any further effect that might occur at $Re = 12{,}300$, the T-2 wing model itself was remounted in such a way that the torque meter registered lift. The wing angle of attack was made adjustable so that a lift curve could be determined. The resulting data are plotted in Figure 13. It is seen that there is a discontinuity in the curve, with two values of $C_{L_{max}}$ being required to give the best fit of the data. However, a single value of $C_{L_\alpha} = .05$ gives a reasonable approximation - within about 13% - for all the data. A check for the effect of aspect

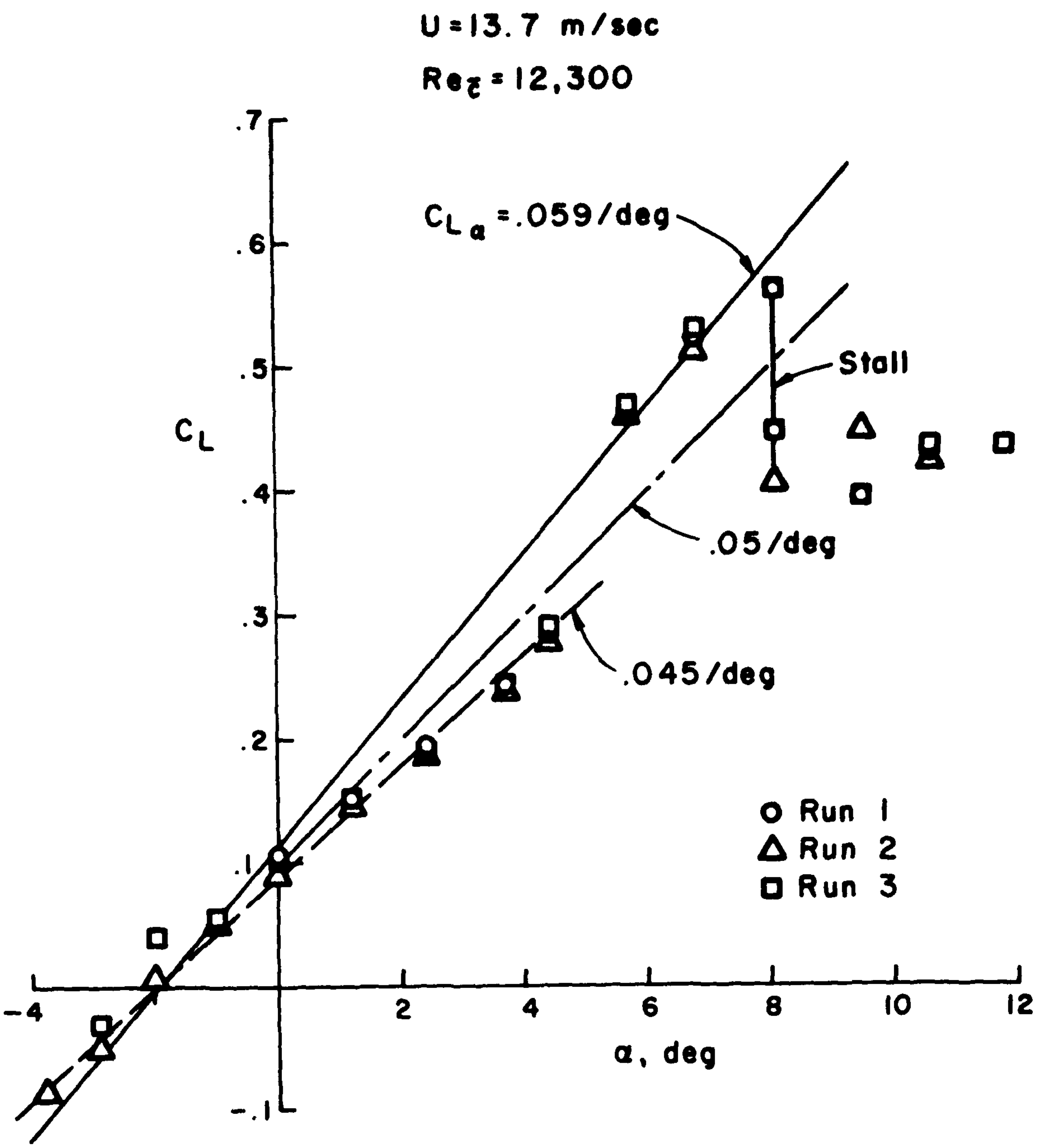

Figure 13. Measured lift curve of T-2 wing model.

ratio on C_{L_α} can be made using the method of Ref. 5. If a sectional value of .1 per degree is assumed, and with $A = 5.07$ for the T-2 wing, a three-dimensional value of .07 results. Thus it appears that a significant portion of the reduction in C_{L_α} can be accounted for by three-dimensional effects.

The measurement of the model lift-curve slope made it possible to compare the experimental C_ℓ values with the results of a computation run based on the conditions of the model tests. Reasonable agreement in such a comparison would support the validity of the computation method when applied to the full-scale case. For this purpose, a computation was made to simulate lateral traverses through the flow field of the vortex pair at two vertical locations. A lift curve slope of .05 per degree was used as shown in Figure 13 with stall occurring at an angle of attack of 8°. A constant value $C_L = .43$ was used above 8°. The comparison for these cases is shown in Figure 14, where the data are taken from those to be presented in the next section. The abscissa in this figure is the lateral position y in the flow made nondimensional by the wingspan b of the T-2. It is seen that the agreement is reasonable, with the computations, as expected, exceeding the measurements by approximately 20%. In view of this, it is concluded that the computation method should give reliable results when applied to the full-scale test case. It is also concluded that the vortex velocity profile in the wind tunnel test must have been reasonably similar to that used for the computation.

C. Results and Comparison with Computations

The torque meter was used to measure the rolling moment coefficient C_ℓ of the model T-2 wing at a number of points in a cross-plane of the vortex flow field. Two cases were investigated, one with the wing horizontal ($\phi=0°$) and one with the wing vertical ($\phi=90°$). The rolling moment was induced in the former case by vertical velocity components and in the latter case by horizontal velocity components. The test grids showing the locations at which C_ℓ was measured are shown in Figures 15 and 16. In both cases sufficient points were used to permit the mapping of

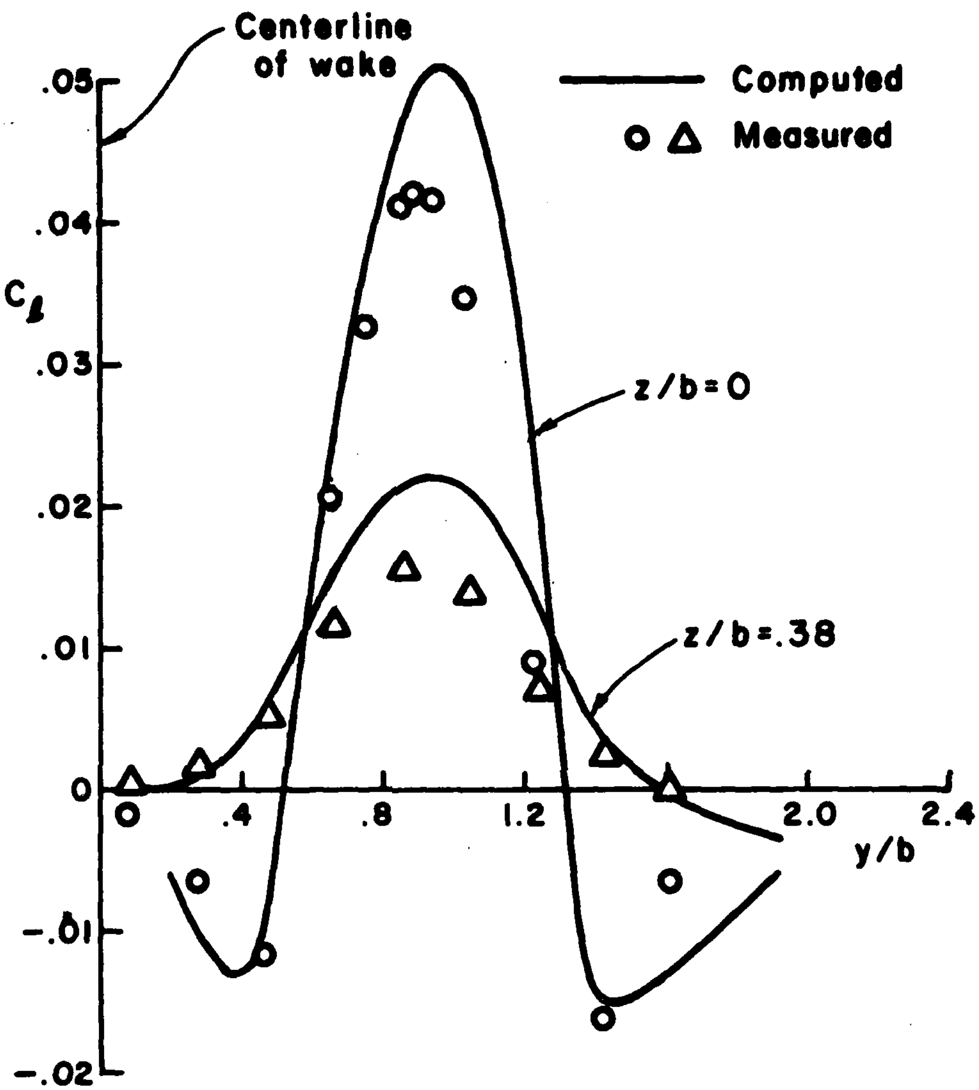

Figure 14. Comparison of computed and measured C_ℓ distributions for model tests of T-2 wing.

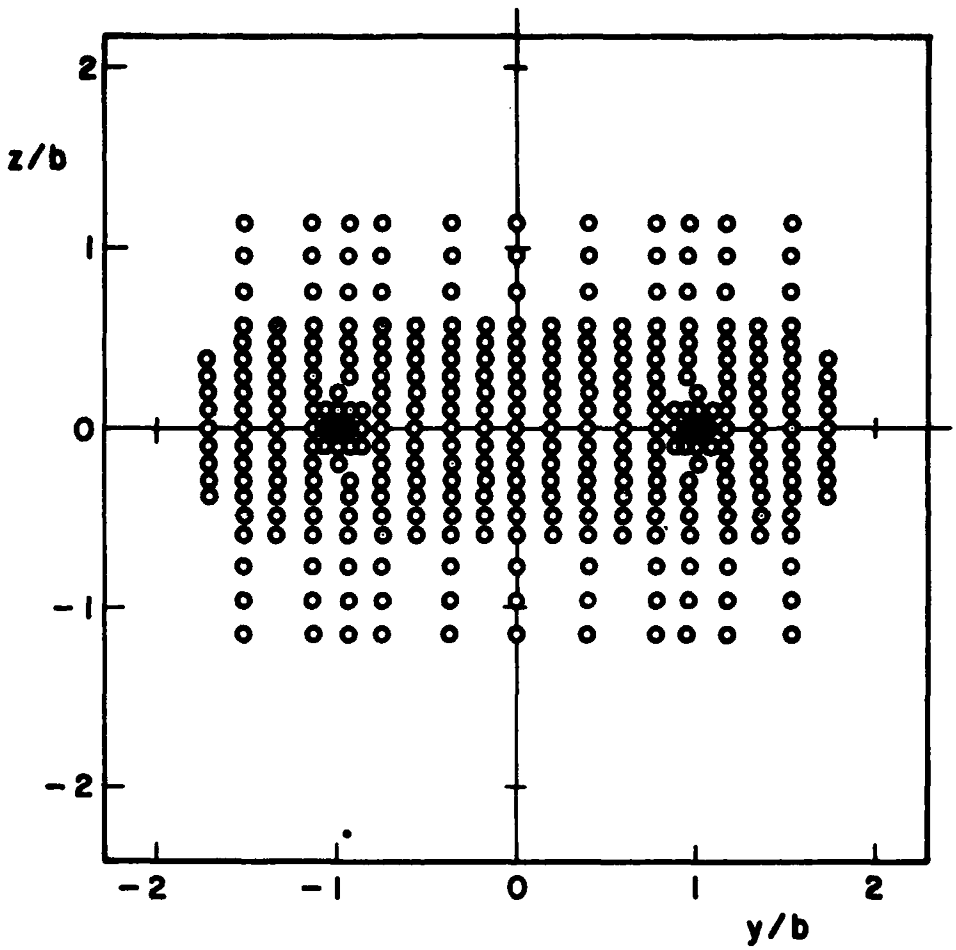

Figure 15. Test grid for measurements of rolling moment with wing horizontal (ϕ=0°).

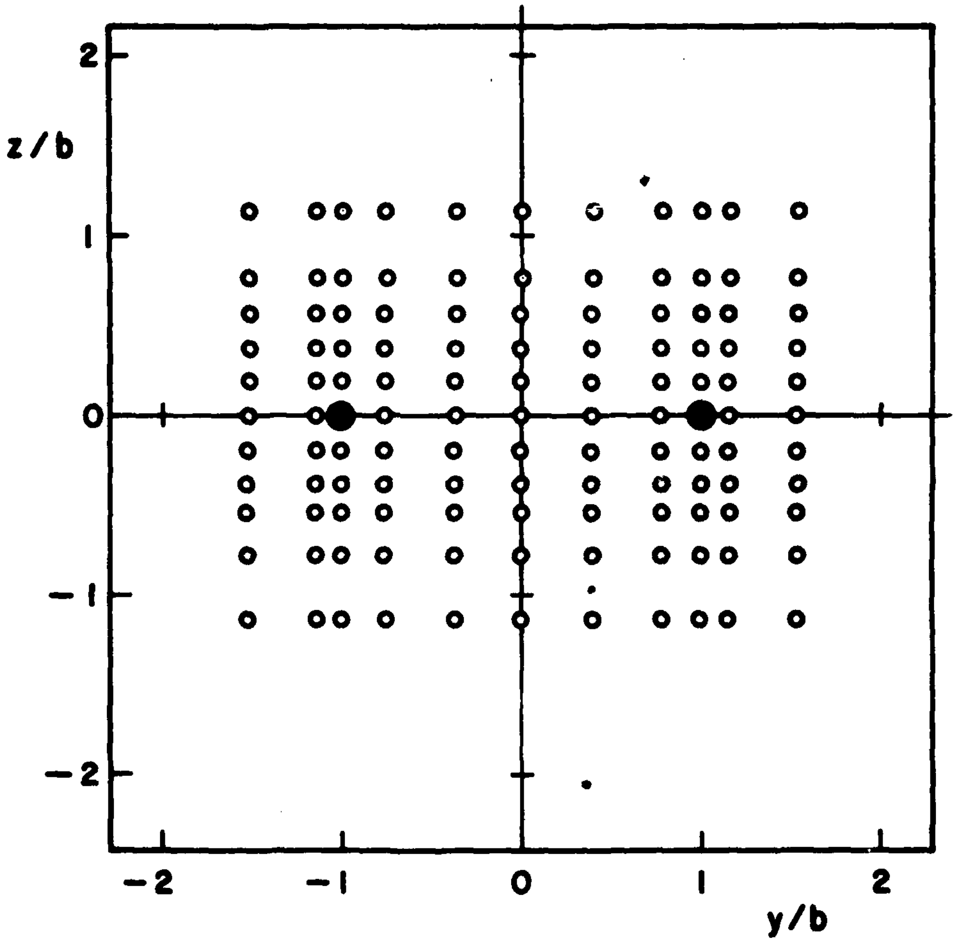

Figure 16. Test grid for measurements of rolling moment with wing vertical (ϕ=90°).

the wake field in isopleths of constant C_ℓ, with somewhat more detail possible for $\phi = 0°$. The measurements were all made at an axial location $x = 1.01$ m downstream of the vortex generators and with a tunnel speed $U_\infty = 13.7$ m/sec.

Plots of the measured lateral distributions of C_ℓ are presented in Figures 17 and 18 for $\phi = 0°$ and $90°$, respectively. For $\phi = 0°$ there are 19 vertical locations z/b, and for $\phi = 90°$ there are 11. The data show that the wind tunnel flow field had reasonable symmetry and that the magnitudes of induced C_ℓ are about the same for both vortices. In Figure 17 it is seen that a lateral traverse through the vortex centers ($z/b=0$) involves five reversals of C_ℓ. For $|z/b| > .5$ a lateral traverse involves only one reversal. With the wings vertical ($\phi=90°$), it is seen in Figure 18 that a lateral traverse at $z/b = 0$ also involves only one reversal, while farther above and below the plane of the vortices the response is more complex. In particular, a vertical traverse through one of the vortices results, as might be expected, in two reversals. The situation is more readily appreciated by an examination of isopleth plots which portray the measured rolling moments as contours of constant value. Isopleths for the $\phi = 0°$ and $\phi = 90°$ cases are shown in Figures 19 and 20. It is seen that for $\phi = 0°$, the region of five reversals is confined to small values of z/b. In the $\phi = 90°$ case, there are small regions above and below the plane of the vortices where reversals occur. (Due to slight asymmetry in the measurements, the region of negative C_ℓ below the $y/b = +1$ vortex was not resolved on this plot.)

Comparisons of measured C_ℓ distributions with computed distributions for the full-scale encounter are shown in Figures 21 and 22, for $\phi = 0°$ and $\phi = 90°$, respectively. Two vertical locations are represented, one through the plane of the vortices, and one displaced above the vortices.

The comparisons all show that the computation defines the lateral distribution of rolling moment quite well, with positive and negative peaks matching the measurements. The general agreement in shape of the distributions is also indicative of a similarity in response to the vortex velocity profiles encountered.

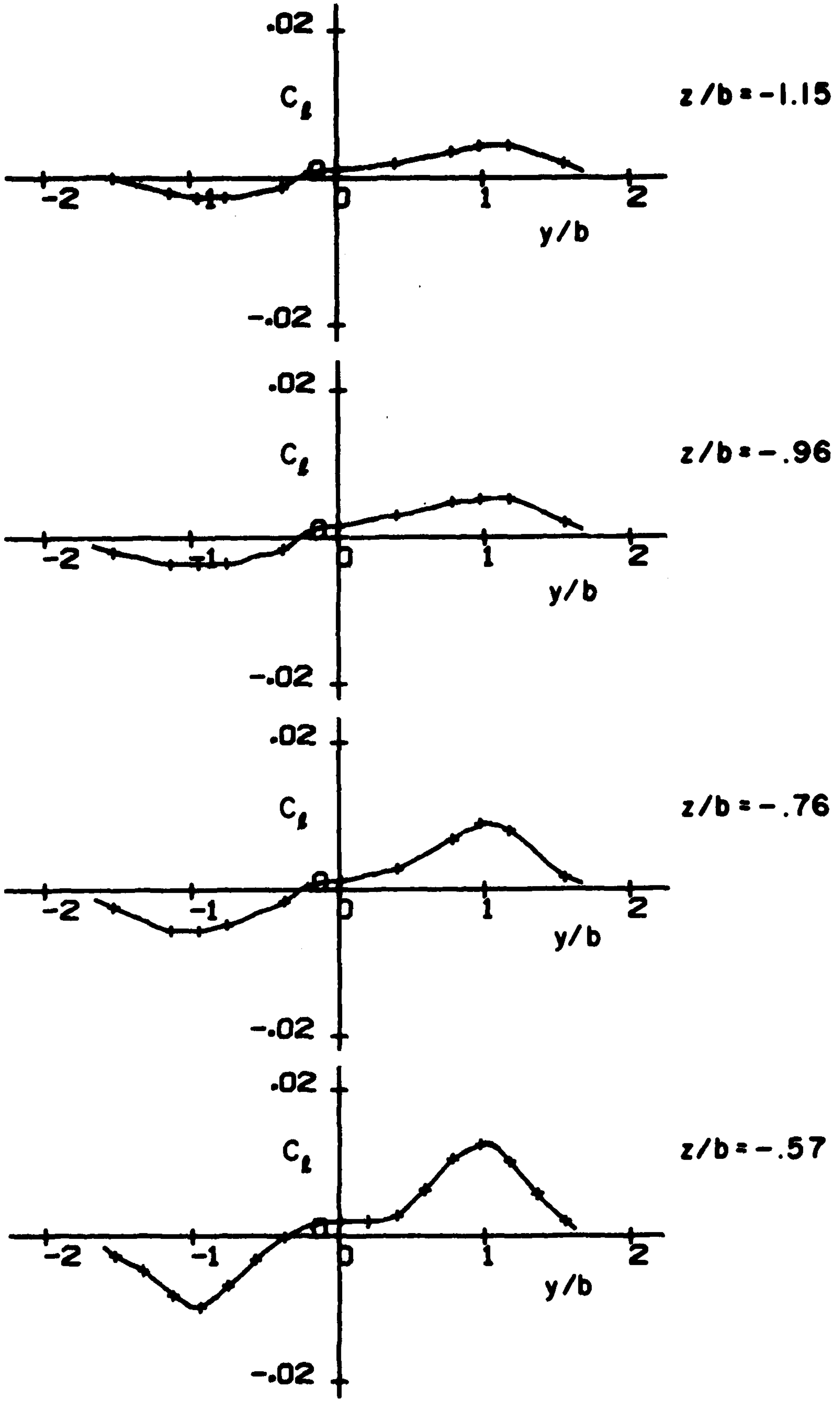

Figure 17. Measured lateral profiles of rolling moment coefficient for the T-2 model wing at $\phi = 0°$ for several vertical locations z/b .

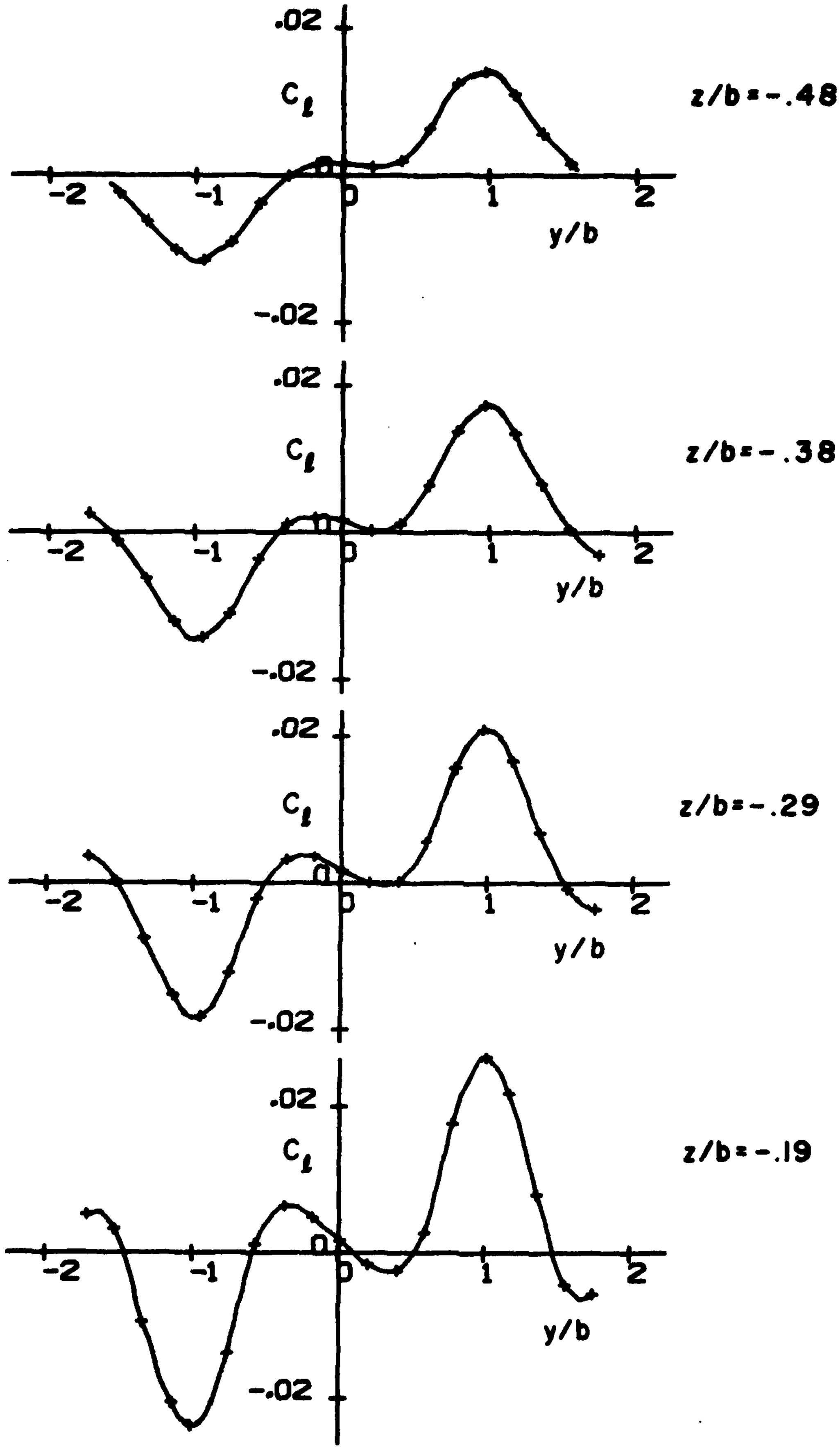

Figure 17. (cont.)

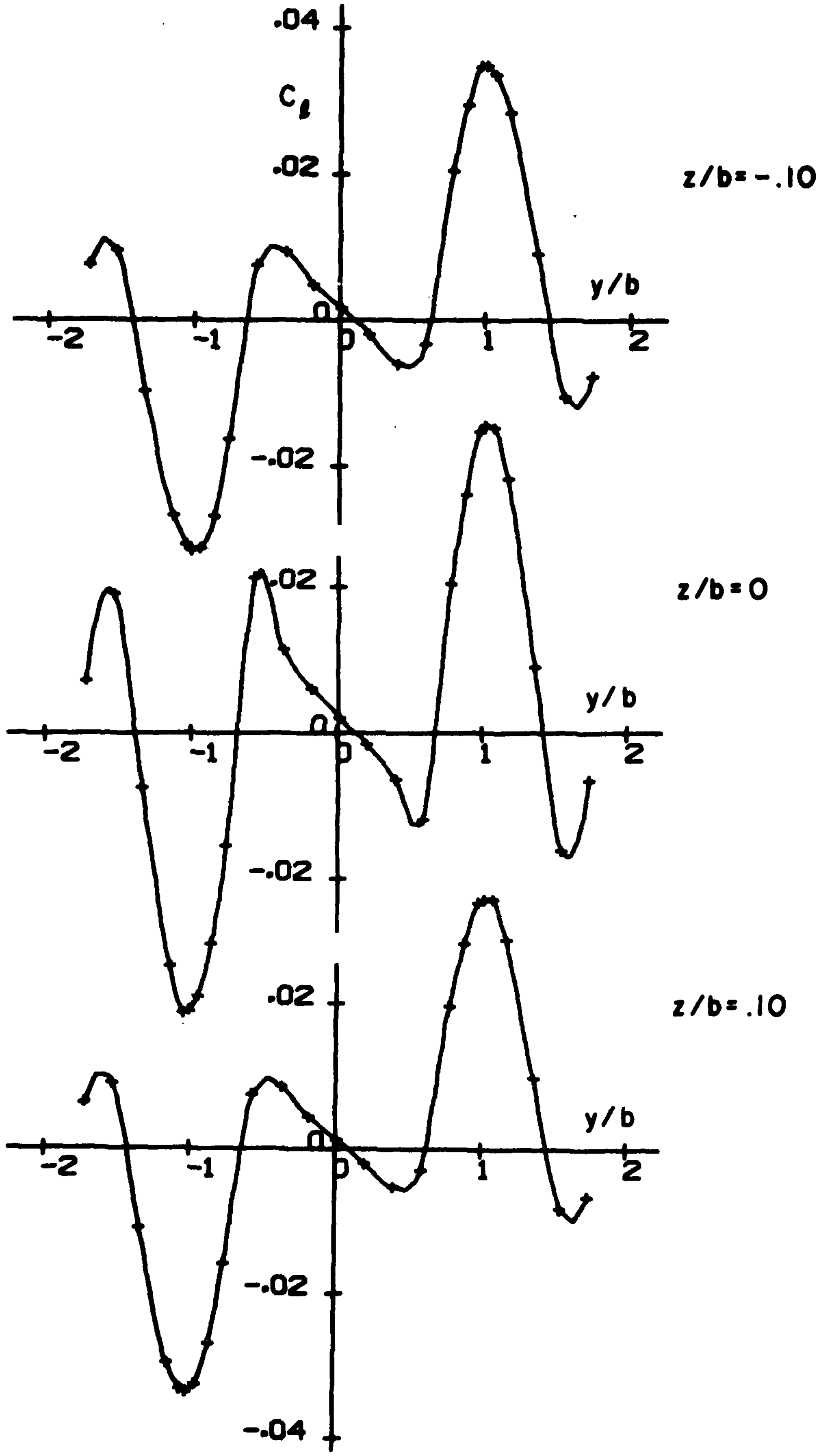

Figure 17. (cont.)

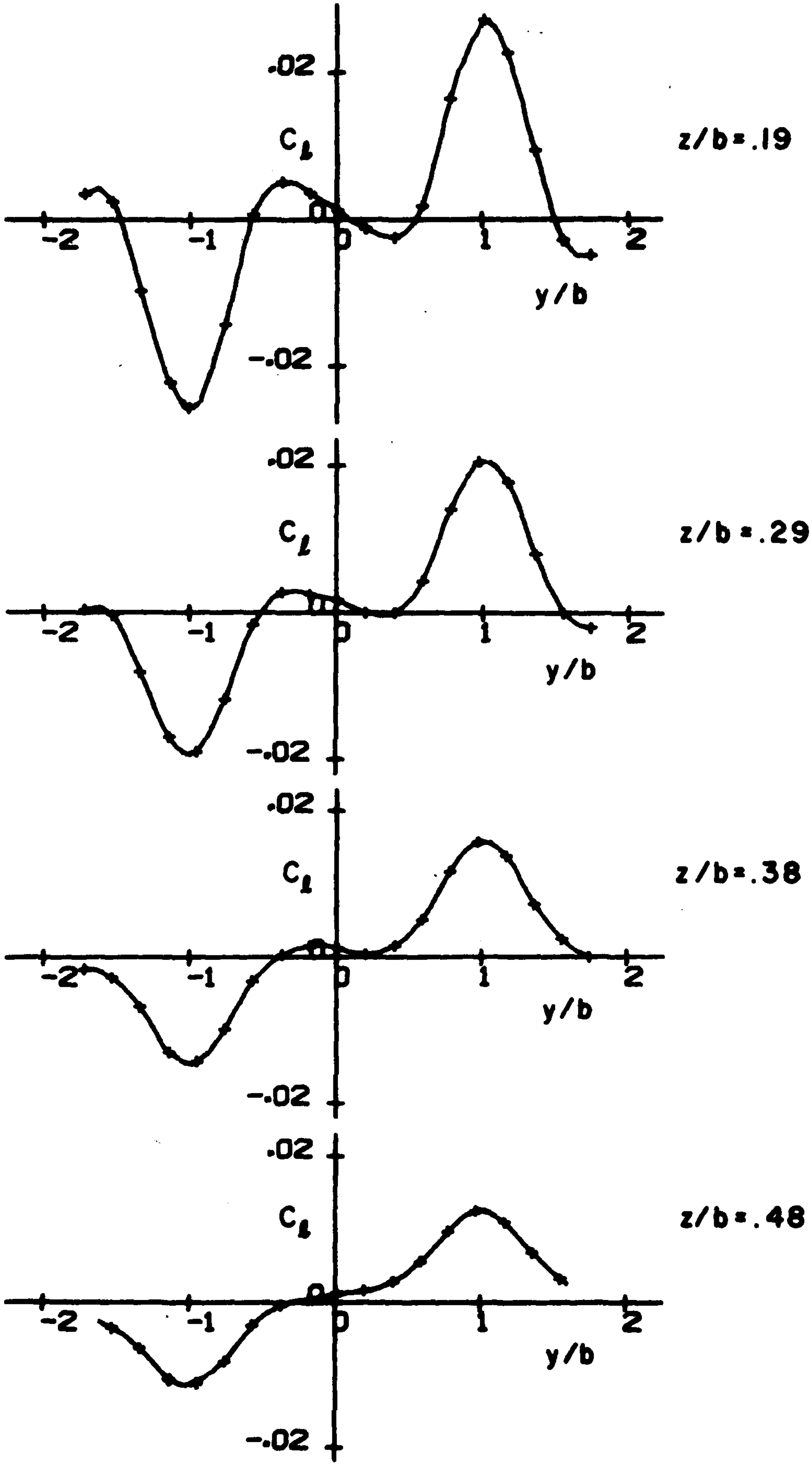

Figure 17. (cont.)

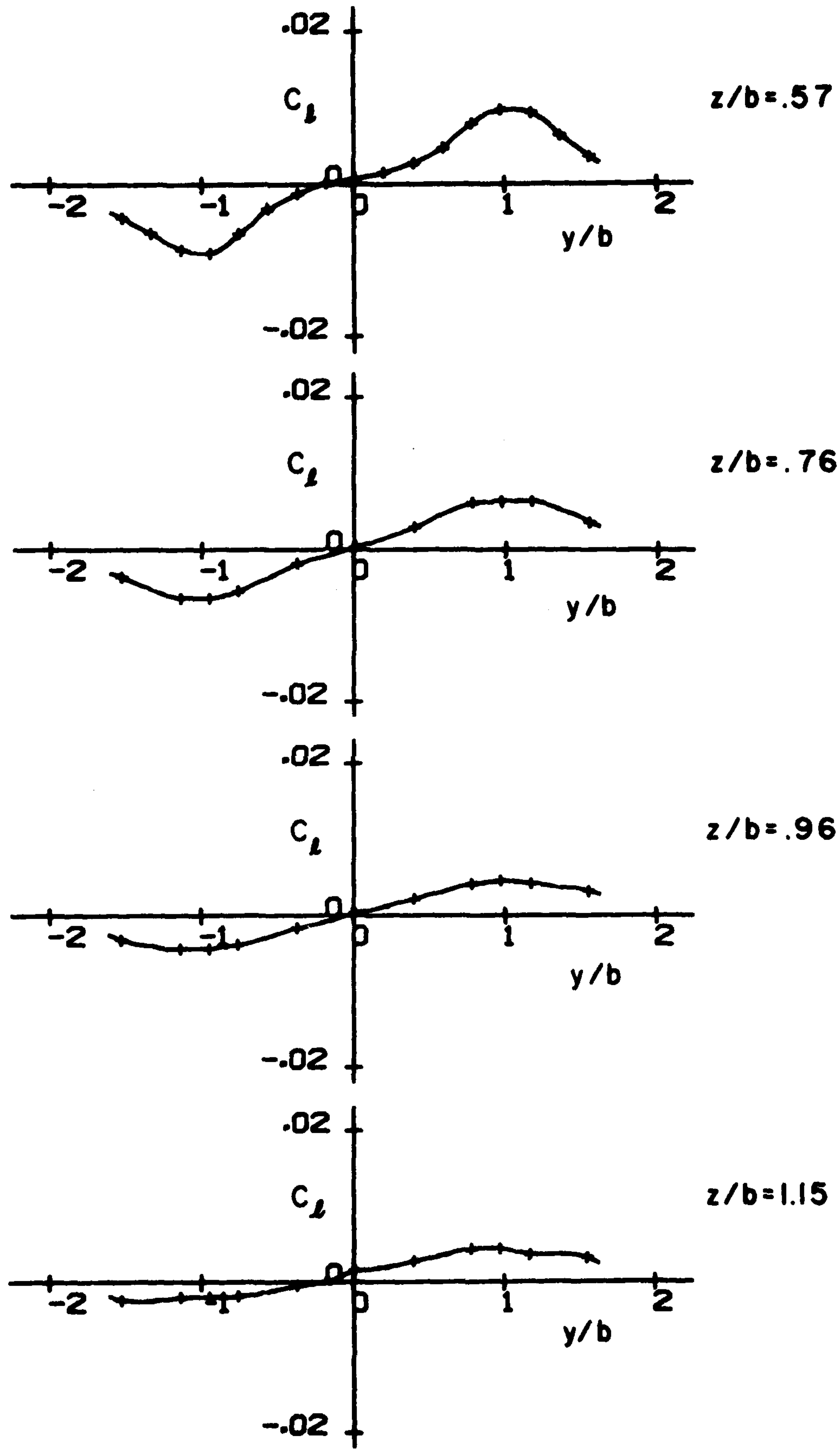

Figure 17. (concluded)

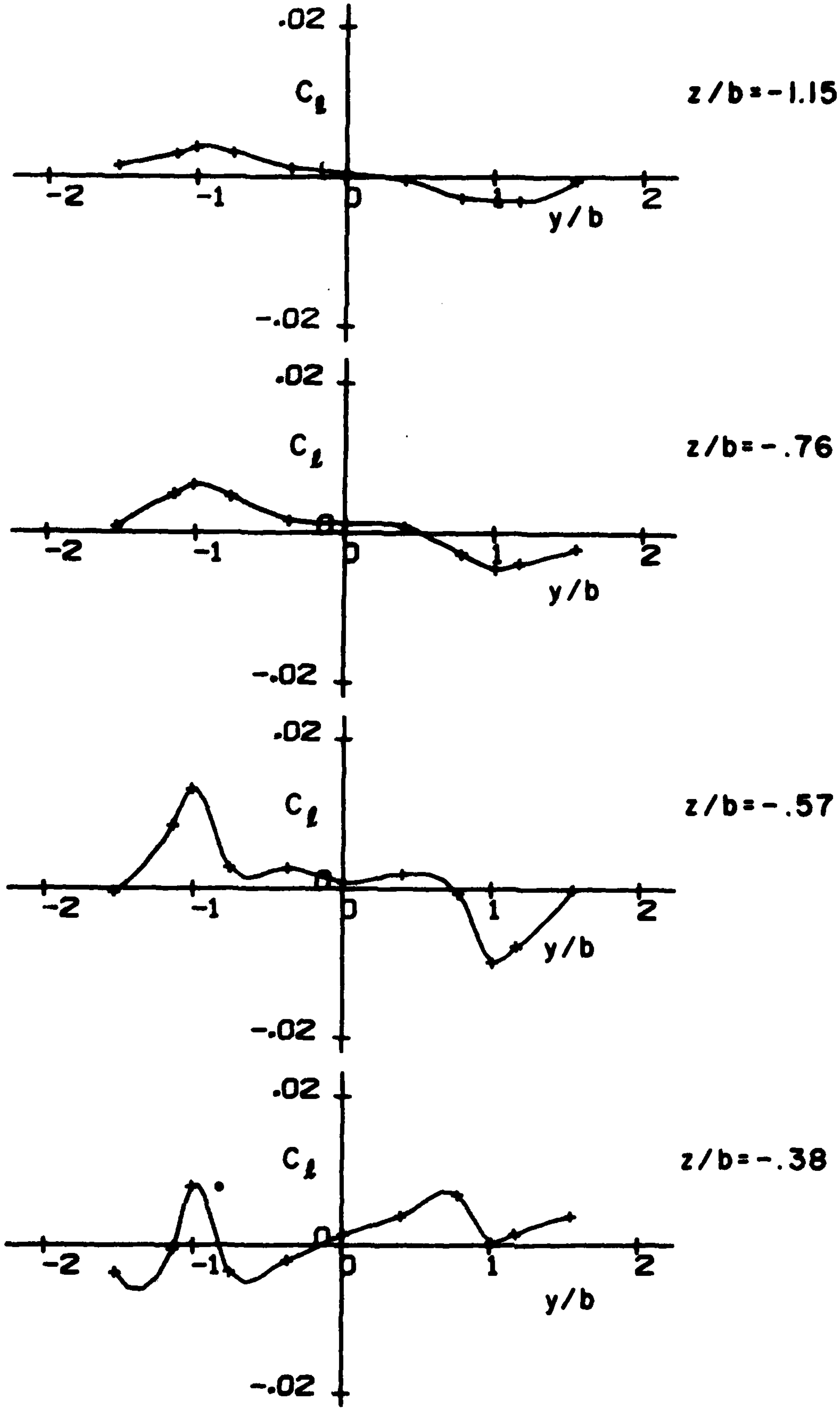

Figure 18. Measured lateral profiles of rolling moment coefficient for the T-2 model wing at $\phi = 90°$ for several vertical locations z/b .

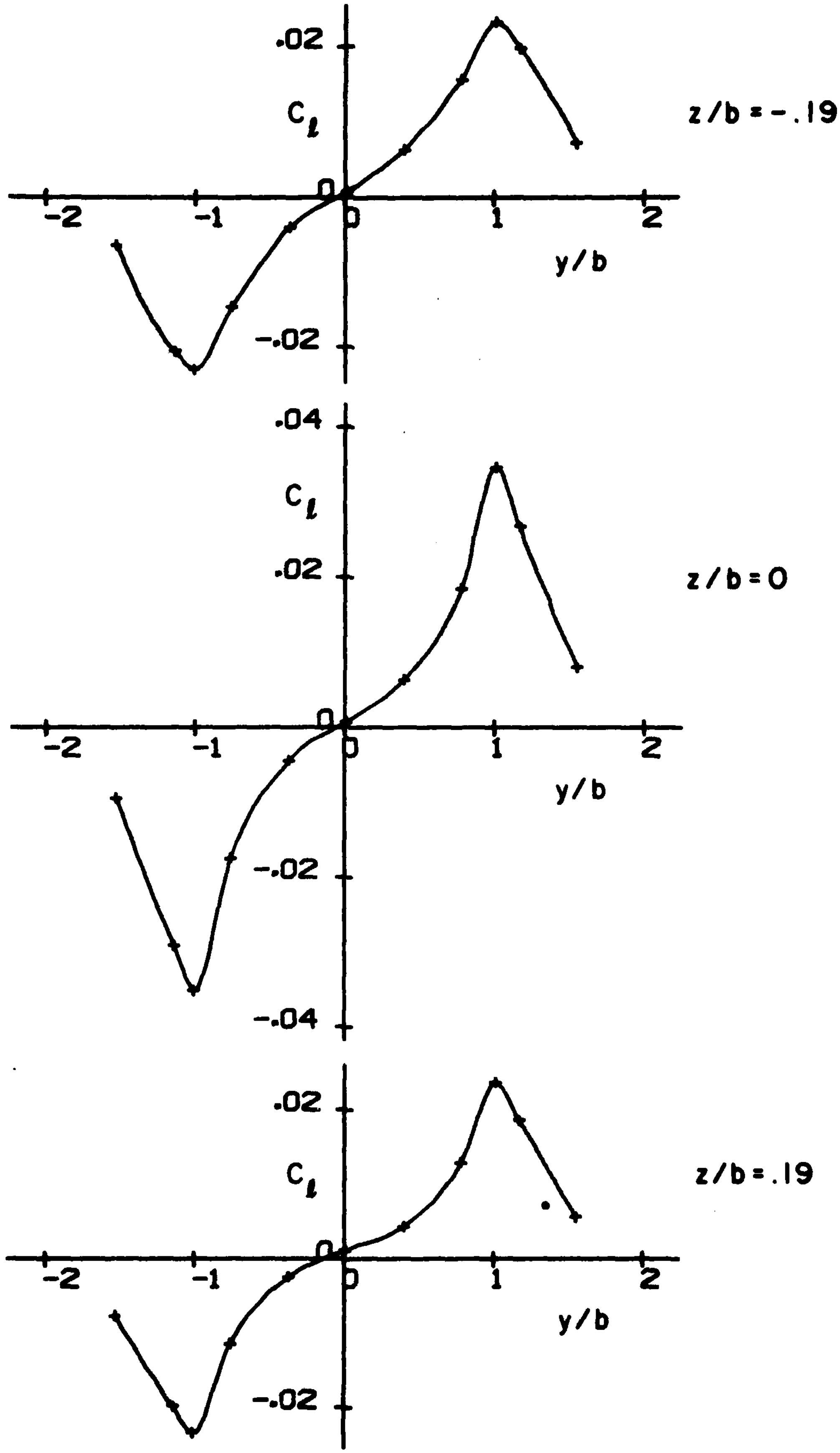

Figure 18. (cont.)

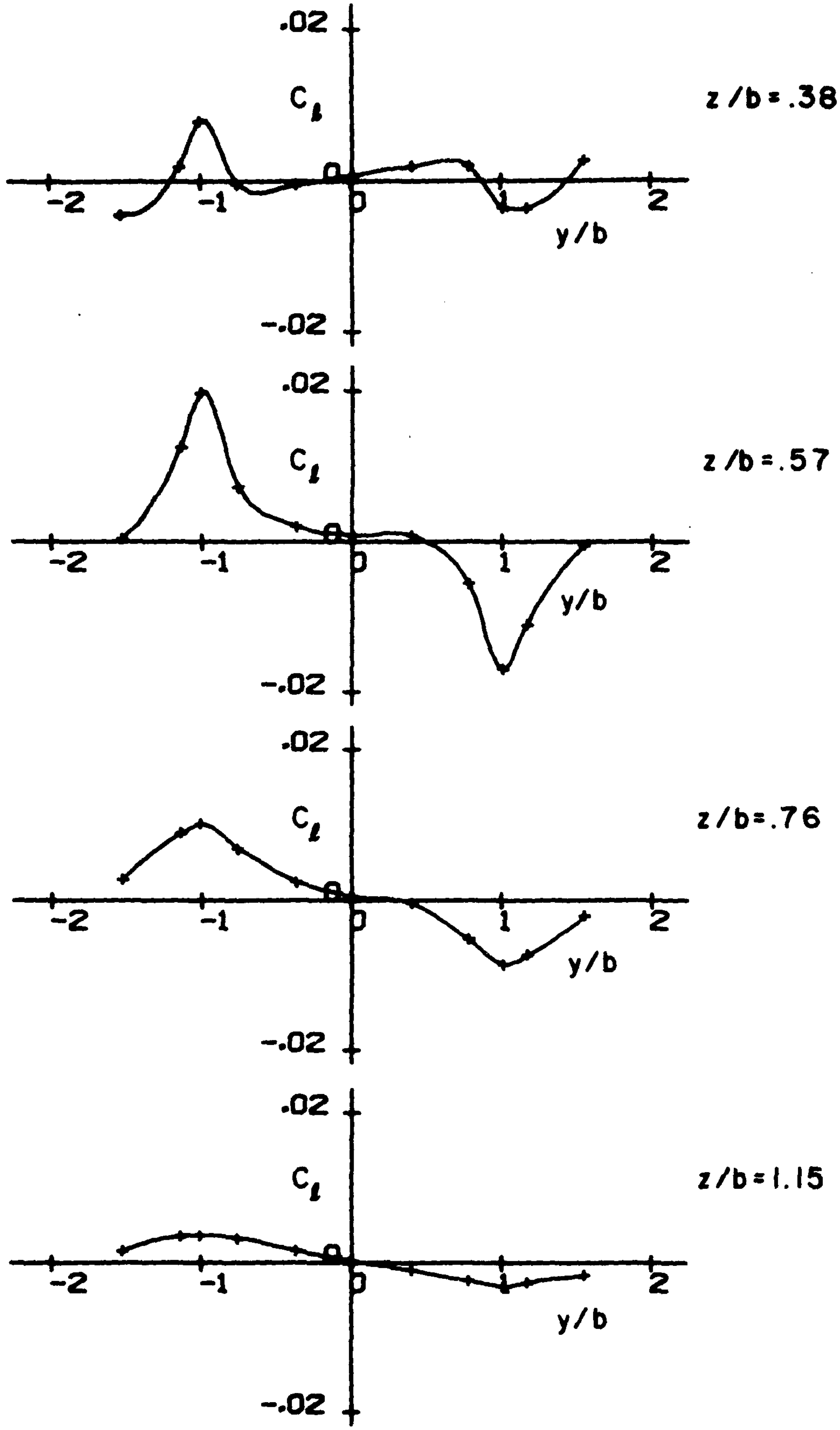

Figure 18. (concluded)

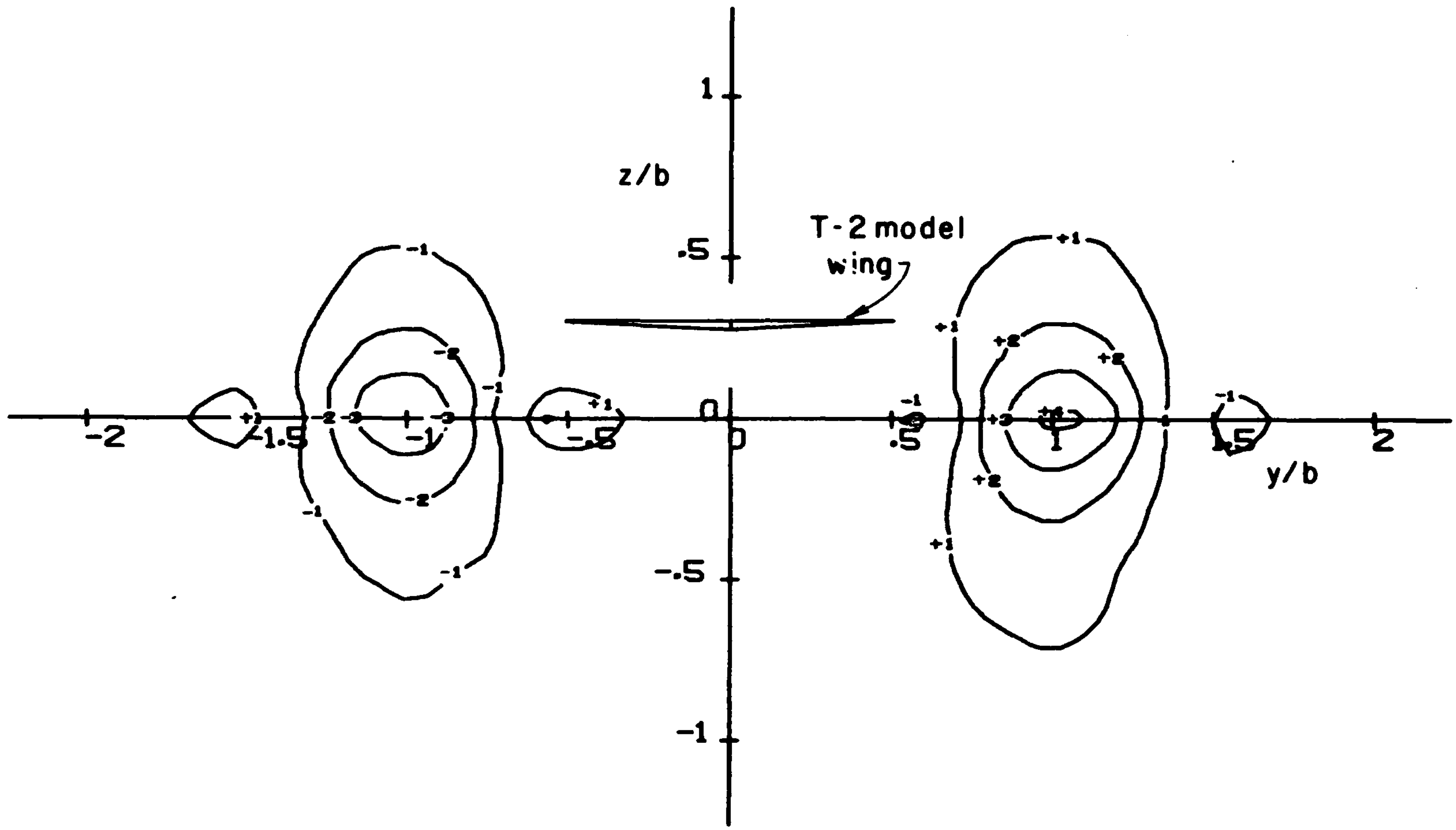

Figure 19. Measured isopleths of constant C_ℓ for the T-2 model wing with $\phi = 0°$. The numerals denote values of C_ℓ in hundredths.

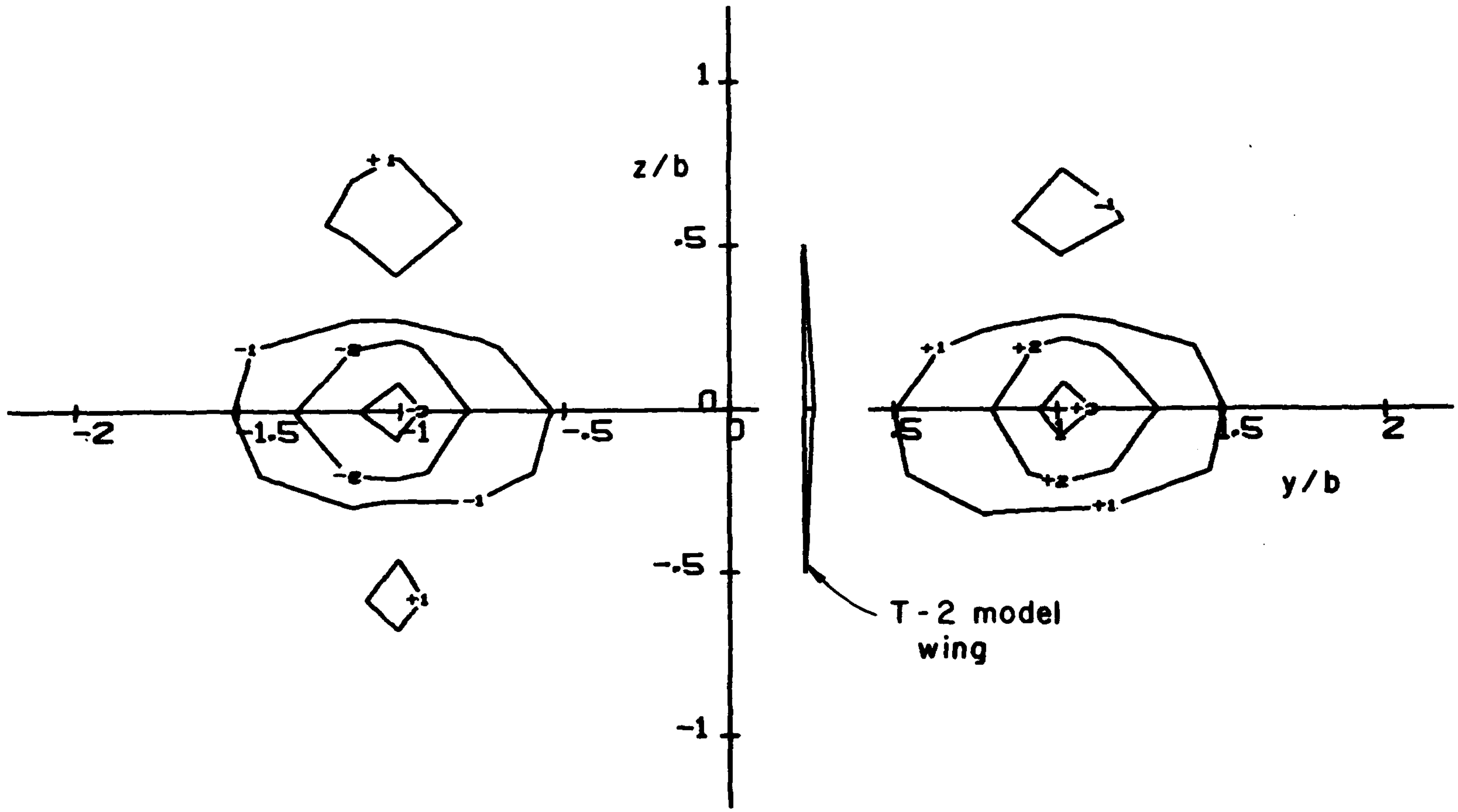

Figure 20. Measured isopleths of constant C_ℓ for the T-2 model wing with $\phi = 90°$. The numerals denote values of C_ℓ in hundredths.

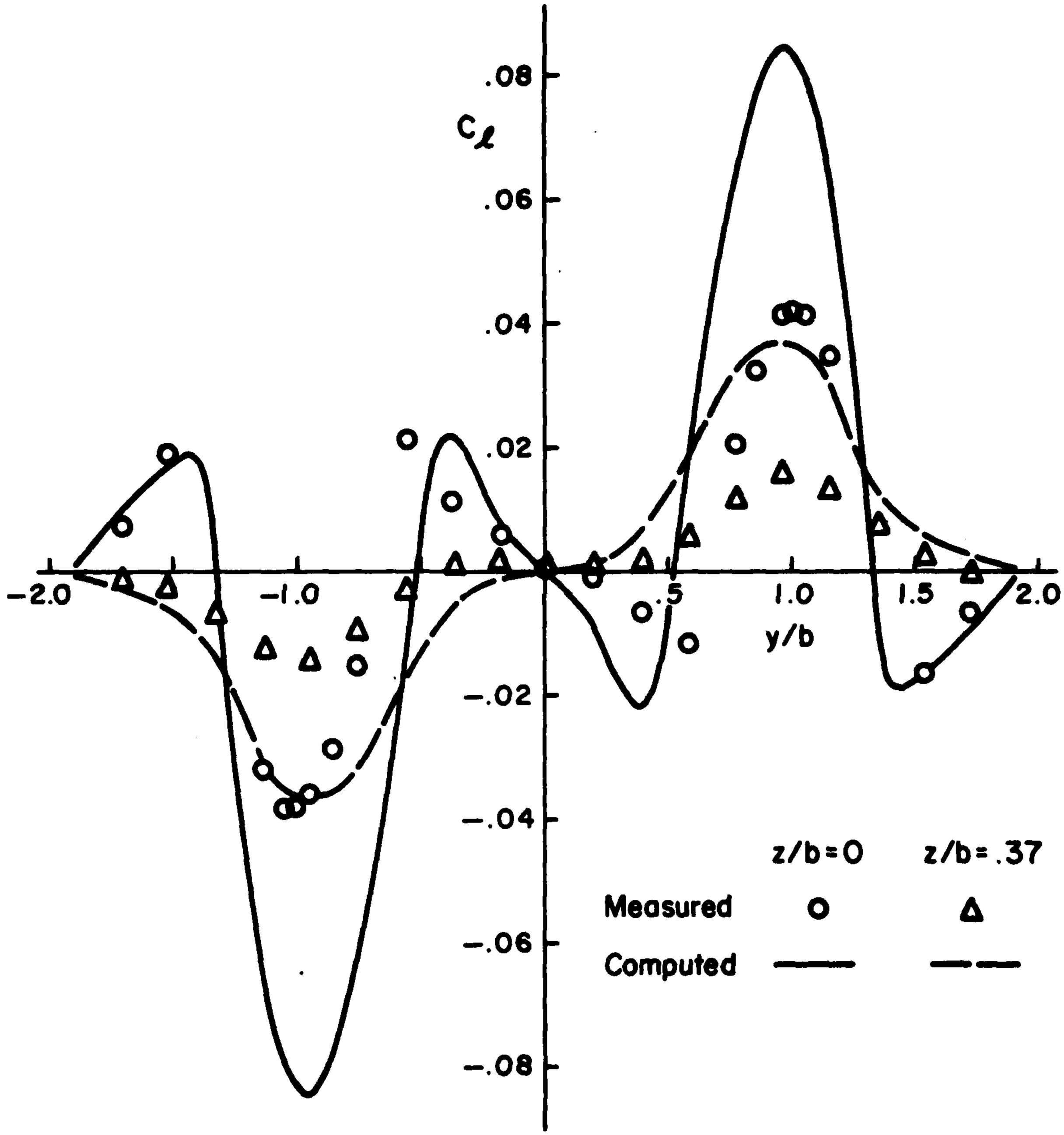

Figure 21. Comparisons of measured values of C_ℓ for the T-2 model wing with computed values for a full-scale encounter. $\phi = 0°$.

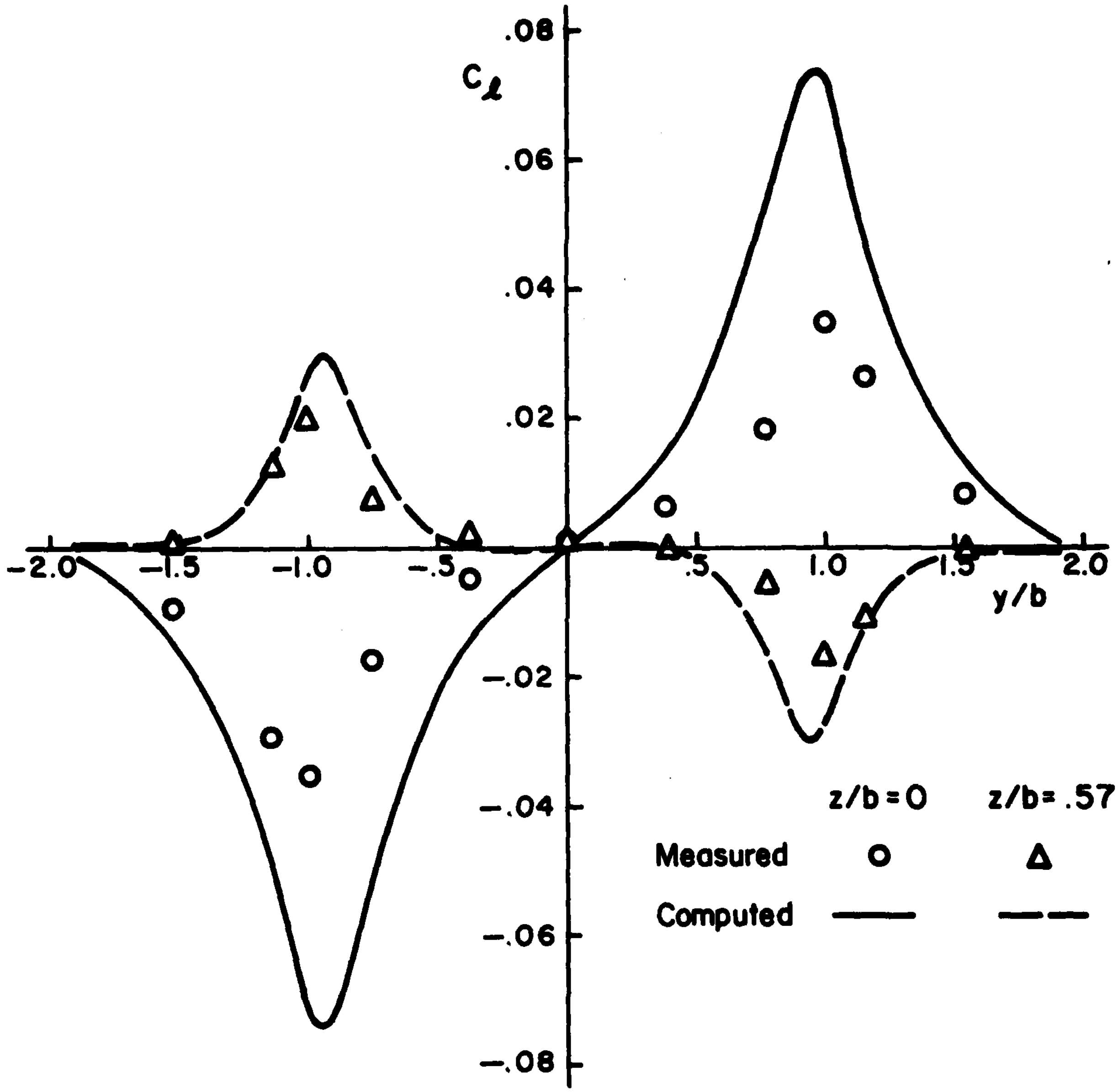

Figure 22. Comparisons of measured values of C_ℓ for the T-2 model wing with computed values for a full-scale encounter. $\phi = 90^\circ$.

In the computation, of course, the profile was that to be expected for an elliptically loaded P-3 wing, whereas for the model tests the profile was that actually produced by the vortex generators in the wind tunnel. In both cases, the vortex cores were small in comparison to the T-2 wingspan and the total circulation was scaled by matching C_L of the generators. No comparison of the detailed shapes of the rest of the vortex profiles was possible, but the similar response indicates that they must have been similar. It is felt that as long as the circulation is scaled and the core size is small compared with the wingspan of the encountering aircraft, any slight differences in the velocity profiles from a generator aircraft in a clean configuration will have only secondary effects on induced rolling moments.

Referring again to the comparisons shown in Figures 21 and 22, it is seen that the principal rolling moment peaks exceed the measured values by as much as 100%. To understand the meaning of this difference in magnitude refer again to the computed and measured model data shown in Figure 14. In that case it was found that when the computation made use of a lift curve that was actually measured for the wing model, the agreement was reasonably good, with the computed peak values exceeding the measurements by about 20%. Since for the full-scale computation of Figures 21 and 22, an actual lift curve was also used - that of a full-scale T-2 based on flight tests - it appears that the difference between the computed full-scale results and the model measurements is traceable primarily to the lift curves themselves. For the model, a value of $C_{L_\alpha} = .05$/degree was used, whereas for the full-scale T-2, the value was $C_{L_\alpha} = .08$/degree. The values of $C_{L_{max}}$ occurred for the model and full-scale T-2 at 8° and 14°, respectively. As has already been discussed, the primary reason for the particular characteristics of the model lift curve is felt to be the low Reynolds number of the tests.

In view of the foregoing considerations, it is felt that the computational method is capable of predicting rolling moment coefficients with reasonable accuracy. Thus, the peak values shown in Figures 21 and 22 are felt to be representative of values that should be expected in full-scale encounters.

4. CALCULATION OF THE FORCES AND MOMENTS ON THE WAKE-RIDING AIRCRAFT

The forces and moments on the wake riding aircraft are calculated in nondimensional form by summing contributions due to the static aerodynamics, control deflections, and aircraft angular rates.

The contributions due to the angular rates are assumed proportional to the rates and not a function of α or β (the standard rotary derivative approach). The contributions due to control deflections are proportional to the deflection and a nonlinear function of α and β. Values of each control derivative are stored on a grid of α,β points in a computer file. The four values of the control derivative bracketing the desired α,β are obtained and the desired values found by two-dimensional linear interpolation.

The static aerodynamic coefficients are also nonlinear functions of α and β and are obtained in the same manner as the control derivatives. The values of α and β used in this process include the effect of the wake flow as calculated at the aircraft c.g.

$$\alpha_{CG} = \tan^{-1}\left(\frac{w_{inertial} + w_{w(CG)}}{U}\right)$$

$$\beta_{CG} = \tan^{-1}\left(\frac{v_{inertial} + v_{w(CG)}}{U}\right)$$

In addition to this wake effect on the static aerodynamic coefficients, there is also the spanwise nonuniform flow effect. This is evaluated using strip theory. The incremental wing section axial and normal force coefficients on the i^{th} section of the wing, c_{x_i} and c_{z_i}, are given in terms of angle of attack, α_i, and local section area, S_i. They are

$$\alpha_i = \tan^{-1} \frac{w_i}{U}$$

$$c_{x_i} = f_x(\alpha_i)S_i/S_w$$

$$c_{z_i} = f_z(\alpha_i)S_i/S_w$$

The functions f_x , f_z are piecewise linear representations of the three-dimensional normal and axial force data from Ref. 6 for $\beta = 0°$.

These incremental coefficients are then summed and added to four of the six static aerodynamic coefficients as shown below.

$$C_x = C_x(\alpha_{CG},\beta_{CG}) + \sum c_{x_i}$$

$$C_z = C_z(\alpha_{CG},\beta_{CG}) + \sum c_{z_i}$$

$$C_\ell = C_\ell(\alpha_{CG},\beta_{CG}) + \sum y_i c_{z_i}/b$$

$$C_n = C_n(\alpha_{CG} , \beta_{CG}) - \sum y_i c_{x_i}/b$$

The really significant contribution from this strip theory is the contribution to the rolling moment coefficient C_ℓ . This is shown in Figure 23 as a function of lateral position y for two altitudes with zero roll. Wind tunnel test data (Ref. 6) indicate that full T-2 aileron deflection produces a maximum roll moment coefficient of ±.04. It, therefore, appears that the ailerons will not be able to counterbalance the moment produced by the wake when operating within 15 ft (4.57 m) of the center of a vortex. The aircraft is automatically rolled out of this region and exits from the wake in the downward direction as shown in Figure 27 and discussed in Section 5.

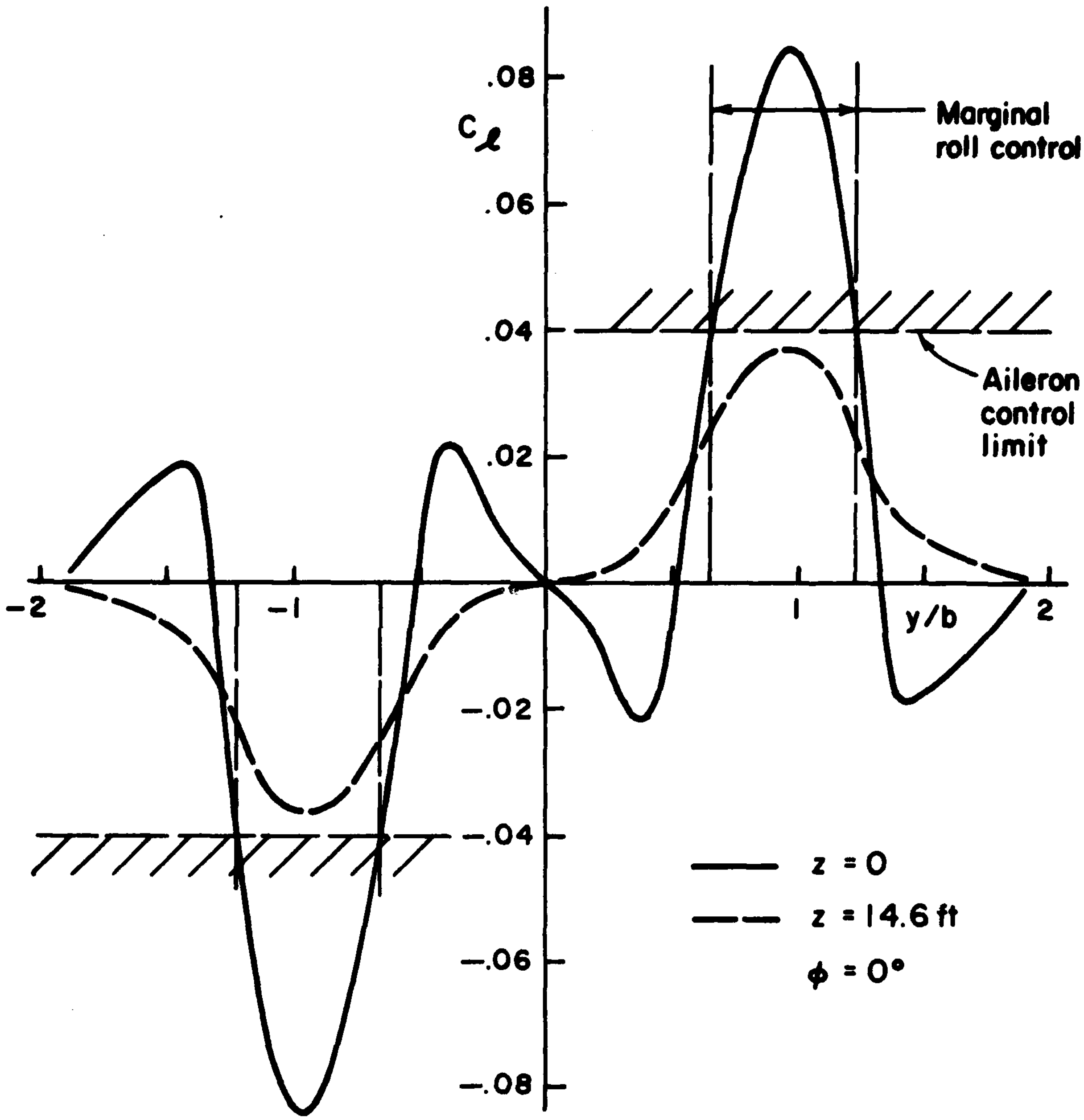

Figure 23. Comparison of rolling moment due to wake and from ailerons.

5. NUMERICAL SIMULATION OF WAKE-RIDER DYNAMICS

A.R.A.P.'s six-degree-of-freedom Aircraft Digital Simulation Program has been used to simulate the flight of the T-2 in the wake of two P-3's. Geometric, mass, and aerodynamic characteristics have been obtained from Refs. 6, 7, and 8 and are tabulated in Appendix A.

In order to obtain estimates of the maximum structural loads and to crudely evaluate the piloting task, over forty simulations were run. From these, six have been chosen for presentation in this report. The first three illustrate the advantage of approaching the wake from above. The last three represent worst-case encounters and also give a feel for what the pilot must do in order to ride the wake.

Figure 24 shows the T-2 being flown with altitude stabilization:

$$\delta_e = k_h(z - z_{des}) + k_\gamma \gamma + k_\alpha(\alpha - \alpha_{des})$$

$$T = T_o + k_V(V - V_{des})$$

$$k_h = .001 \text{ rad/ft}$$

$$k_\gamma = .5$$

$$k_\alpha = 3$$

$$k_V = -40 \text{ lb/ft}$$

where δ_e = elevator deflection

T = thrust

γ = flight path angle

This is not meant to represent typical pilot control but merely to provide stable altitude changes. The solid curve in Figure 24 indicates how a 100 ft (30.5 m) altitude decrease is accomplished

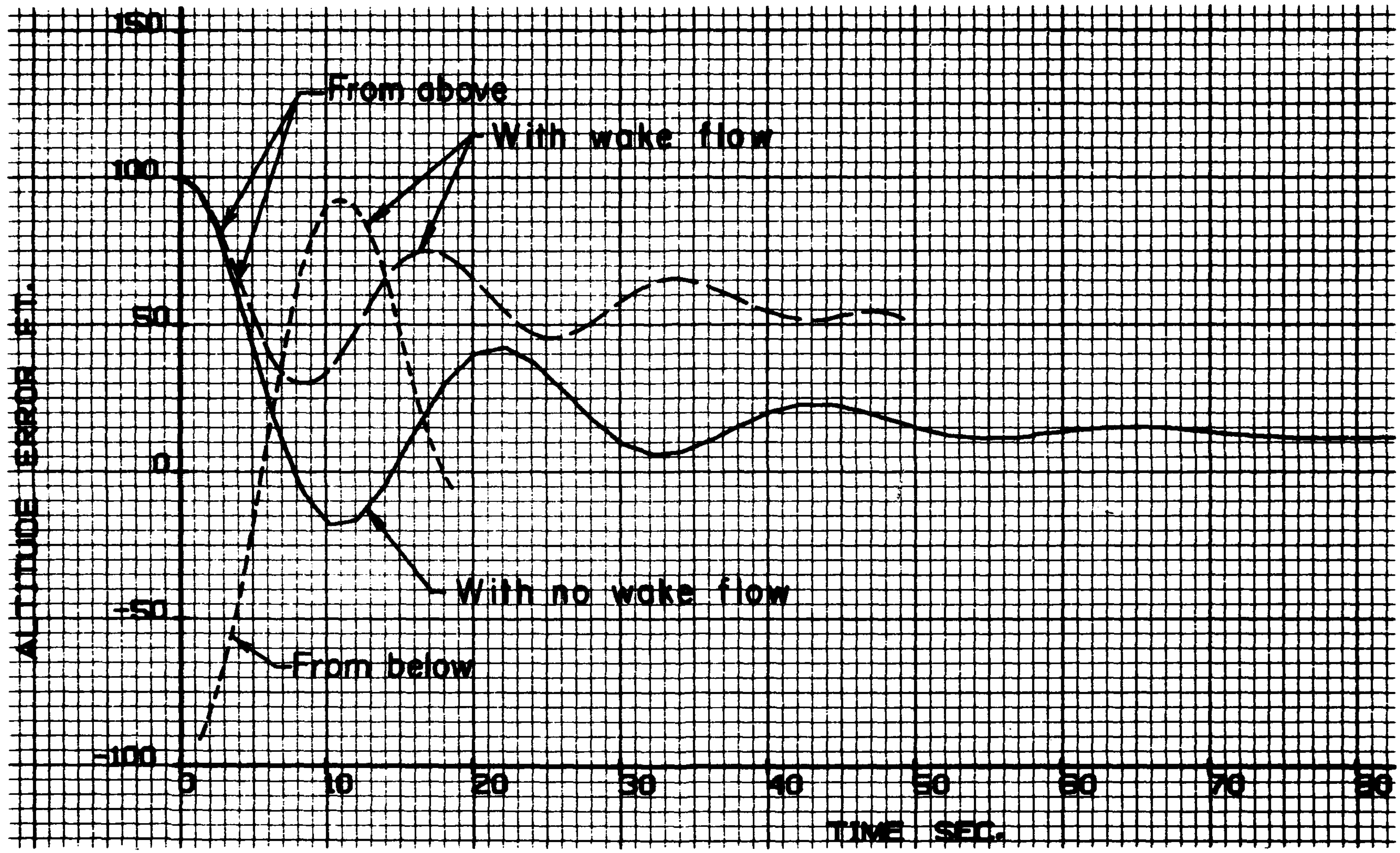

Figure 24. Altitude time history for wake entry from below and from above.

with no wake present. The long dashed curve shows what happens with the wake present. Note that the control, while not accurate, is quite stable. On the other hand, if the approach is made from below, the increasing upwash and high power setting force the aircraft through the center of the wake, and the approach from above must then be used. It, therefore, appears that entry into the wake should be done from above.

Having chosen this entry technique, the altitude stabilization was removed and entry was studied using a constant thrust reduction. This is successful as long as the sink rate is well below the maximum upwash in the wake (say, 5 fps (1.52 mps) sink rate for a 14 fps (4.27 mps) upwash).

For the previous simulations, the aircraft started with no lateral position error in order to concentrate on the longitudinal problems. To examine the combined problem, the aircraft is initially positioned 7 ft (2.13 m) to the right and 50 ft (15.24 m) up. The trajectory of the aircraft with the controls held fixed is shown in Figures 25 and 26. The small horizontal wake velocity component v_w causes the aircraft to drift to the right as it descends. The more it drifts to the right, the larger v_w becomes. The aircraft is also rolled by the vortices, causing the vertical component of the lift vector to decrease and and the aircraft to descend through the wake. Time histories of α , β , ϕ , ψ , p , r , $\dot{p}$, and $\dot{r}$ as well as the position errors are also shown for this simulation in Figure 26.

In the next simulation (Figures 27 and 28), the ailerons are used to help keep the wings level

$$\delta_a = k_\phi \phi$$

$$k_\phi = 1$$

where δ_a = aileron deflection.

Again, the aircraft drifts to the right but at a reduced rate since the lift vector is more nearly vertical. The aircraft passes through the wake near the center of the closest vortex

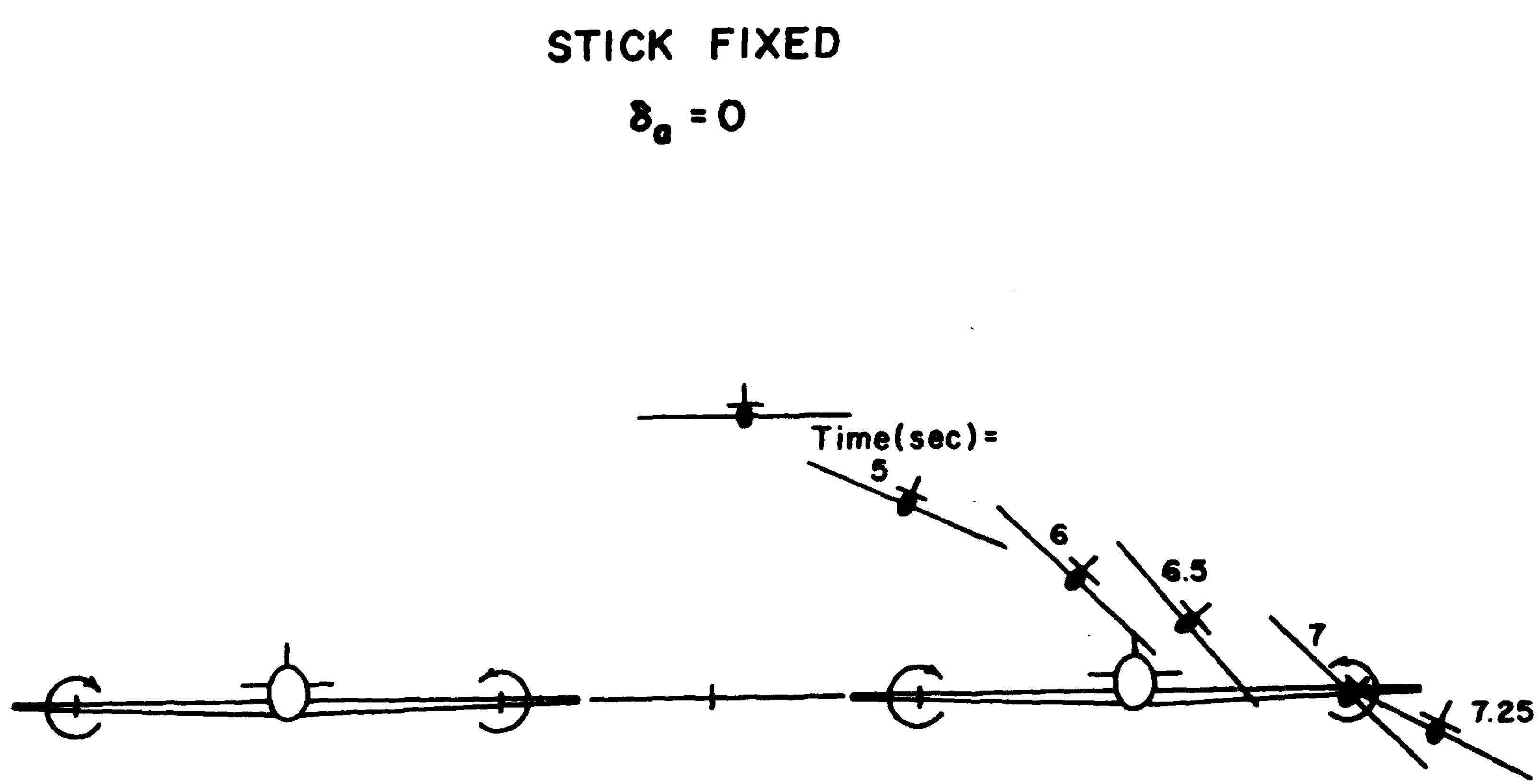

Figure 25. Time sequence of T-2 wake riding with no control inputs.

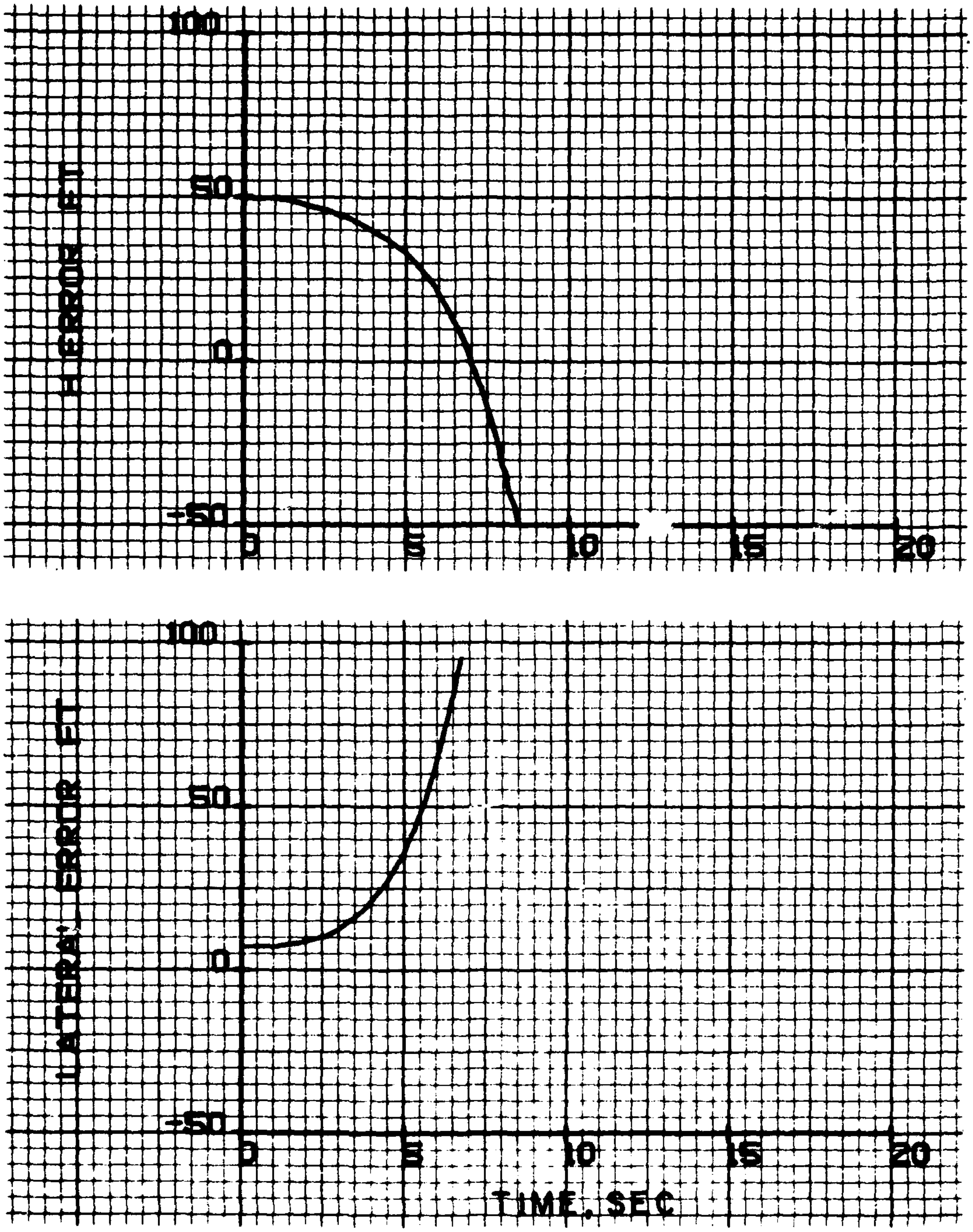

Figure 26. Time histories of T-2 wake riding with no control.

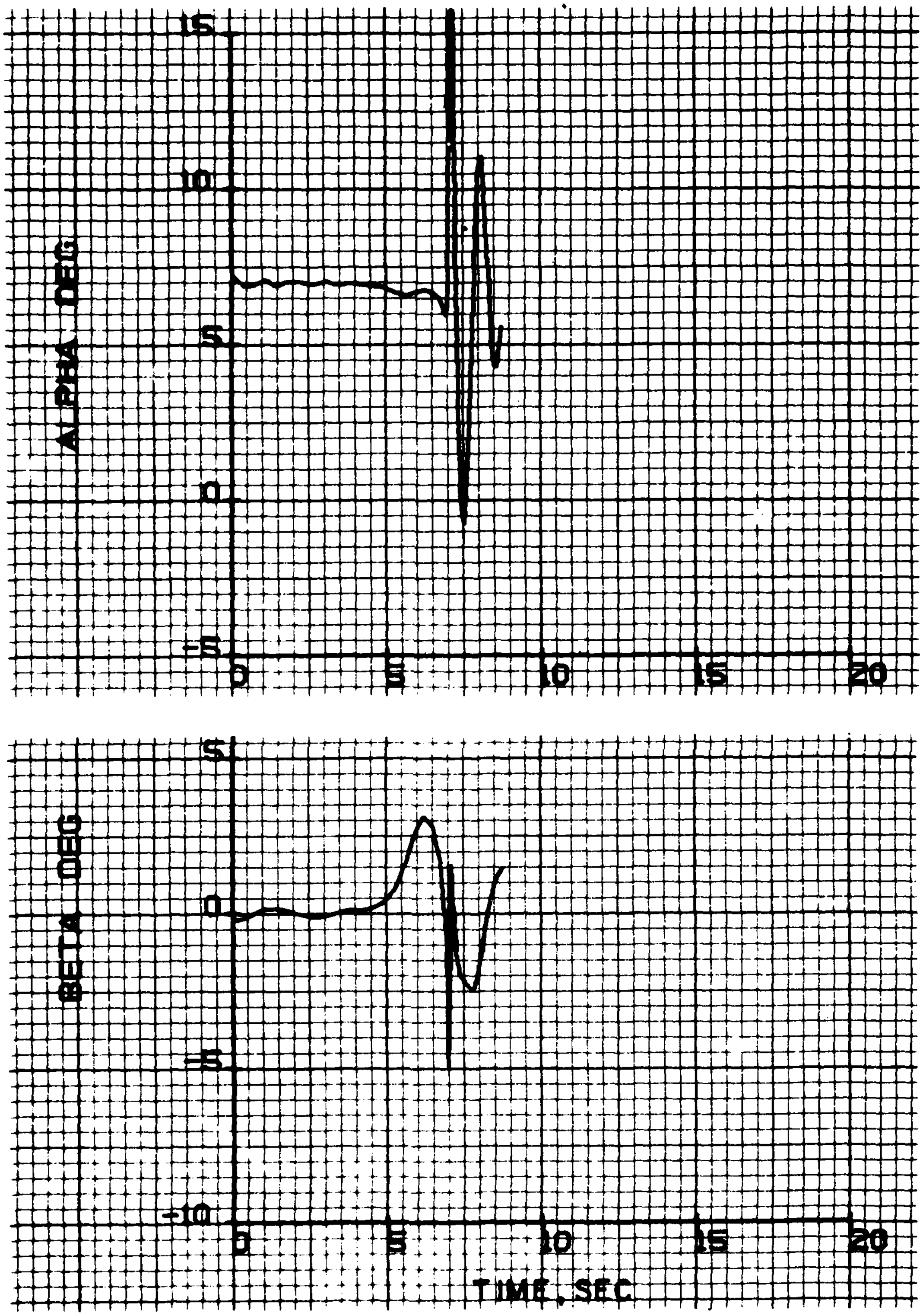

Figure 26. (cont.)

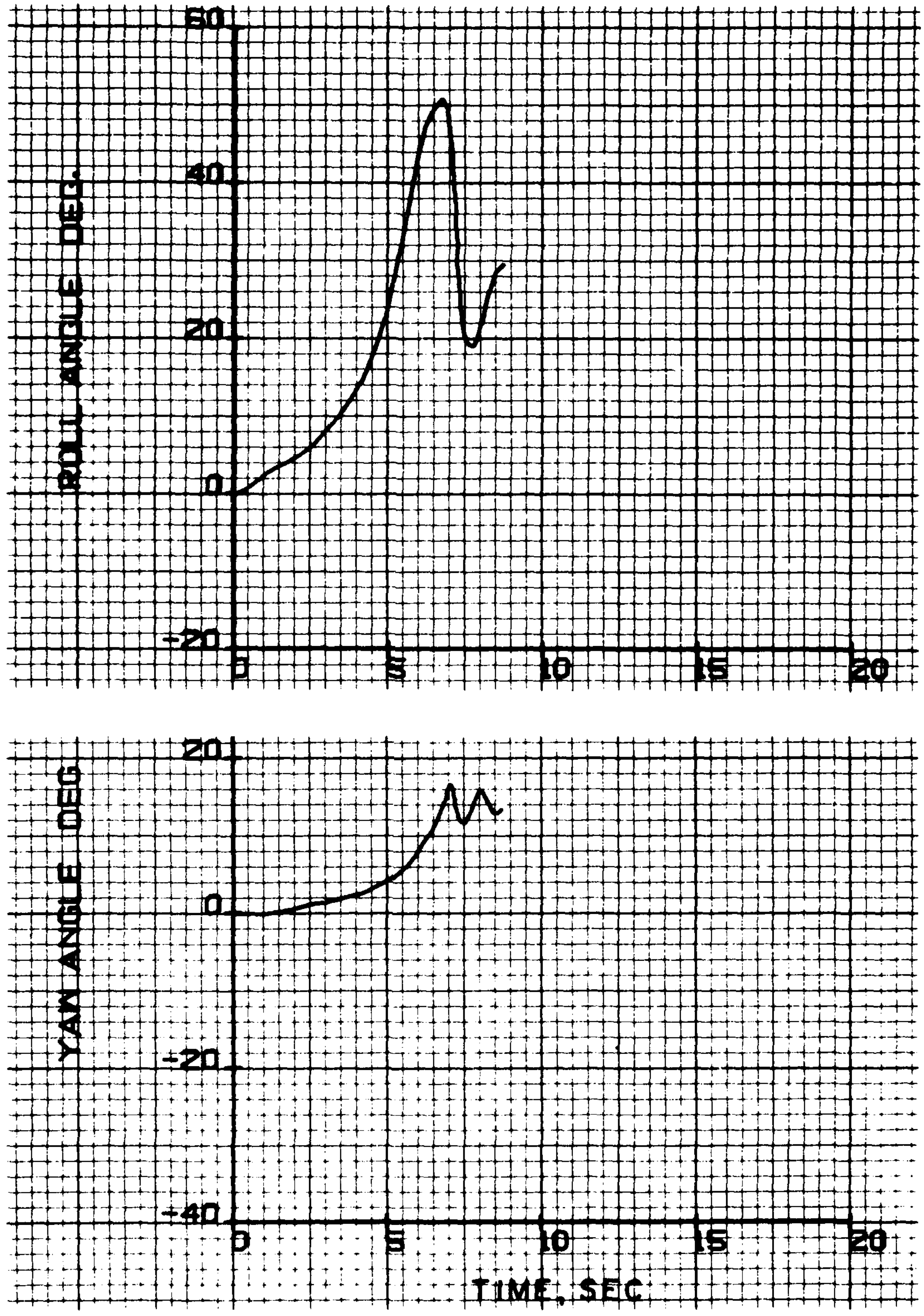

Figure 26. (cont.)

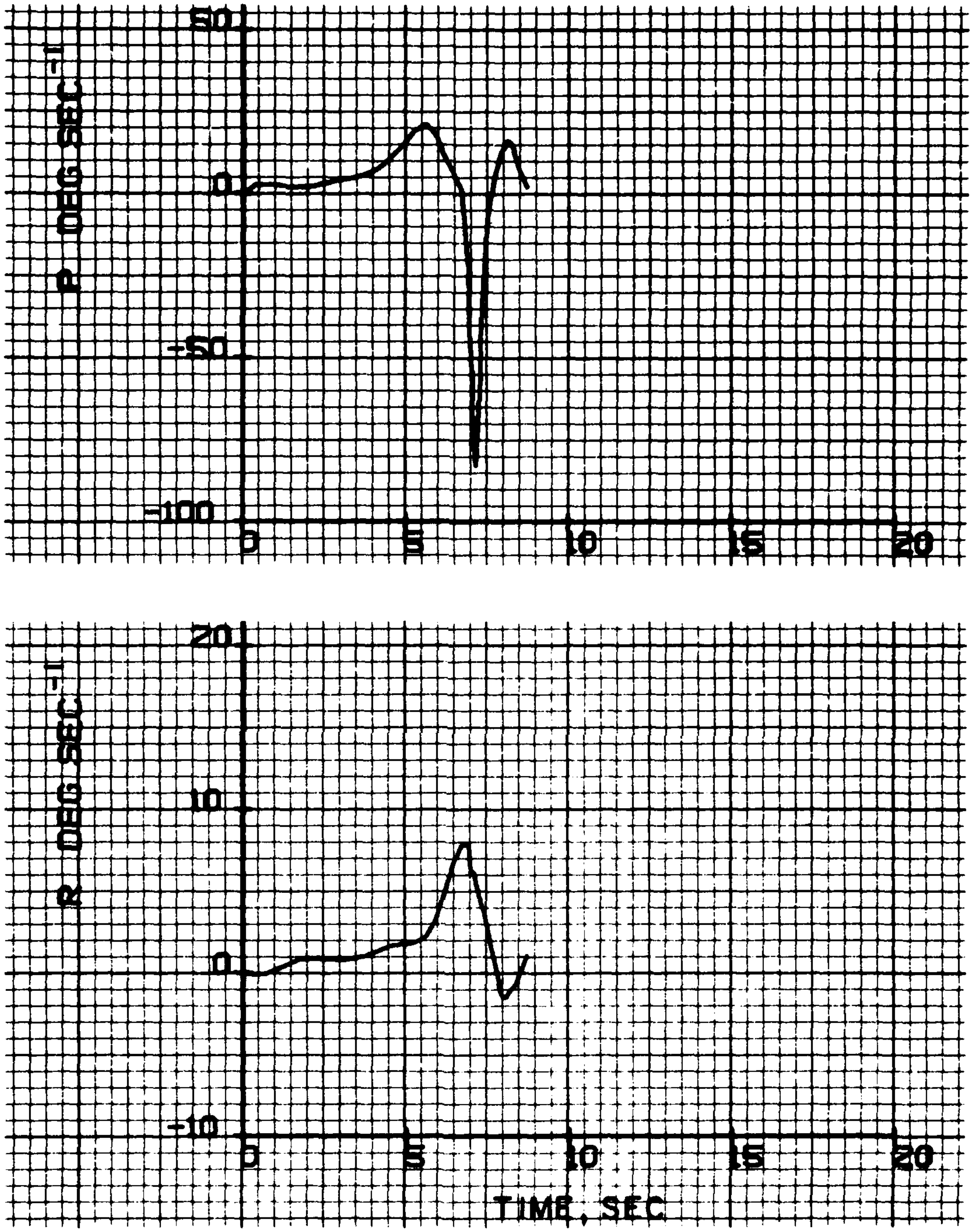

Figure 26. (cont.)

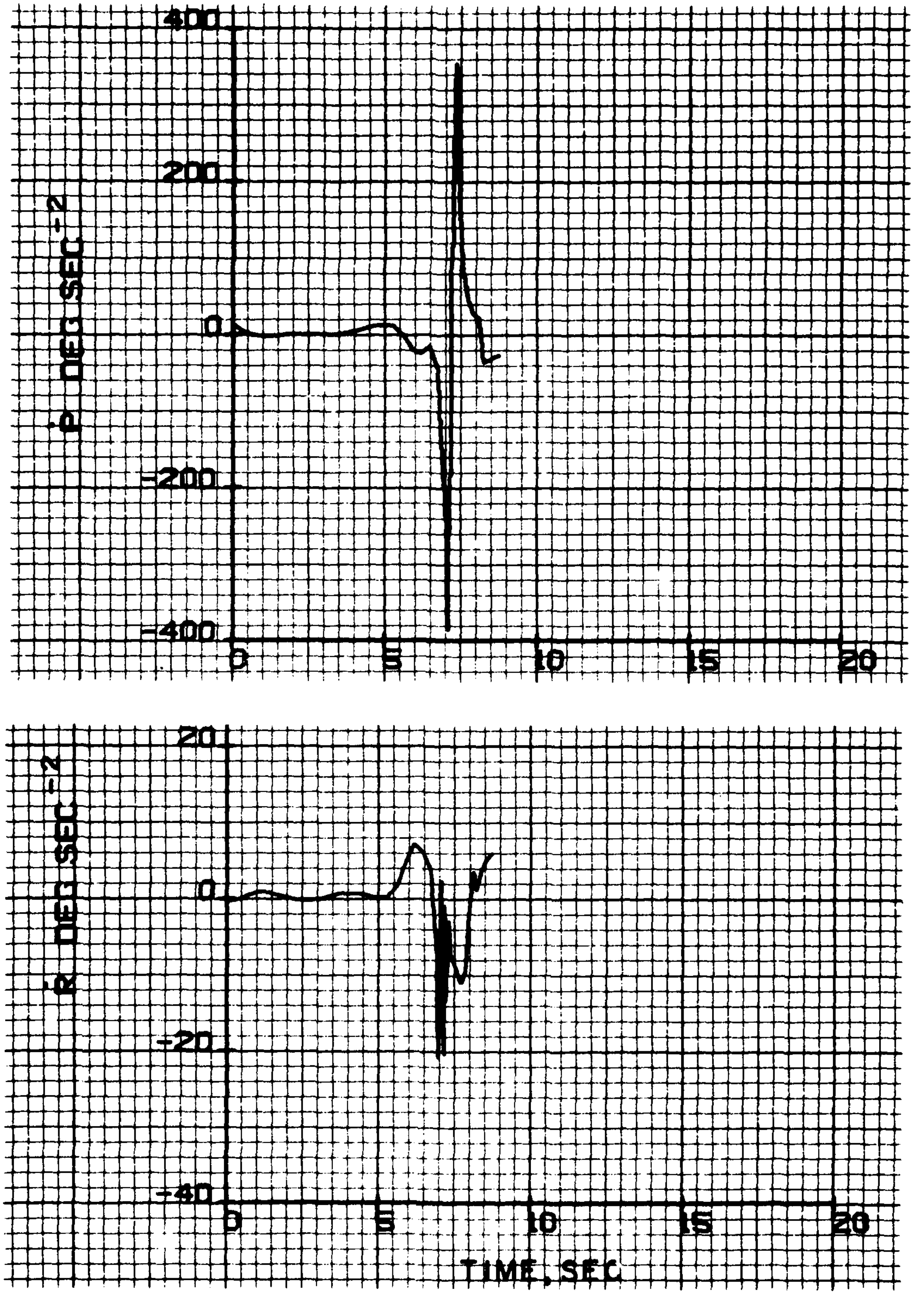

Figure 26. (concluded)

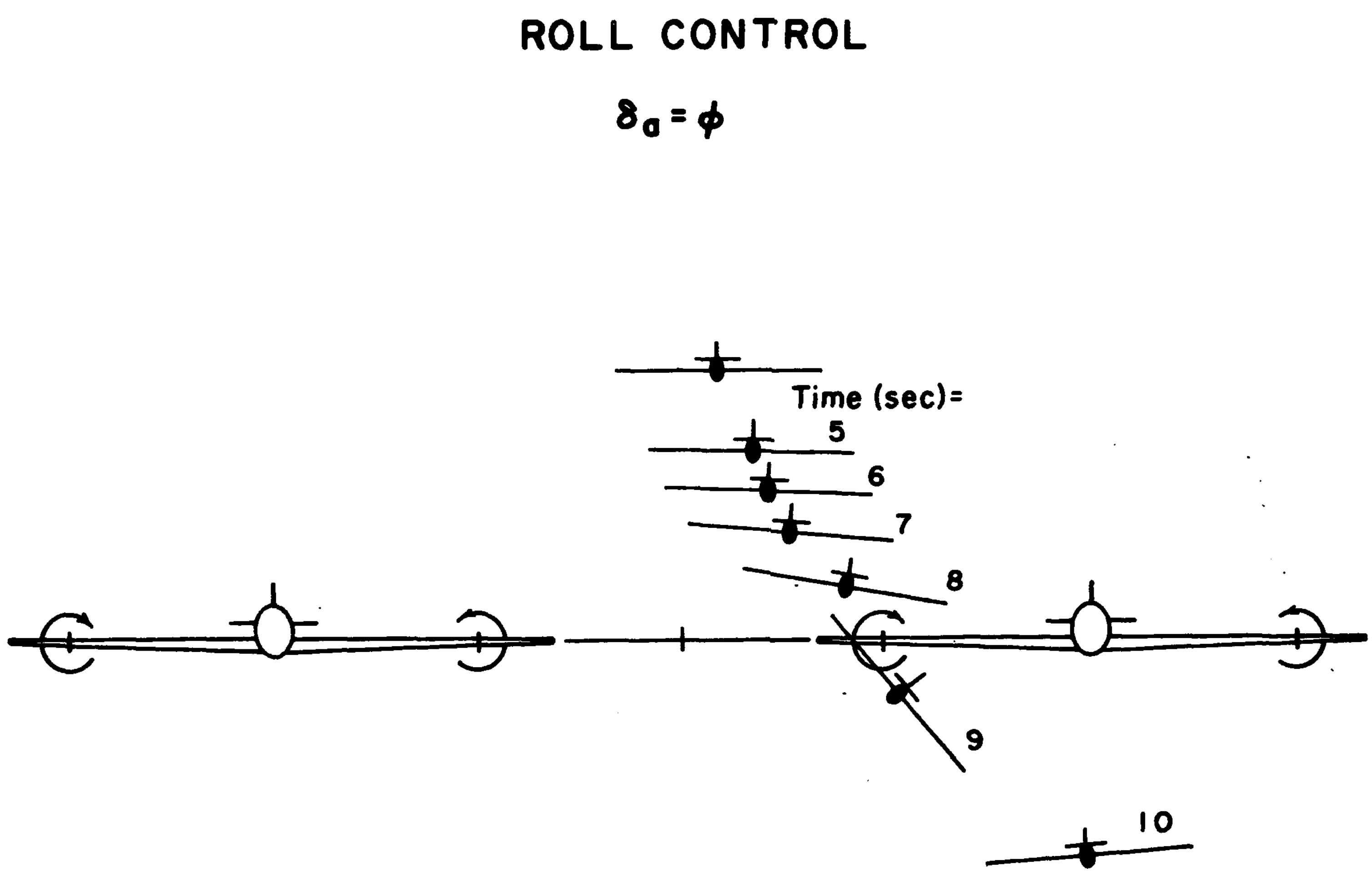

Figure 27. Time sequence of T-2 wake riding with roll angle feedback to ailerons.

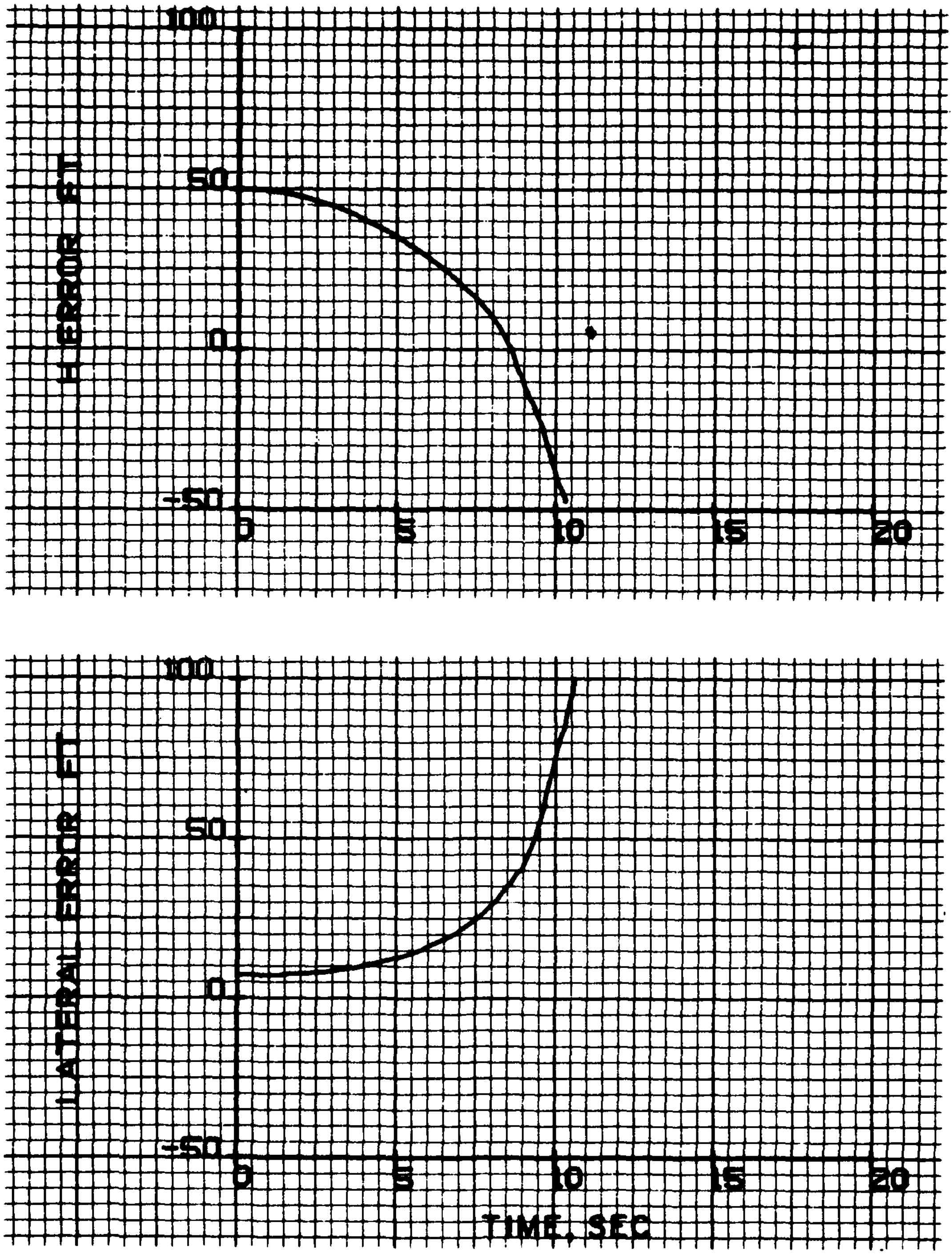

Figure 28. Time histories of T-2 wake riding with roll angle feedback to ailerons.

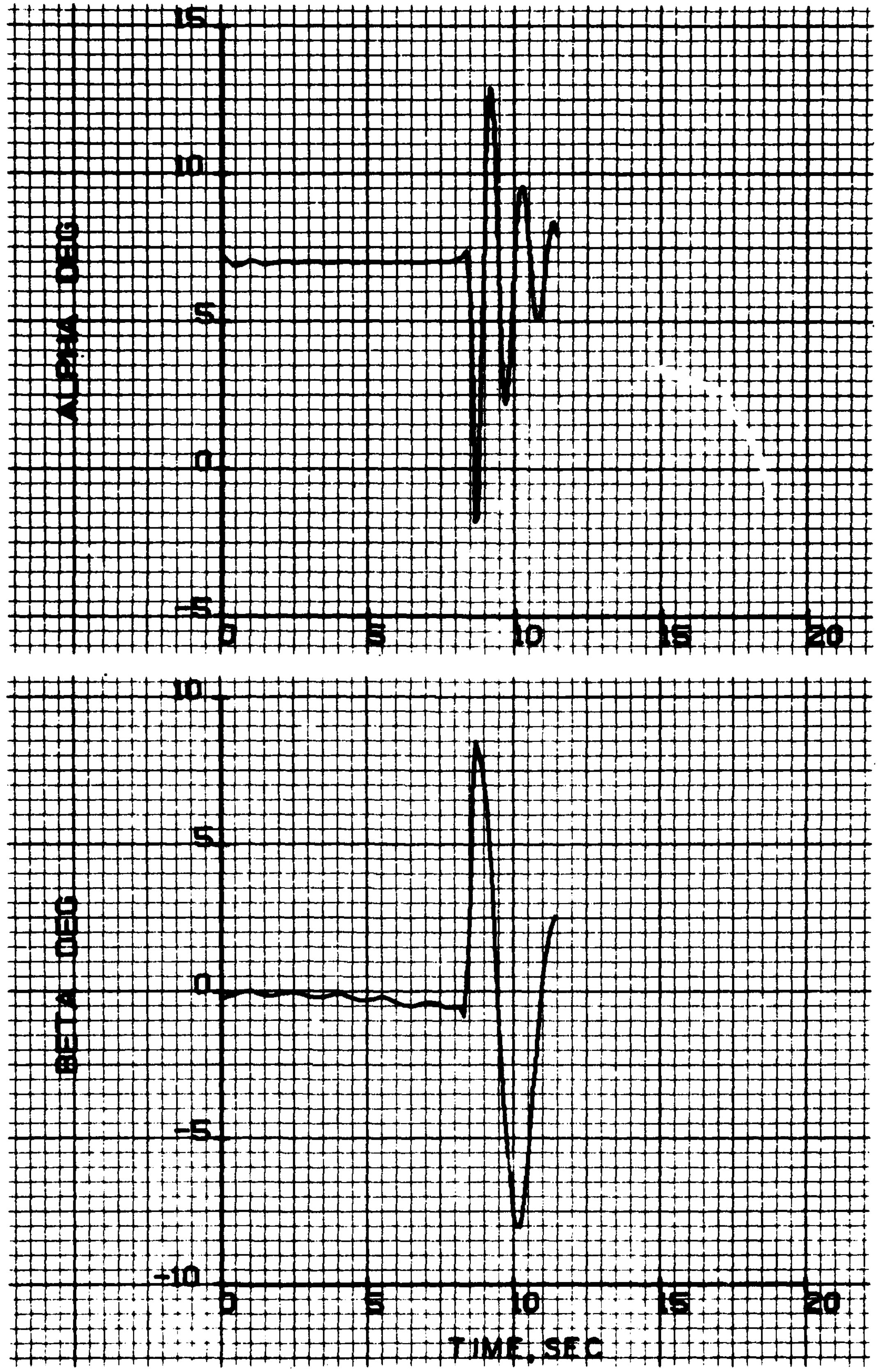

Figure 28. (cont.)

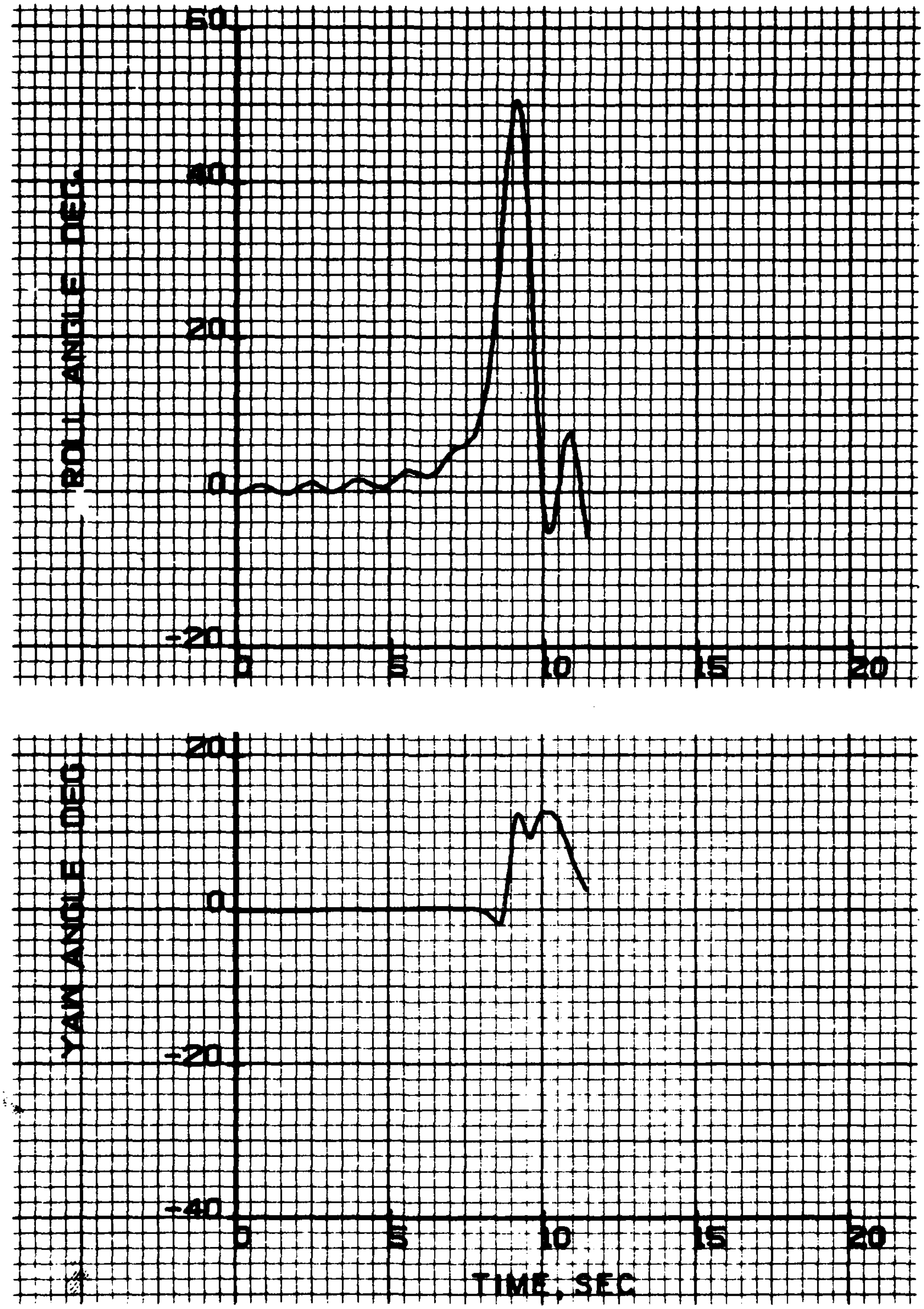

Figure 28. (cont.)

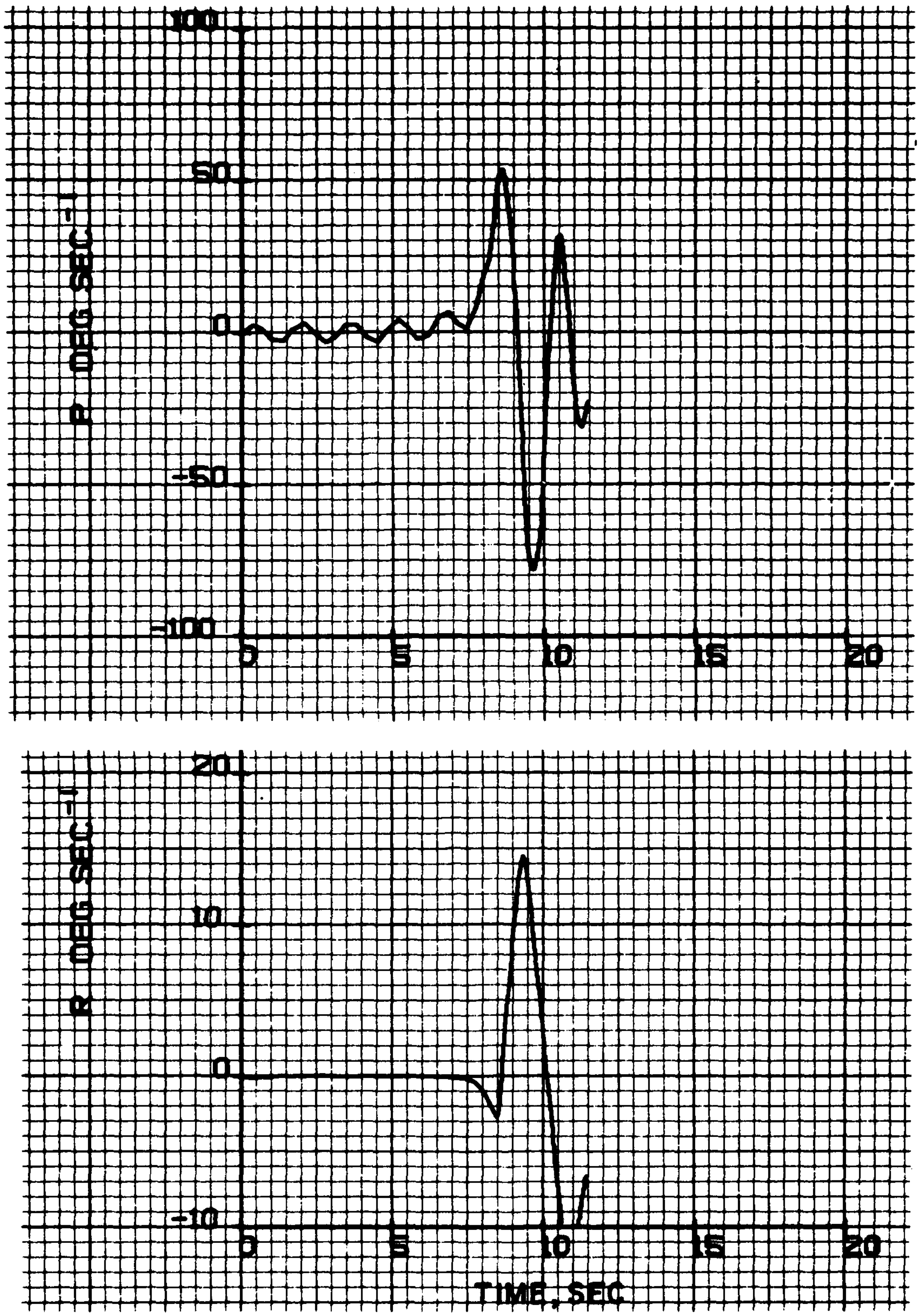

Figure 28. (cont.)

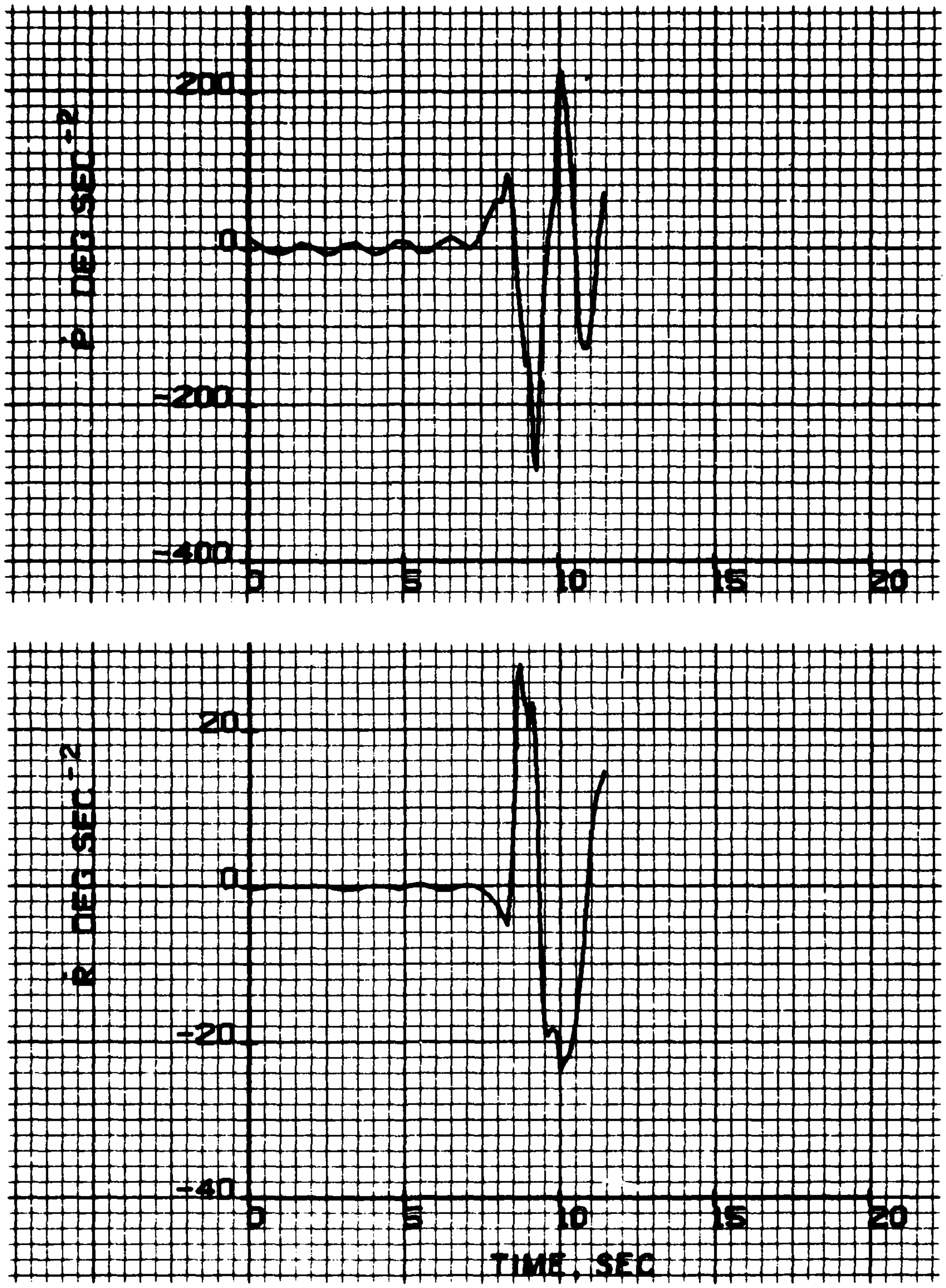

Figure 28. (cont.)

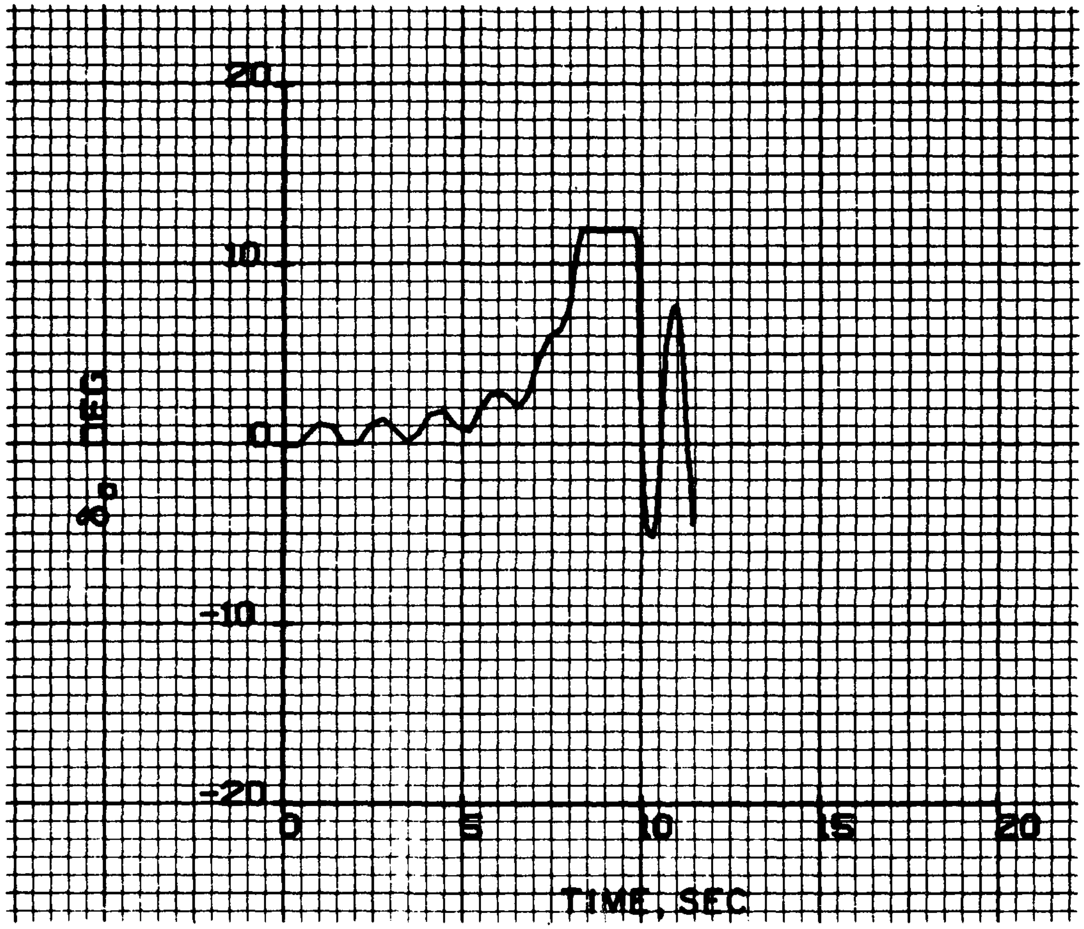

Figure 28. (concluded)

and is rolled because the roll torque from the vortex is greater than the maximum aileron roll torque.

In the third simulation (Figures 29 and 30), the ailerons are used to control lateral error as well as roll angle

$$\delta_a = k_y y + k_\phi \phi$$

$$k_y = .0033 \text{ rad/ft}$$

$$k_\phi = 1$$

There is, therefore, a slight negative roll (Figure 30) due to the initial 7 ft (2.14 m) lateral error. The error is reduced and the vehicle descends slightly into the lower part of the wake but then rises again. At this point, the pilot should further reduce power and attempt to stabilize the aircraft at $z = 10$ ft (3.05 m). He can then concentrate on holding his lateral position with respect to the vortex field.

The small, slow aileron motions (Figure 30) required to stabilize the lateral oscillations indicate that a pilot should be able to perform this function if he has good visual cues for locating the vortices. In reality, however, the pilot's task may be complicated by P-3 position-keeping variations, ambient turbulence and crosswind effects on the wake, and turbulence within the wake. It is felt that these effects are best evaluated in the flight test program.

ROLL + LATERAL POSITION CONTROL

$$\delta_a = \phi + .0033\epsilon_y$$

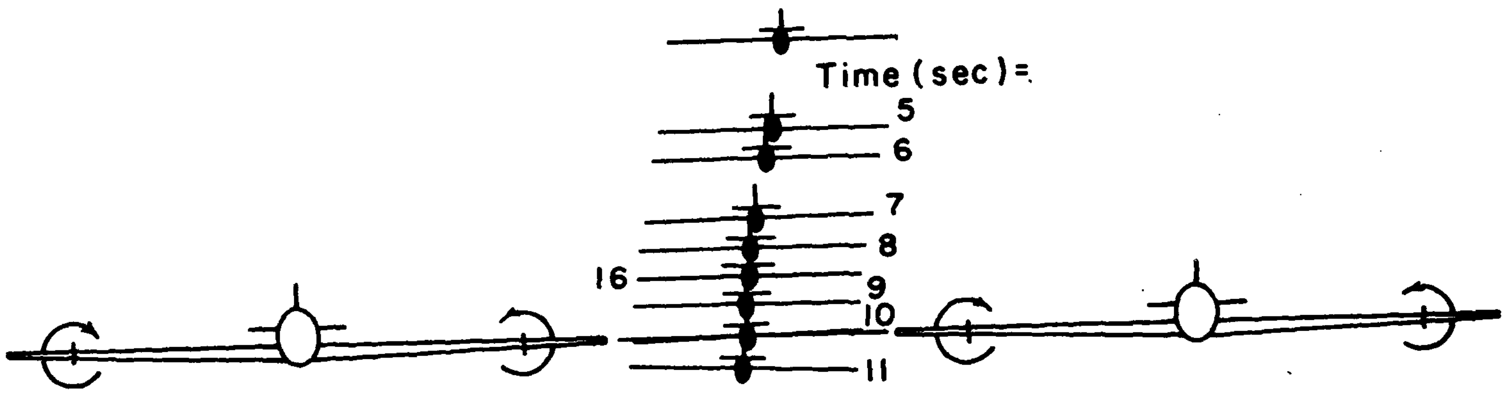

Figure 29. Time sequence of T-2 wake riding with lateral position and roll angle feedback to ailerons.

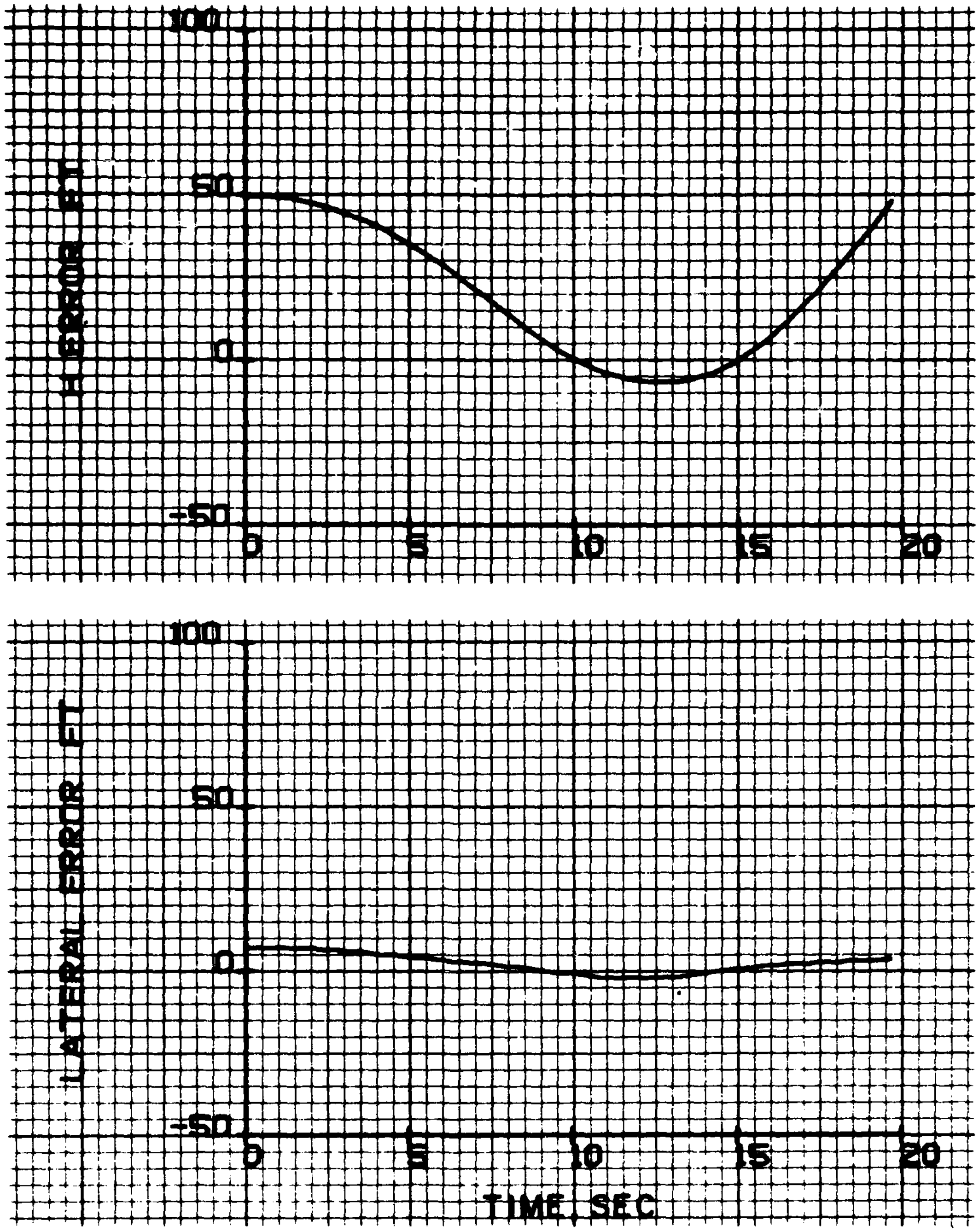

Figure 30. Time histories of T-2 wake riding with lateral position and roll angle feedback to ailerons.

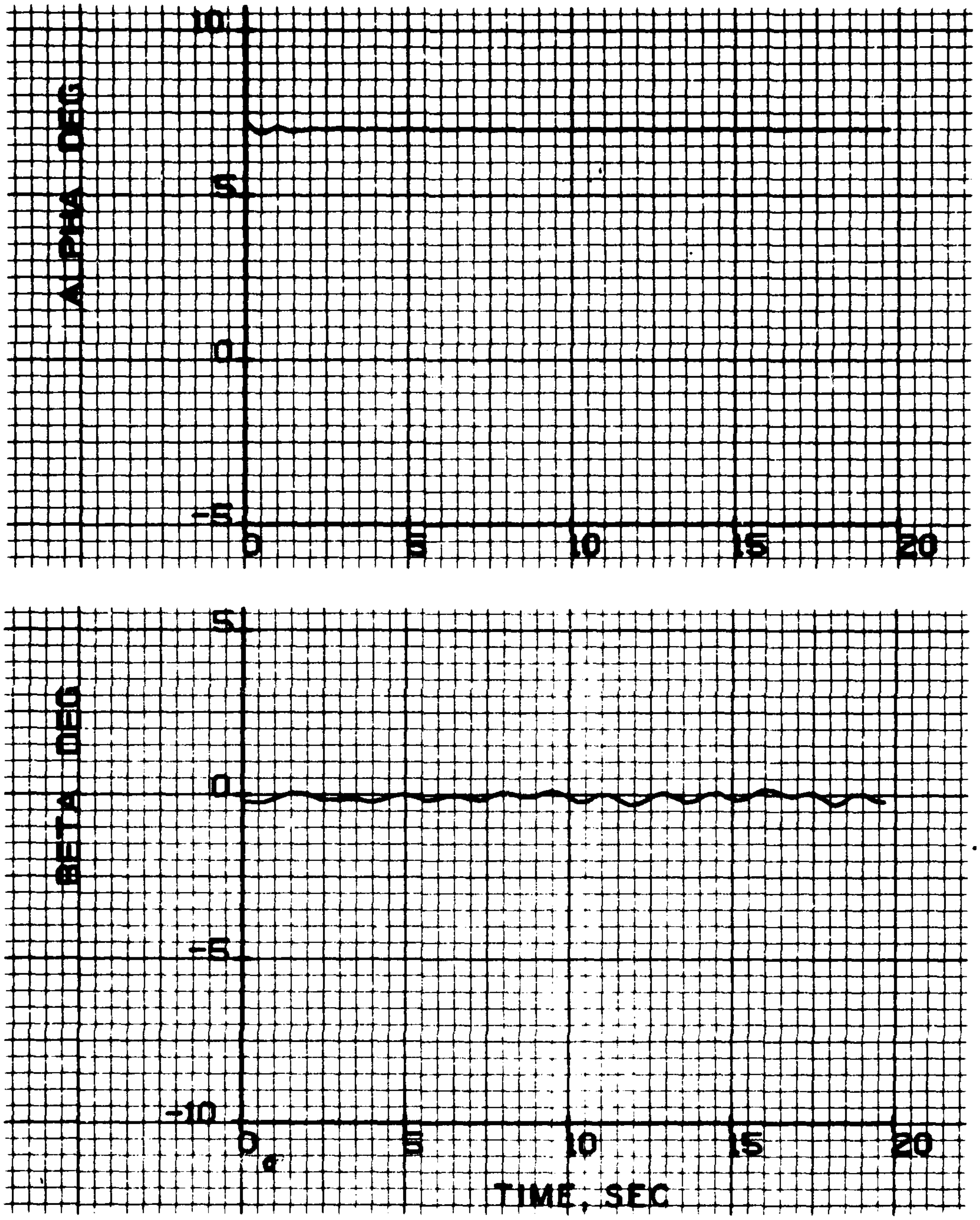

Figure 30. (cont.)

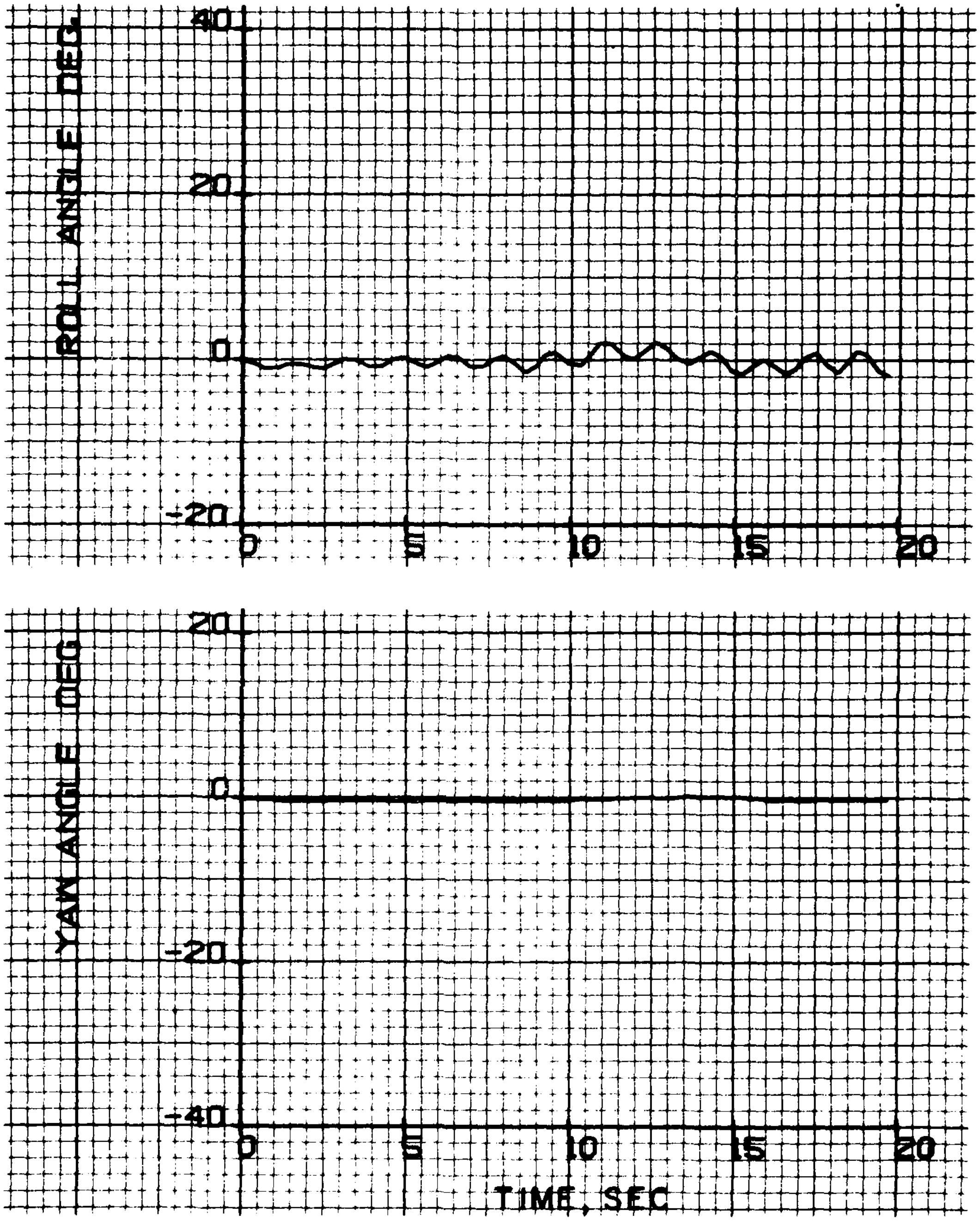

Figure 30. (cont.)

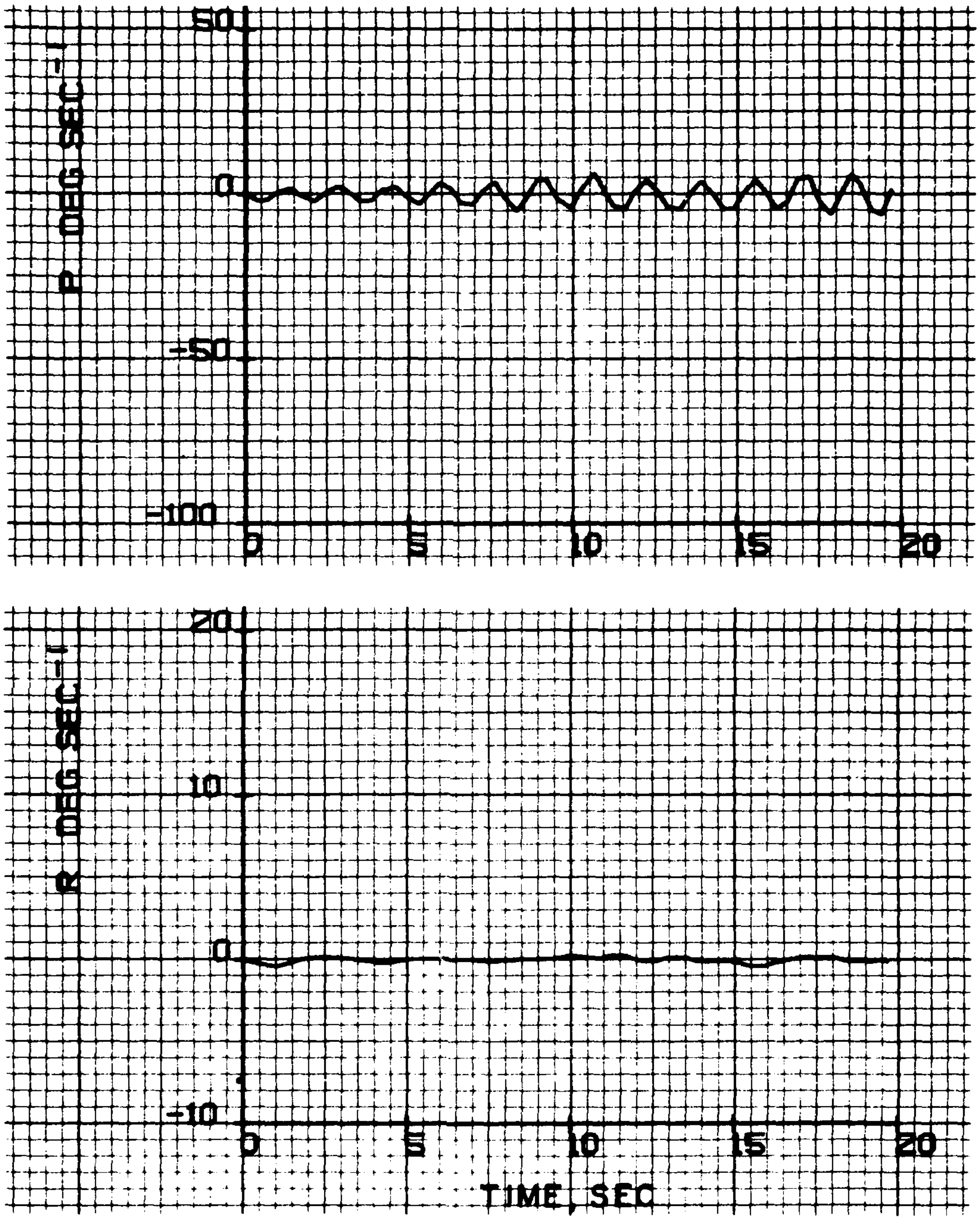

Figure 30. (cont.)

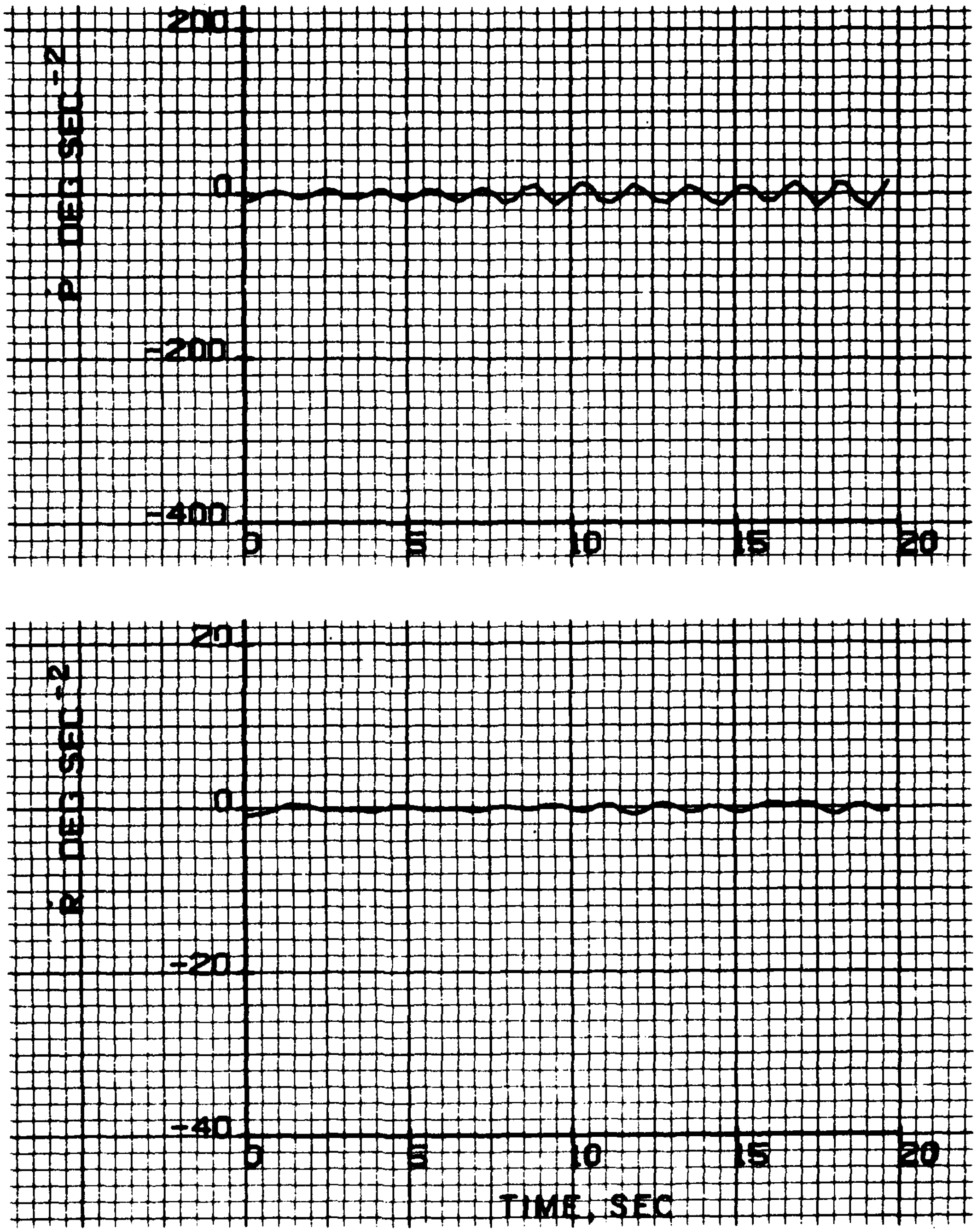

Figure 30. (cont.)

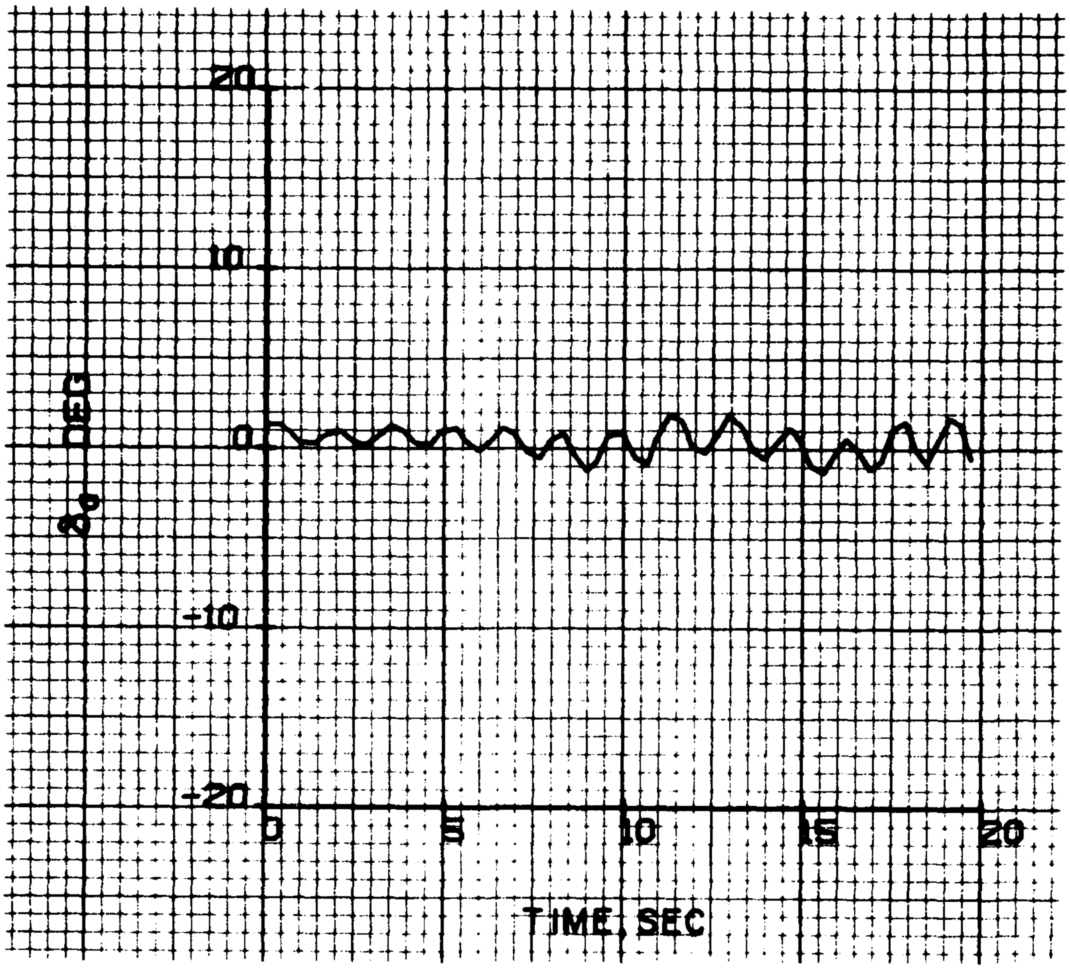

Figure 30. (concluded)

6. STRUCTURAL LOAD CALCULATIONS

Dynamic simulations presented in Section 5 suggest that aircraft upset motions occurring during direct vortex encounters are not sufficiently violent to factor heavily into loads estimation. In particular, the angular aircraft rates resulting from the encounter are not large enough to produce dangerous misorientation of the aircraft after exiting from the vortex. In addition, the aircraft accelerations resulting in inertial loadings on the T-2 can be neglected when compared to aerodynamic loading. In general, it is also true that inertial loadings tend to alleviate structural loading and this approximation is conservative. It is appropriate to estimate static aerodynamic loadings when the T-2 is immersed in the vortex flowfield since conservative estimates are sought.

A. Wing Loading

Overloading the wings of the T-2 during vortex encounter does not appear to be a problem. Using a strip theory estimate of the loading on one wing coaxially encountering the vortex specified in Section 2 gives a load of approximately 6370 lbs (2887 kg). This calculation has assumed an average value of lift curve slope equal to 0.08/deg. This loading, doubled to account for the other wing, can only result in accelerations experienced by the pilot of ±1 incremental g's. These loads are well within the wing structural design limits.

B. Horizontal Tail

The loading induced on either the port or starboard horizontal tail estimated by strip theory during worst-case encounter is approximately 2120 lbs (962 kg). This load approaches the horizontal tail root shear design load of 2550 lbs (1157 kg). The horizontal tail root bending moment during worst-case coaxial encounter is estimated to be 9540 ft-lbs (1320 kgm) which is also below the design value of 13,600 ft-lbs (1880 kgm). These

estimated loads are still to be reduced by interference with the wing flowfield, and this effect will be discussed below.

C. Vertical Tail

The loading induced on the horizontal tail has been estimated by strip theory to be approximately 1890 lbs (867 kg) during worst-case encounter. To this, in addition to static loading, the rudder deflected full over will increase this load by approximately 1300 lbs (590 kg) to bring the total load to 3200 lbs (1450 kg). Since the vertical tail design load is 7000 lbs (3175 kg), no problems regarding vertical tail root shear are anticipated.

The vertical tail root bending moment requires special attention since the horizontal tail is located on the rudder. Therefore, asymmetric loading of the horizontal tail results in an additional increment to the root bending moment of the vertical tail. Including this increment, the rudder root bending moment is 33,500 ft-lbs (4631 kgm). The vertical tail root bending moment is estimated to reach 116% of its design value, making the tail root the most highly stressed location on the aircraft. This loading is conservative and will be adjusted in the next subsection to account for wing interference effects.

D. Wing Flowfield Tail Loads Alleviation

During coaxial vortex penetration, the T-2 aircraft will shed a strong vortex flowfield which will tend to lessen the aerodynamic loads on the tail by countering the vortex flow from the P-3 aircraft. A simple estimate of this alleviation has been made, and all tail loads and moments are reduced by about 15%. The tail root bending moment is estimated to be 27,600 ft-lbs (3815 kgm) which is 96% of the design value.

Experience gained by NASA while probing the wake of a 747 aircraft in flaps-down configuration with a T-37 (an aircraft very similar to but smaller than the T-2) has shown, as we have found, that the root bending moment on the vertical tail of the T-37 was the most serious tail load problem. In these NASA tests,

negative wing loads were also a problem. A direct comparison with these tests is not possible because the T-37 penetrated the vortex wake of a 747 in flaps-down configuration, thus the vortex, though far stronger, is more diffuse than that of the P-3. Further, the T-37 made these penetrations at lower dynamic pressures than are envisaged for the wake rider experiments. In addition, the pilot of the T-37 made every effort to force his aircraft to remain in the center of the vortex as long as he possibly could.

7. CONCLUSIONS AND RECOMMENDATIONS

A study has been made of the dynamics of a T-2 aircraft attempting to establish a wake-riding position behind two P-3 aircraft. The following conclusions may be drawn from the data gathered in this study.

(1) An approach to the wake-riding position should be made from above by a reduction in power slightly less than that which may ultimately be possible and maintaining constant airspeed (and, hence, position) by setting up the appropriate rate of descent.

(2) The lateral position from which a wake rider attempts to descend into the wake-riding position would appear to be an important element of the wake-riding problem for, initially, the pilot cannot "sense" the proper position from rolling cues. Once in the wake-riding position, rolling cues may be sufficient to enable the pilot to maintain position. Thus, it would appear desirable (in the absence of engine smoke to mark the vortices) to perform these flight tests either in still air or with flight directions aligned with the wind so that visual cues of lateral position are as accurate as possible.

(3) The provision to the pilot of visual cues marking the vortices (smoke or condensation) would be most helpful in assuring the success of wake-riding experiments.

(4) Once in the wake-riding slot, the piloting task of maintaining position in still air should not be too heavy.

(5) Aileron control of roll orientation will be marginal with the T-2 fuselage centerline within 15 ft (4.57 m) of the center of a trailing vortex. If the T-2 is allowed to enter this region, it is anticipated that the aircraft will be rolled out of the wake into the region below the vortex. If no aileron control is used, a roll acceleration of 385 deg/sec^2 could occur although a roll rate of 90 deg/sec would probably not be exceeded.

(6) If the T-2 inadvertently passes through the center of a vortex, yaw angles of the order of 16° might be experienced. The maximum yawing acceleration is less than 30°/sec^2.

(7) Structural loads on the tail of the T-2 aircraft passing directly through a vortex are computed to be large, approximately equal to the design load in the case of the root bending moment on the vertical tail (the most loaded aircraft component). This situation results from the fact that the tails of aircraft are not designed for the level of asymmetric horizontal tail loading that is experienced when passing through a vortex.

(8) The structural load calculations that have been made are, in general, supported by the results of flight tests performed by NASA using a T-37 aircraft to penetrate the wake of a 747. In these tests, vertical tail loads were high but not critical. A direct comparison is not possible because the T-37 penetrated the vortex wake of a 747 in flaps-down configuration, thus, the vortex, though far stronger, is more diffuse than that of the P-3. Further, the T-37 made these penetrations at lower dynamic pressures than are envisaged for the wake-rider experiments.

The following recommendations can be made as a result of this study:

(1) The wake-rider flight tests, as originally envisaged, must be considered as high risk experiments unless the tail of the T-2 were to be strengthened to take the root bending moments that might be incurred if a pass through the center of a trailing vortex occurred.

(2) It is desirable to approach the wake-riding position from above using a reduced-power, constant-airspeed approach.

(3) If wake-riding experiments are carried out, every effort should be made to mark the vortices between which the T-2 is to ride in order to provide the T-2 pilot with visual cues for lateral positioning.

APPENDIX A

MASS, GEOMETRIC AND AERODYNAMIC DATA USED IN THE SIMULATIONS OF THE FLIGHT OF THE T-2

Mass Properties

W	11,000 lbs	4990 kg
cg	21% mac	
I_{xx}	9000 slug ft^2	13,000 kg m^2
I_{yy}	14,600 slug ft^2	19,790 kg m^2
I_{zz}	19,000 slug ft^2	25,754 kg m^2
I_{xy}	0	
I_{xz}	0	
I_{yz}	0	

Geometric Properties

S	254.86 ft^2	23.68 m^2
$\bar{c}$	7.407 ft	2.257 m
b	38.13 ft	11.62 m

Aerodynamic Properties

Static Aerodynamic Coefficients and Control Deflection Derivatives Evaluated on a Grid of α, β Points

(on pages following)

Pages 77-86 are the best copies available

BETA= 0.0000000E 00

ALFA	-0.800000E 01	0.000000E 00	0.300000E 01	0.150000E 02	0.200000E 02	0.300000E 02
CX	0.320000E-01	-0.400000E-01	0.240000E-01	0.140000E 00	-0.260000E-01	-0.330000E-01
CY	0.000000E 00	0.000000E 00	0.000000E 00	0.000000E 00	0.000000E 00	0.000000E 00
CZ	0.600000E 00	-0.800000E-01	-0.600000E 00	-0.105000E 01	-0.900000E 00	-0.105000E 01
CL	0.000000E 00	0.000000E 00	0.000000E 00	-0.200000E-01	-0.100000E-01	-0.160000E-01
CM	0.110000E 00	-0.400000E-01	-0.180000E 00	-0.320000E 00	-0.360000E 00	-0.490000E 00
CN	0.000000E 00	0.000000E 00	0.000000E 00	-0.600000E-02	0.500000E-02	0.160000E-01
CXM1	0.000000E 00	0.000000E 00	0.000000E 00	0.000000E 00	0.000000E 00	0.000000E 00
CXM2	0.000000E 00	0.000000E 00	0.000000E 00	0.000000E 00	0.000000E 00	0.000000E 00
CXM3	0.000000E 00	0.000000E 00	0.000000E 00	0.000000E 00	0.000000E 00	0.000000E 00
CXM4	0.000000E 00	0.000000E 00	0.000000E 00	0.000000E 00	0.000000E 00	0.000000E 00
CYDA	0.000000E 00	0.000000E 00	0.000000E 00	0.000000E 00	0.000000E 00	0.000000E 00
CYDU	0.000000E 00	0.000000E 00	0.000000E 00	0.000000E 00	0.000000E 00	0.000000E 00
CYDR	0.460000E-01	0.460000E-01	0.410000E-01	0.420000E-01	0.200000E-01	0.250000E-01
CZM1	0.141000E 00	0.141000E 00	0.153000E 00	0.164000E 00	0.140000E 00	0.157000E 00
CZM2	-0.156000E 00	-0.156000E 00	-0.160000E 00	-0.120000E 00	-0.700000E-01	-0.700000E-01
CZM3	0.000000E 00	0.000000E 00	0.000000E 00	0.000000E 00	0.000000E 00	0.000000E 00
CZM4	0.000000E 00	0.000000E 00	0.000000E 00	0.000000E 00	0.000000E 00	0.000000E 00
CLM1	0.000000E 00	0.000000E 00	0.000000E 00	0.000000E 00	0.000000E 00	0.000000E 00
CLM2	0.000000E 00	0.000000E 00	0.000000E 00	0.000000E 00	0.000000E 00	0.000000E 00
CLDA	-0.390000E-01	-0.390000E-01	-0.360000E-01	-0.250000E-01	-0.150000E-01	-0.120000E-01
CLDU	0.000000E 00	0.000000E 00	0.000000E 00	0.000000E 00	0.000000E 00	0.000000E 00
CLDR	0.600000E-02	0.600000E-02	0.600000E-02	0.100000E-02	0.400000E-02	0.600000E-02
CMM1	0.320000E 00	0.320000E 00	0.360000E 00	0.360000E 00	0.290000E 00	0.350000E 00
CMM2	-0.325000E 00	-0.325000E 00	-0.325000E 00	-0.260000E 00	-0.150000E 00	-0.145000E 00
CMM3	0.000000E 00	0.000000E 00	0.000000E 00	0.000000E 00	0.000000E 00	0.000000E 00

BETA= 0.0000000E 00

ALFA	-0.8000000E 01	0.0000000E 00	0.8000000E 01	0.1500000E 02	0.2000000E 02	0.3000000E 02
CNMA	0.0000000E 00	0.0000000E 00	0.0000000E 00	0.0000000E 00	0.0000000E 00	0.0000000E 00
CNM1	0.0000000E 00	0.0000000E 00	0.0000000E 00	0.0000000E 00	0.0000000E 00	0.0000000E 00
CNM2	0.0000000E 00	0.0000000E 00	0.0000000E 00	0.0000000E 00	0.0000000E 00	0.0000000E 00
CNDA	-0.2000000E-02	-0.2000000E-02	-0.1500000E-02	0.2000000E-02	0.3000000E-02	-0.8000000E-03
CNDO	0.0000000E 00	0.0000000E 00	0.0000000E 00	0.0000000E 00	0.0000000E 00	0.0000000E 00
CNDR	-0.2300000E-01	-0.2500000E-01	-0.2100000E-01	-0.1950000E 00	-0.9000000E-02	-0.9000000E-02

DELTA= 0.5000000E 01

ALFA	-0.800000E 01	0.000000E 00	0.800000E 01	0.150000E 02	0.200000E 02	0.300000E 02
CA	0.330000E-01	-0.400000E-01	0.240000E-01	0.140000E 00	-0.260000E-01	-0.400000E-01
CY	-0.650000E-01	-0.650000E-01	-0.530000E-01	-0.500000E-01	-0.600000E-01	-0.600000E-01
CZ	0.580000E 00	-0.800000E-01	-0.600000E 00	-0.105000E 01	-0.910000E 00	-0.105000E 01
CL	-0.150000E-01	-0.150000E-01	-0.170000E-01	0.200000E-02	-0.190000E-01	-0.260000E-01
CM	0.100000E 00	-0.500000E-01	-0.190000E 00	-0.320000E 00	-0.360000E 00	-0.460000E 00
CN	0.900000E-02	0.900000E-02	0.700000E-02	0.800000E-02	0.300000E-02	0.100000E-01
CAM1	0.000000E 00	0.000000E 00	0.000000E 00	0.000000E 00	0.000000E 00	0.000000E 00
CAM2	0.000000E 00	0.000000E 00	0.000000E 00	0.000000E 00	0.000000E 00	0.000000E 00
CAM3	0.000000E 00	0.000000E 00	0.000000E 00	0.000000E 00	0.000000E 00	0.000000E 00
CAM4	0.000000E 00	0.000000E 00	0.000000E 00	0.000000E 00	0.000000E 00	0.000000E 00
CYDA	0.000000E 00	0.000000E 00	0.000000E 00	0.000000E 00	0.000000E 00	0.000000E 00
CYDD	0.000000E 00	0.000000E 00	0.000000E 00	0.000000E 00	0.000000E 00	0.000000E 00
CYDR	0.460000E-01	0.460000E-01	0.410000E-01	0.420000E-01	0.200000E-01	0.250000E-01
CZM1	0.141000E 00	0.141000E 00	0.153000E 00	0.164000E 00	0.110000E 00	0.157000E 00
CZM2	-0.156000E 00	-0.156000E 00	-0.160000E 00	-0.120000E 00	-0.700000E-01	-0.700000E-01
CZM3	0.000000E 00	0.000000E 00	0.000000E 00	0.000000E 00	0.000000E 00	0.000000E 00
CZM4	0.000000E 00	0.000000E 00	0.000000E 00	0.000000E 00	0.000000E 00	0.000000E 00
CLM1	0.000000E 00	0.000000E 00	0.000000E 00	0.000000E 00	0.000000E 00	0.000000E 00
CLM2	0.000000E 00	0.000000E 00	0.000000E 00	0.000000E 00	0.000000E 00	0.000000E 00
CLDA	-0.390000E-01	-0.390000E-01	-0.360000E-01	-0.250000E-01	-0.150000E-01	-0.120000E-01
CLDD	0.000000E 00	0.000000E 00	0.000000E 00	0.000000E 00	0.000000E 00	0.000000E 00
CLDR	0.600000E-02	0.600000E-02	0.600000E-02	0.100000E-02	0.400000E-02	0.600000E-02
CMM1	0.320000E 00	0.320000E 00	0.360000E 00	0.360000E 00	0.290000E 00	0.330000E 00
CMM2	-0.325000E 00	-0.325000E 00	-0.325000E 00	-0.280000E 00	-0.150000E 00	-0.145000E 00
CMM3	0.000000E 00	0.000000E 00	0.000000E 00	0.000000E 00	0.000000E 00	0.000000E 00

BETA= 0.5000000E 01 PAGE 4

ALFA	-0.8000000E 01	0.0000000E 00	0.8000000E 01	0.1500000E 02	0.2000000E 02	0.5000000E 02
CMM4	0.0000000E 00	0.0000000E 00	0.0000000E 00	0.0000000E 00	0.0000000E 00	0.0000000E 00
CMM1	0.0000000E 00	0.0000000E 00	0.0000000E 00	0.0000000E 00	0.0000000E 00	0.0000000E 00
CMM2	0.0000000E 00	0.0000000E 00	0.0000000E 00	0.0000000E 00	0.0000000E 00	0.0000000E 00
CNDA	-0.2000000E-02	-0.2000000E-02	-0.1500000E-02	0.2000000E-02	0.5000000E-02	-0.8000000E-03
CNDO	0.0000000E 00	0.0000000E 00	0.0000000E 00	0.0000000E 00	0.0000000E 00	0.0000000E 00
CNDR	-0.2300000E-01	-0.2300000E-01	-0.2100000E-01	-0.1950000E 00	-0.9000000E-02	-0.9000000E-02

BETA= 0.1000000E 02

ALFA	-0.600000E 01	0.000000E 00	0.800000E 01	0.150000E 02	0.200000E 02	0.300000E 02
CX	0.350000E-01	-0.900000E-02	0.700000E-01	0.100000E 00	-0.140000E-01	-0.620000E-01
CY	-0.135000E 00	-0.135000E 00	-0.135000E 00	-0.110000E 00	-0.135000E 00	-0.125000E 00
CZ	0.560000E 00	-0.110000E 00	-0.750000E 00	-0.110000E 01	-0.960000E 00	-0.110000E 01
CL	-0.260000E-01	-0.260000E-01	-0.290000E-01	-0.900000E-02	-0.360000E-01	-0.400000E-01
CM	0.700000E-01	-0.600000E-01	-0.200000E 00	-0.340000E 00	-0.370000E 00	-0.460000E 00
CN	0.150000E-01	0.150000E-01	0.140000E-01	-0.600000E-02	0.110000E-01	-0.500000E-02
CXH1	0.000000E 00	0.000000E 00	0.000000E 00	0.000000E 00	0.000000E 00	0.000000E 00
CXH2	0.000000E 00	0.000000E 00	0.000000E 00	0.000000E 00	0.000000E 00	0.000000E 00
CXH3	0.000000E 00	0.000000E 00	0.000000E 00	0.000000E 00	0.000000E 00	0.000000E 00
CXH4	0.000000E 00	0.000000E 00	0.000000E 00	0.000000E 00	0.000000E 00	0.000000E 00
CYDA	0.000000E 00	0.000000E 00	0.000000E 00	0.000000E 00	0.000000E 00	0.000000E 00
CYDO	0.000000E 00	0.000000E 00	0.000000E 00	0.000000E 00	0.000000E 00	0.000000E 00
CYDR	0.450000E-01	0.460000E-01	0.410000E-01	0.420000E-01	0.200000E-01	0.250000E-01
CZH1	0.141000E 00	0.141000E 00	0.153000E 00	0.164000E 00	0.110000E 00	0.157000E 00
CZH2	-0.156000E 00	-0.156000E 00	-0.160000E 00	-0.120000E 00	-0.700000E-01	-0.700000E-01
CZH3	0.000000E 00	0.000000E 00	0.000000E 00	0.000000E 00	0.000000E 00	0.000000E 00
CZH4	0.000000E 00	0.000000E 00	0.000000E 00	0.000000E 00	0.000000E 00	0.000000E 00
CLH1	0.000000E 00	0.000000E 00	0.000000E 00	0.000000E 00	0.000000E 00	0.000000E 00
CLH2	0.000000E 00	0.000000E 00	0.000000E 00	0.000000E 00	0.000000E 00	0.000000E 00
CLDA	-0.390000E-01	-0.390000E-01	-0.360000E-01	-0.250000E-01	-0.150000E-01	-0.120000E-01
CLDO	0.000000E 00	0.000000E 00	0.000000E 00	0.000000E 00	0.000000E 00	0.000000E 00
CLDR	0.600000E-02	0.600000E-02	0.600000E-02	0.100000E-02	0.400000E-02	0.600000E-02
CMH1	0.320000E 00	0.320000E 00	0.360000E 00	0.360000E 00	0.290000E 00	0.350000E 00
CMH2	-0.325000E 00	-0.325000E 00	-0.325000E 00	-0.280000E 00	-0.150000E 00	-0.145000E 00
CMH3	0.000000E 00	0.000000E 00	0.000000E 00	0.000000E 00	0.000000E 00	0.000000E 00

BETA= 0.1000000E 02

ALFA	-0.8000000E 01	0.0000000E 00	0.8000000E 01	0.1500000E 02	0.2000000E 02	0.3000000E 02
CNM4	0.0000000E 00	0.0000000E 00	0.0000000E 00	0.0000000E 00	0.0000000E 00	0.0000000E 00
CNM1	0.0000000E 00	0.0000000E 00	0.0000000E 00	0.0000000E 00	0.0000000E 00	0.0000000E 00
CNM2	0.0000000E 00	0.0000000E 00	0.0000000E 00	0.0000000E 00	0.0000000E 00	0.0000000E 00
CNDA	-0.2300000E-02	-0.2000000E-02	-0.1500000E-02	0.2000000E-02	0.3000000E-02	-0.8000000E-03
CNDD	0.0000000E 00	0.0000000E 00	0.0000000E 00	0.0000000E 00	0.0000000E 00	0.0000000E 00
CNDR	-0.2300000E-01	-0.2500000E-01	-0.2100000E-01	-0.1950000E 00	-0.9000000E-02	-0.9000000E-02

BETA= 0.200000E 02

ALFA	-0.800000E 01	0.000000E 00	0.800000E 01	0.150000E 02	0.200000E 02	0.300000E 02
CX	0.360000E-01	-0.700000E-02	0.660000E-01	0.130000E 00	0.200000E-01	-0.140000E-01
CY	-0.310000E 00	-0.310000E 00	-0.300000E 00	-0.320000E 00	-0.265000E 00	-0.295000E 00
CZ	0.500000E 00	-0.120000E 00	-0.680000E 00	-0.115000E 01	-0.109000E 01	-0.117000E 01
CL	-0.450000E-01	-0.450000E-01	-0.450000E-01	-0.460000E-01	-0.700000E-01	-0.670000E-01
CM	0.400000E-01	-0.700000E-01	-0.160000E 00	-0.290000E 00	-0.390000E 00	-0.400000E 00
CN	0.250000E-01	0.250000E-01	0.230000E-01	-0.600000E-02	0.110000E-01	-0.500000E-02
CXH1	0.000000E 00	0.000000E 00	0.000000E 00	0.000000E 00	0.000000E 00	0.000000E 00
CXH2	0.000000E 00	0.000000E 00	0.000000E 00	0.000000E 00	0.000000E 00	0.000000E 00
CXH3	0.000000E 00	0.000000E 00	0.000000E 00	0.000000E 00	0.000000E 00	0.000000E 00
CXH4	0.000000E 00	0.000000E 00	0.000000E 00	0.000000E 00	0.000000E 00	0.000000E 00
CYDA	0.000000E 00	0.000000E 00	0.000000E 00	0.000000E 00	0.000000E 00	0.000000E 00
CYDD	0.000000E 00	0.000000E 00	0.000000E 00	0.000000E 00	0.000000E 00	0.000000E 00
CYDR	0.790000E-01	0.790000E-01	0.760000E-01	0.630000E-01	0.620000E-01	0.590000E-01
CZH1	0.141000E 00	0.141000E 00	0.153000E 00	0.164000E 00	0.110000E 00	0.157000E 00
CZH2	-0.156000E 00	-0.156000E 00	-0.160000E 00	-0.120000E 00	-0.700000E-01	-0.700000E-01
CZH3	0.000000E 00	0.000000E 00	0.000000E 00	0.000000E 00	0.000000E 00	0.000000E 00
CZH4	0.000000E 00	0.000000E 00	0.000000E 00	0.000000E 00	0.000000E 00	0.000000E 00
CLH1	0.000000E 00	0.000000E 00	0.000000E 00	0.000000E 00	0.000000E 00	0.000000E 00
CLH2	0.000000E 00	0.000000E 00	0.000000E 00	0.000000E 00	0.000000E 00	0.000000E 00
CLDA	-0.340000E-01	-0.340000E-01	-0.320000E-01	-0.250000E-01	-0.260000E-01	-0.250000E-01
CLDD	0.000000E 00	0.000000E 00	0.000000E 00	0.000000E 00	0.000000E 00	0.000000E 00
CLDR	0.750000E-02	0.750000E-02	0.750000E-02	0.800000E-02	0.100000E-01	0.950000E-02
CMH1	0.390000E 00	0.390000E 00	0.330000E 00	0.380000E 00	0.330000E 00	0.270000E 00
CMH2	-0.220000E 00	-0.220000E 00	-0.220000E 00	-0.230000E 00	-0.210000E 00	-0.145000E 00
CMH3	0.000000E 00	0.000000E 00	0.000000E 00	0.000000E 00	0.000000E 00	0.000000E 00

BETA= 0.20000000E 02

ALFA	-0.8000000E 01	0.0000000E 00	0.8000000E 01	0.1500000E 02	0.2000000E 02	0.3000000E 02
CNH4	0.0000000E 00	0.0000000E 00	0.0000000E 00	0.0000000E 00	0.0000000E 00	0.0000000E 00
CNH1	0.0000000E 00	0.0000000E 00	0.0000000E 00	0.0000000E 00	0.0000000E 00	0.0000000E 00
CNH2	0.0000000E 00	0.0000000E 00	0.0000000E 00	0.0000000E 00	0.0000000E 00	0.0000000E 00
CNDA	-0.1000000E-02	-0.1000000E-02	-0.5000000E-03	0.2500000E-02	0.3000000E-02	-0.8000000E-03
CNDO	0.0000000E 00	0.0000000E 00	0.0000000E 00	0.0000000E 00	0.0000000E 00	0.0000000E 00
CNDR	-0.3400000E-01	-0.3400000E-01	-0.3200000E-01	-0.2200000E-01	-0.2500000E-01	-0.2100000E-01

BETA= 0.300000E 02

ALFA	-0.800000E 01	0.000000E 00	0.800000E 01	0.150000E 02	0.200000E 02	0.300000E 02
CX	0.280000E-01	0.400000E-02	0.720000E-01	0.153000E 00	0.460000E-01	-0.130000E-01
CY	-0.510000E 00	-0.510000E 00	-0.550000E 00	-0.640000E 00	-0.500000E 00	-0.480000E 00
CZ	0.390000E 00	-0.150000E 00	-0.620000E 00	-0.108000E 01	-0.112000E 01	-0.124000E 01
CL	-0.570000E-01	-0.570000E-01	-0.550000E-01	-0.550000E-01	-0.700000E-01	-0.670000E-01
CM	0.200000E-01	-0.800000E-01	-0.120000E 00	-0.300000E 00	-0.360000E 00	-0.460000E 00
CN	0.300000E-01	0.300000E-01	0.300000E-01	-0.600000E-02	0.110000E-01	-0.500000E-02
CXH1	0.000000E 00	0.000000E 00	0.000000E 00	0.000000E 00	0.000000E 00	0.000000E 00
CXH2	0.000000E 00	0.000000E 00	0.000000E 00	0.000000E 00	0.000000E 00	0.000000E 00
CXH3	0.000000E 00	0.000000E 00	0.000000E 00	0.000000E 00	0.000000E 00	0.000000E 00
CXH4	0.000000E 00	0.000000E 00	0.000000E 00	0.000000E 00	0.000000E 00	0.000000E 00
CYDA	0.000000E 00	0.000000E 00	0.000000E 00	0.000000E 00	0.000000E 00	0.000000E 00
CYDD	0.000000E 00	0.000000E 00	0.000000E 00	0.000000E 00	0.000000E 00	0.000000E 00
CYDR	0.790000E-01	0.790000E-01	0.760000E-01	0.650000E-01	0.620000E-01	0.590000E-01
CZH1	0.141000E 00	0.141000E 00	0.153000E 00	0.164000E 00	0.140000E 00	0.157000E 00
CZH2	-0.156000E 00	-0.156000E 00	-0.160000E 00	-0.120000E 00	-0.700000E-01	-0.700000E-01
CZH3	0.000000E 00	0.000000E 00	0.000000E 00	0.000000E 00	0.000000E 00	0.000000E 00
CZH4	0.000000E 00	0.000000E 00	0.000000E 00	0.000000E 00	0.000000E 00	0.000000E 00
CLH1	0.000000E 00	0.000000E 00	0.000000E 00	0.000000E 00	0.000000E 00	0.000000E 00
CLH2	0.000000E 00	0.000000E 00	0.000000E 00	0.000000E 00	0.000000E 00	0.000000E 00
CLDA	-0.340000E-01	-0.340000E-01	-0.320000E-01	-0.250000E-01	-0.200000E-01	-0.250000E-01
CLDD	0.000000E 00	0.000000E 00	0.000000E 00	0.000000E 00	0.000000E 00	0.000000E 00
CLDR	0.750000E-02	0.750000E-02	0.750000E-02	0.800000E-02	0.100000E-01	0.950000E-02
CMH1	0.390000E 00	0.390000E 00	0.330000E 00	0.360000E 00	0.330000E 00	0.270000E 00
CMH2	-0.220000E 00	-0.220000E 00	-0.220000E 00	-0.230000E 00	-0.210000E 00	-0.145000E 00
CMH3	0.000000E 00	0.000000E 00	0.000000E 00	0.000000E 00	0.000000E 00	0.000000E 00

BETA= 0.3000000E 02

ALFA	-0.8000000E 01	0.0000000E 00	0.8000000E 01	0.1500000E 02	0.2000000E 02	0.3000000E 02
CMM4	0.0000000E 00	0.0000000E 00	0.0000000E 00	0.0000000E 00	0.0000000E 00	0.0000000E 00
CNH1	0.0000000E 00	0.0000000E 00	0.0000000E 00	0.0000000E 00	0.0000000E 00	0.0000000E 00
CNH2	0.0000000E 00	0.0000000E 00	0.0000000E 00	0.0000000E 00	0.0000000E 00	0.0000000E 00
CNDA	-0.1000000E-02	-0.1000000E-02	-0.5000000E-03	0.2500000E-02	0.3000000E-02	-0.8000000E-03
CNDD	0.0000000E 00	0.0000000E 00	0.0000000E 00	0.0000000E 00	0.0000000E 00	0.0000000E 00
CNDR	-0.3400000E-01	-0.3400000E-01	-0.3200000E-01	-0.2200000E-01	-0.2500000E-01	-0.2100000E-01

where

CX	axial force coefficient, C_x
CY	side force coefficient, C_y
CZ	normal force coefficient, C_z
CL	rolling moment coefficient, C_ℓ
CM	pitching moment coefficient, C_m
CN	yawing moment coefficient, C_n
CYDR	side force due to rudder derivative, $C_{y_{\delta_r}}$
CZH1	normal force due to elevator derivative, $\delta_e < 0$, $C_{m_{\delta_e}}$
CZH2	normal force due to elevator derivative, $\delta_e \geq 0$, $C_{m_{\delta_e}}$
CLDA	rolling moment due to aileron derivative, $C_{\ell_{\delta_a}}$
CLDR	rolling moment due to rudder derivative, $C_{\ell_{\delta_r}}$
CMH1	pitching moment due to elevator derivative, $\delta_e < 0$, $C_{m_{\delta_e}}$
CMH2	pitching moment due to elevator derivative, $\delta_e \geq 0$, $C_{m_{\delta_e}}$
CNDA	yawing moment due to aileron derivative, $C_{n_{\delta_a}}$
CNDR	yawing moment due to rudder derivative, $C_{n_{\delta_r}}$

Rotary Derivatives

c_{y_p}	-.08	c_{m_q}	-10.57
c_{y_r}	.485	$c_{m_{\dot\alpha}}$	- 3.94
c_{ℓ_p}	-.5436	c_{n_p}	-.023
c_{ℓ_r}	.1125	c_{n_r}	- .16

SIGN CONVENTIONS FOR AIRCRAFT VARIABLES

δ_h: Horizontal tail deflection, positive for nose down command (i.e., horizontal tail trailing edge down)

δ_a: Aileron (or flaperon) deflection, positive for left roll command (i.e., right aileron trailing edge down)

δ_r: Rudder deflection, positive for nose left command (i.e., rudder trailing edge left)

δ_D: Differential horizontal tail

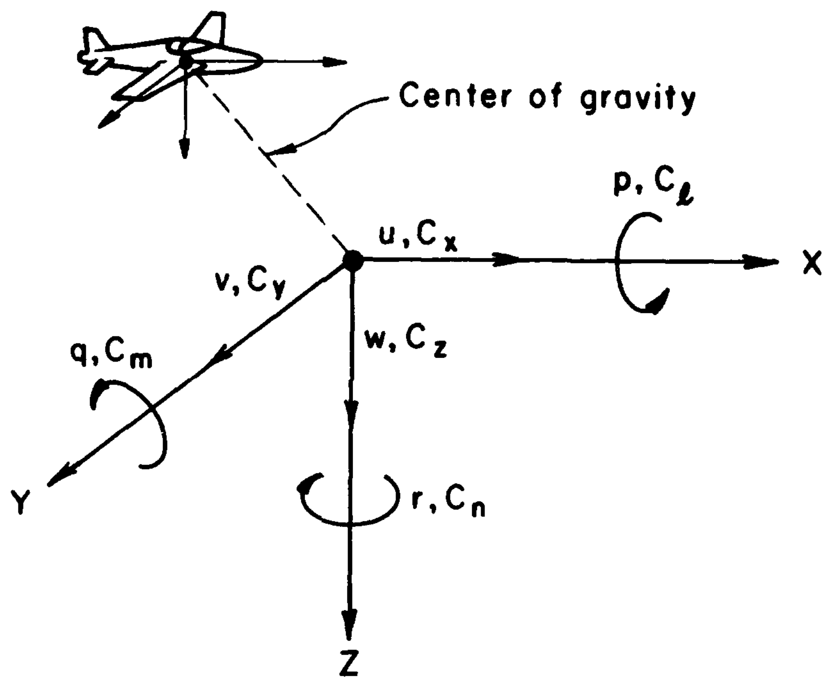

u	linear velocity along x axis
v	linear velocity along y axis
w	linear velocity along z axis
C_x	force coefficient along x axis
C_y	force coefficient along y axis
C_z	force coefficient along z axis
P	angular velocity about x axis
q	angular velocity about y axis
r	angular velocity about z axis
C_ℓ	rolling moment coefficient
C_m	pitching moment coefficient
C_n	yawing moment coefficient